

Using spectral variability across space and time to improve ecological understanding and management of invaded mid-Atlantic temperate successional vegetation communities

Kelsey Huelsman

Leesburg, VA

B.S. Environmental Science, University of Virginia, 2010

M.S. Environmental Science, University of Virginia, 2019

A Dissertation Presented to the Graduate Faculty
of the University of Virginia in Candidacy for the Degree of Doctor of Philosophy

University of Virginia

July 2024

Abstract

Connecting the spectral variability in aerial remote sensing imagery to plant communities across time and space has great potential for conservation efforts. Variability among species at different points in the growing season, across years, across platforms, and across scales can elucidate the best times and approaches to detect invasive plant species for management efforts. Spectral variability within species can be used to better understand functional trait variation and ecosystem functioning through remote sensing. Variability in images can also be used to understand plant community dynamics across time and space.

This dissertation explores the temporal and spatial variability in species-specific spectral signatures and vegetation communities in northwestern Virginia at the biological field station Blandy Experimental Farm, which contains 80 ha of fields in various stages of succession with abundant invasive plant species. The first two chapters explore the remote detection of three invasive plant species that outcompete and displace native plants and that are of interest to land managers in Virginia and much of the U.S., *Ailanthus altissima* (tree of heaven), *Elaeagnus umbellata* (autumn olive), and *Rhamnus davurica* (Dahurian buckthorn). First, within a single growing season using fine resolution drone-based imagery, then across multiple growing seasons using aerial hyperspectral imagery collected by fixed-wing aircraft by the National Ecological Observatory Network (NEON), a different platform, sensor, and spatial resolution.

The results demonstrate that both UAV and NEON (fixed-wing aircraft) hyperspectral imagery can be used to detect the three species of interest, however, accuracies varied over time and were greatest when algorithms were produced using *in situ* data (e.g. from the same platform, on the same date). Drone-based algorithms were most consistent across the growing season for *E. umbellata*, while NEON-based detection was least consistent. NEON-based detection of *R.*

davurica was most consistent across growing seasons and platforms. *A. altissima* algorithms were also relatively consistent across years but used different spectral features in the drone-based and NEON-based algorithms. These results demonstrate the usefulness of flexible sampling times within and across growing seasons.

The last two chapters explore the partitioning of spectral variability at different scales and their ecological implications. First, at multiple organizational scales (at the leaf, canopy, species, and community levels) within a single growing season in drone-based images, then at multiple spatial scales (within and among plots) by pairing field surveys of species composition and NEON-based images. Within a growing season, spectral variability in biochemical-associated spectral regions within individual canopies and among canopies of the same species exceeded among-species variability, suggesting a lack of agreement with the SVH as biochemical traits become increasingly variable at finer organizational scales as leaves mature over a growing season. Spectral variability within plots was greater in biochemical traits than in structural traits, but among-plot spectral variability was greater in structural traits than biochemical traits, suggesting vegetation communities are stable in different traits at different scales. These violations of the SVH were driven by both spatial and temporal factors.

This dissertation demonstrates that species-based assumptions about traits and spectra are not necessarily accurate across space and time and the importance of considering the wide range of spectral and trait variability within a species. Understanding trait variation at different scales and times can facilitate answering major questions in community ecology to further the understanding of plant communities and ecosystems. Spectroscopy can be used to this end and will benefit from increasingly available hyperspectral airborne data and new satellite missions.

Doctoral Dissertation Committee

Howard Epstein (Advisor)

Department of Environmental Sciences

Xi Yang (Advisor)

Department of Environmental Sciences

Lawrence Band

Department of Environmental Sciences

Bradley Cantrell

School of Architecture

Acknowledgments

Many people made this research not only possible but also enjoyable:

- My advisor, Howie Epstein, who took a leap of faith and let me into graduate school with little research experience. He gave me freedom to explore my broad interests, and the space to make mistakes and learn from them, all of which helped me to grow into the well-rounded scientist I am today.
- My adoptive co-advisor, Xi Yang, who introduced me to remote sensing, which became the lens through which I view ecological patterns and processes in this dissertation.
- My additional committee members, Larry Band from the Department of Environmental Science and Brad Cantrell from the School of Architecture, who provided helpful insights and rigor to this dissertation.
- My community collaborator Rod Walker, from the Blue Ridge Program for Regional Invasive Species Management (PRISM). His passion for finding creative ways to manage invasive plant species provided inspiration for this project, and his enthusiasm and investment in this project kept me moving forward.
- My collaborator Lucie Cervena, from Charles University in Prague, Czechia, without whom I would have struggled to learn how to collect drone images.
- Dave Carr, T'ai Roulston, and Kyle Haynes at Blandy Experimental Farm, who allowed frequent drone flights at the field station and helped me navigate safety protocols during a pandemic shutdown to keep my research moving forward.
- Judy Masi and Elizabeth Jackson, the office administrators who consistently have fast answers delivered with kindness and patience and who make the difficult-to-navigate world of research manageable and painless.

- My lab mates in the Epstein and Yang labs and fellow Blandy researchers, who provided years of feedback and support and years of inspiration with their own research, especially Allie Parisien and Andrew Jablonski, whose research interests and enthusiasm complement my own.
- My undergraduate mentees over the years, especially Lydia Mullori and Anthony Murphy-Neilson, who helped extract and analyze thousands of spectra.
- My internship supervisors Abby Benson and Steve Formel, who allowed me to find a niche in the GBIF world that complemented this dissertation.
- The ultimate support system of my loving and supportive parents, partner, and chosen family.

Table of Contents

Abstract	2
Acknowledgments	5
Chapter 1: Introduction	8
Chapter 2: Using phenology to improve invasive plant detection in fine-scale hyperspectral drone-based images: A case study in temperate successional fields	14
Chapter 3: Scaling fine-resolution drone-based hyperspectral algorithms to the landscape scale: A case study in invasive plant species detection	43
Chapter 4: Fine-scale ecological organization contributes substantively to spectral variability in Virginia successional forests	82
Chapter 5: Spectral variability and biodiversity across scales in an early successional plant community	109
Chapter 6: Conclusion	133
References	139
Appendix A: Supplemental Figures Chapter 2	168
Appendix B: Supplemental Figures Chapter 3	173
Appendix C: Supplemental Figures Chapter 4	176
Appendix D: Supplemental Figures Chapter 5	178
Appendix E: Spectral variability in fine-scale drone-based imaging spectroscopy does not impede detection of target invasive plant species	180

Chapter 1: Introduction

Global environmental change, including land-use change, climate change, and the spread of invasive species, particularly invasive plant species, threaten the biodiversity of ecosystems globally (Bellard et al., 2013; W. Dawson et al., 2017; Gaertner et al., 2009; Kimothi & Dasari, 2010; Peerbhay et al., 2016; Pyšek et al., 2017; Seebens et al., 2017). Changes in community composition and biodiversity caused by invasive plants alter the functioning, stability, and ecosystem services provided by ecosystems (Cardinale, 2011). Invasive plants disrupt anticipated carbon, nutrient, water, and energy cycles by altering the biogeochemistry (e.g. soil chemistry) and structure (e.g. structural heterogeneity) of an ecosystem. They inhibit the growth of native species, which interrupts resources for native wildlife and insects. They can also harm agricultural systems or human health directly, or indirectly via synergistic relationships with other invasive species. From an ecological, conservation, and ecosystem services perspective, invasive plants are important and acknowledged as a global conservation priority.

In Virginia, the estimated annual cost of invasive species is \$1 billion (Virginia Invasive Species Advisory Committee, 2018). Invasive tree and shrub species, including *Ailanthus altissima* (tree of heaven), *Elaeagnus umbellata* (autumn olive), and *Rhamnus davurica* (Dahurian buckthorn) outcompete and displace native plants. They impact soil chemistry, moisture, and nutrient cycling (Heneghan et al., 2006; Knight et al., 2007; Mascaro and Schnitzer, 2007; Malinich et al., 2017; Naumann et al., 2010), and they encourage the encroachment of other plant species that thrive in high-nutrient environments (Gómez-Aparicio & Canham, 2008). *A. altissima* is of particular interest more recently, as it is a preferred host of the agriculturally-costly spotted lanternfly, which feeds on apples, peaches, grapes, and hops crops (Virginia Invasive Species Advisory Committee, 2018).

The global and local interest in managing invasive plant species and protecting biodiversity makes ecosystem observation and biodiversity monitoring imperative. This need can be met in two ways: through field-based observation, or through remote sensing via satellite, fixed-wing aircraft, or unmanned aerial vehicles (UAVs, or drones). Field-based surveys are accurate but are labor-intensive and therefore also cost-prohibitive over large scales (Kays et al., 2015; Pimm et al., 2015). Satellite remote sensing can monitor large areas over time but may lack fine-scale details. UAVs and fixed-wing aircrafts can provide higher spatial resolution than satellites for regional or landscape scales.

Imaging spectroscopy, or hyperspectral remote sensing, can be used in concert with aerial platforms. Hyperspectral remote sensing has become increasingly popular for ecosystem observation (Féret & Asner, 2014; R. Wang & Gamon, 2019), as it provides significant detail about plant traits (Gregory P. Asner & Martin, 2008a; Ustin & Gamon, 2010). Biochemical characteristics and traits of vegetation, e.g. photosynthetic pigments, water, proteins, structural compounds interact in specific ways with solar radiation, which produce a specific “spectral signature” that is detected in hyperspectral remote sensing (Cavender-Bares et al., 2016; McManus et al., 2016). Although green plants have similar spectral signatures, differences in chemical, physiological, and structural properties can cause subtle differences in reflectance signatures, which should cause spectra to differ more among distantly related groups than among close relatives (Cavender-Bares et al., 2016; McManus et al., 2016; Schweiger et al., 2018). The positive relationship between spectral variability and species diversity, known as the spectral variation hypothesis (SVH; Palmer et al., 2002), is grounded in functional variation, with the assumption that functions and therefore spectra differ most among species. Spectral signatures of vegetation are not only shaped by genetics, however; they are also shaped by the abiotic and biotic

characteristics of the surrounding environment (Laliberté et al., 2020; Z. Wang et al., 2020) as well as physical factors inherent to the sensor and platform used.

The long-term evolutionary history of a plant species, including the historical climate and disturbance regimes of its environment, are preserved through the genotype. The physical expression of the genotype, known as “the phenotype” is shaped by environmental conditions and species interactions. A spectral signature is one way a phenotype is expressed. Because genetics and environmental conditions both affect a phenotype, a single genotype can have many phenotypes. This variability is known as phenotypic plasticity (Bradshaw 1965; Scheiner 1993; Des Marais et al. 2013). Phenotypic plasticity can occur across both time and space (e.g. over a growing season, across multiple growing seasons, within a single canopy, across multiple biomes, globally). Characteristics can differ more within a species than among species, due to factors including phenology, biochemical variability, or structural variability. Biological features that can impact spectra can be long-term traits such as canopy architecture, or short-term characteristics such as leaf angle, all of which interact with reflected light and therefore impact spectra. In addition to the biochemical traits and responses that affect the spectral signatures of vegetation, physical factors can also affect how vegetation reflects incoming solar radiation and how that reflected radiation is then perceived by a sensor. Lighting conditions, sensor viewing geometry, spatial resolution (Huelsman et al. 2024, in preparation), and spectral resolutions can all affect a spectral signature. If the spatial resolution (i.e. size of pixels) is greater than the size of plant canopies, linking certain reflectance signatures to species or diversity may also be less straightforward.

Hyperspectral remote sensing is an efficient and robust approach to ecosystem observation (Cavender-Bares et al., 2020; Foody & Cutler, 2003; Nagendra, 2001; Pettorelli et al., 2014; Rocchini et al., 2010; Skidmore et al., 2021), with great potential to both monitor biodiversity and

use in invasive species management applications. Despite this potential, the utility of hyperspectral remote sensing has been underexamined. Evaluating how spatial and temporal scales affect remote sensing is an imperative step toward leveraging existing spectral imagery to increase understanding of ecosystem health and to improve conservation efforts through meaningful and accurate monitoring approaches. Blandy Experimental Farm, a biological field station in northwestern Virginia, United States (39.06°N, 78.07°W) provides an opportunity to assess the spatial and temporal variability in spectral signatures across multiple years and using multiple platforms in successional fields and forests with abundant invasive plant species.

This dissertation explores the utility of hyperspectral remote sensing in invasive plant species detection and the implications of temporal and spatial variability in this practical application. Then it explores the underlying patterns in variability at different spatial and temporal scales that are vital to understand if remote sensing is to be used to make conclusions about ecosystem health, trait diversity, and biodiversity. I address the main questions:

1. When in the growing season and what features allow for the detection of the invasive plant species *A. altissima*, *E. umbellata*, and *R. davurica* in fine-scale hyperspectral imagery collected by UAV?
2. To what extent can *A. altissima*, *E. umbellata*, and *R. davurica* be detected in coarser-scale hyperspectral imagery collected by fixed-wing aircraft?
3. When in the growing season and in what spectral regions is spectral variability within species (within individual canopies and among individuals of a species) greater than variability among species in successional plant communities?
4. What do alpha, beta, and gamma biodiversity and spectral diversity suggest about ecosystem dynamics in an early successional plant community?

In chapter 2, I utilize a drone to collect hyperspectral imagery in heterogeneous plant communities and incorporate species-specific phenology into the methods for a more robust approach to developing effective detection algorithms for the invasive plant species *A. altissima*, *E. umbellata*, and *R. davurica*. I provide a methodological foundation to develop detection algorithms, which can be used to further the understanding of the spatial patterns of invasive plant species in the landscape for management purposes. I also compare the most important spectral features that led to accurate detection of each species over a single growing season, which can be used to maximize the reliability and accuracy of detection.

In chapter 3, I assess the interoperability, scalability, and similarities between drone-based and fixed-wing aircraft-based detection algorithms. Images collected by drone often have much finer spatial resolution than images collected by fixed-wing aircraft, which is potentially beneficial for capturing fine-scale details but comes at the cost of smaller spatial extents. To determine the applicability of fine-scale algorithms at the landscape scale, I apply the drone-based detection algorithms established in chapter 2 to coarser resolution images collected by the National Ecological Observatory Network (NEON), which not only cover a larger area but also include multiple years of images. I then create new algorithms using the NEON images and compare the most important spectral features that led to accurate detection of each species over a single growing season.

In chapter 4, I take advantage of the very fine spatial resolution of drone-based imagery, in which pixels are approximately the size of individual leaves, to examine the effects of seasonality and organizational scale on spectral variability and agreement with the SVH. I partitioning spectral variability in hyperspectral drone imagery collected over the course of a growing season to different levels of organization: within individual canopies, among canopies within the same

species, among species, and among communities. I also examine temporal and spectral patterns in species-specific variability at finer scales.

In chapter 5 I again examine the SVH using plot-level species composition data and coarser-scale remote images (from NEON). I use the species composition data to calculate biodiversity metrics and then compare them to spectral variability within plots, among plots, and across the landscape. I also assess the plot-level (alpha-level) biodiversity and spectral diversity metrics to determine what may drive agreement or disagreement with the SVH at this scale and in this ecosystem.

Genetic information can be inferred from the spectral phenotype and used for invasive plant species detection, although spectra are impacted by more than just species identity. Variability in spectra across space and time, however, suggest that the accuracy of and key spectral features in detection algorithms may vary, and there may be better combinations of times and/or spectral features to use in detection. This inherent temporal, spatial, and spectral variability within species also suggests that species-based assumptions about traits that ignore within-species variability, including the SVH, are not necessarily accurate. This dissertation uses the phenotype to explore the temporal and spatial variability in species-specific spectral signatures and the temporal and spatial patterns in variability at different scales using relatively novel airborne platforms.

Chapter 2: Using phenology to improve invasive plant detection in fine-scale hyperspectral drone-based images: A case study in temperate successional fields

Abstract

Reducing the spread of invasive plants is of global interest but requires extensive ecosystem monitoring. Traditional approaches to invasive species monitoring, such as ground surveys or satellite remote sensing, can be cost prohibitive, labor intensive, or lack fine-scale details. Unoccupied aerial vehicles (UAVs) and hyperspectral remote sensing can be useful tools, providing greater coverage than ground surveys and finer spatial resolution than satellites. I utilized a UAV equipped with a Nano-Hyperspec imager to collect fine resolution (3 cm) hyperspectral images on seven dates from April to November during the 2020 growing season. I used these images to develop hyperspectral detection algorithms for three different invasive plant species within heterogeneous vegetation communities with 12 other native and nonnative plant species. The three species are invasive in much of the U.S., and specifically in Virginia, where the data were collected: *Ailanthus altissima* (tree of heaven), *Elaeagnus umbellata* (autumn olive), and *Rhamnus davurica* (Dahurian buckthorn). Given that invasive plants likely differ from native species in phenology, photosynthetic rates, and nutrient concentrations, I anticipated that hyperspectral data would capture differentiating biophysical and biochemical characteristics. I examined when each species could be accurately detected and what spectral features allowed for

detection in seven algorithms over the growing season. All three species could be detected well in June. Only *E. umbellata* had consistently accurate algorithms (6 of the 7) and used consistent features (blue, green, red, and red edge) across the growing season. *A. altissima* and *R. davurica* were both detectable mid- and late-growing season, with little overlap in key spectral features, indicating the usefulness of including dates outside of peak greenness in data collection and algorithm generation to incorporate species-specific phenological traits. I demonstrate that UAV hyperspectral imagery can be used to accurately detect invasive plant species in heterogeneous plant communities, incorporating phenology into detection algorithms. These methods provide a foundation for land managers and communities to monitor ecosystems, find new occurrences and populations of invasive plants that have not yet dominated local ecosystems, determine and prioritize management approaches, as well as understanding the ecological impact of invasive plant species on vegetation communities.

1. Introduction

Invasive plants threaten the biodiversity of ecosystems globally (Bellard et al., 2013; W. Dawson et al., 2017; Gaertner et al., 2009; Kimothi & Dasari, 2010; Peerbhay et al., 2016; Pyšek et al., 2017; Seebens et al., 2017). Reducing the spread of invasive plants is of global interest but requires extensive ecosystem monitoring. Traditional approaches to monitoring are satellite-based and ground-based, each of which have caveats. The coarse resolution of satellite images fails to detect fine-scale features and individuals. On the other hand, ground surveys are detail-oriented but labor requirements inhibit data collection over large areas. Ecological observations have been limited both spatially and temporally due to cost-prohibitive and labor-intensive survey methods (Kays et al., 2015; Pimm et al., 2015).

Data provided by unoccupied aerial vehicles (UAVs) have higher spatial resolution than satellite-based data as well as greater spatial coverage than ground surveys (Alvarez-Vanhard et al., 2021), merging advantages of traditional satellite-based and ground-based monitoring (Sun & Scanlon, 2019). Thus, UAVs are becoming an increasingly popular platform to observe ecosystems, including invasive plant species monitoring. As the high spatial resolution of UAV images was not found to impede detection of invasive plants due to spectral variability (Huelsenman et al., 2023), it instead can serve to detect small plants early in an invasion, increasing the possibility for earlier intervention and mitigation of impacts (Reaser et al., 2020). UAVs also provide the ability to survey more remote areas in a repeatable and standardized way (Besson et al., 2022), providing timely and accurate maps for detection and monitoring that can influence management decisions (Rodriguez et al., 2021).

In addition to the limitations in spatial resolution of most traditional satellite-based monitoring, there are also spectral limitations. Much of the remotely sensed data provided by

satellite is multispectral, consisting of 4 to 20 discrete spectral bands. Hyperspectral data, on the other hand, includes many adjacent bands that are narrower than multispectral bands. Plants vary in biophysical and biochemical properties (Matongera et al., 2016; Z. Wang et al., 2020; Yang et al., 2016), and pigments, proteins, and structural molecules associated with those properties all interact with light differently to impact spectra (Homolova et al., 2013). Thus, the high spectral resolution of hyperspectral data provide a detailed “electromagnetic signature,” which can provide information on a variety of plant functional and structural traits (Gregory P. Asner et al., 2015; Hill et al., 2019; Homolova et al., 2013).

With current understanding of plant chemical and structural properties, hyperspectral data can be used not only to detect general assemblages of plants (Hochberg et al., 2015; Sanchez-Azofeifa et al., 2013; Schmidt & Skidmore, 2003) but also to differentiate among species (M. Clark et al., 2005; Cochrane, 2000). Relative to native plants at the same sites, invasive plants tend to have higher specific leaf areas, photosynthetic rates, growth rates, and leaf nutrient and pigment concentrations (Ehrenfeld, 2004; Ehrenfeld et al., 2001), which should lead to spectral differences (Gregory P. Asner & Martin, 2008b; Azadnia et al., 2023; Chance et al., 2016; Ely et al., 2019; Kothari et al., 2023; Mahlein et al., 2010; Mutanga et al., 2004; Serbin et al., 2014; Thenkabail et al., 2014; Xiao et al., 2014). In addition to the theoretical underpinnings, hyperspectral imagery has also been used to identify invasive plant species (Aneece & Epstein, 2017; G. Asner & Vitousek, 2005; Gregory P. Asner & Martin, 2008b; Castro et al., 2004; Chance et al., 2016; Kganyago et al., 2017; Skowronek et al., 2017).

Hyperspectral imagery is useful for detecting plant traits, and when used in concert with a drone, imagery can capture temporal variability in those traits, as the flexible operation of UAVs allows for flights to take place readily at multiple points in the growing season (Castro-Esau et al.,

2006; Ecke et al., 2022). Because properties change over the course of a growing season (e.g. phenological traits) and respond to changes in environment (e.g. drought), reflectance spectra should also be expected to change. The use of UAVs for hyperspectral image collection incorporates temporal variability and phenological features, which may further improve invasive plant detection during certain times of the year.

Whereas a few drone-based studies have been successful in identifying individual plant species, this has often been accomplished with traditional photography or in large monocultures, where it is straightforward to differentiate the species of interest from the neighboring plants (Huang & Asner, 2009). Using hyperspectral imagery in concert with a drone is novel, and in recent years this methodology has been used to monitor invasive milkweed in Hungary (Papp et al., 2021), invasive plants in Russia using vegetation indices (Dmitriev et al., 2022), aquatic weeds in France (Diruit et al., 2022), and for early detection of insect infestation in forests in Northeast China (Gao et al., 2023). Sabat-Tomala et al. (2022) used hyperspectral datasets from three times in a growing season to detect invasive plant species in Southern Poland, with a spatial resolution of 0.5 m.

This project incorporates the fine spatial resolution and high coverage data that can be collected with a UAV with the fine spectral resolution of hyperspectral imagery to detect three plant species that are invasive in much of the U.S., and specifically in Virginia where this study is focused: *Ailanthus altissima* (tree of heaven), *Elaeagnus umbellata* (autumn olive), and *Rhamnus davurica* (Dahurian buckthorn). Given that *A. altissima*, *R. davurica*, and *E. umbellata* are invasive and are therefore likely to have high photosynthetic rates and leaf nutrient concentrations, and that hyperspectral data serve as an indication of these biophysical and biochemical characteristics of

plants (Matongera et al., 2016), these characteristics should aid in differentiation from other species.

Although others have successfully differentiated some of these three invasive plant species using hyperspectral imagery, all were done either in the lab (Burkholder et al., 2011) or near the ground using handheld spectrometers (Aneece & Epstein, 2017). I not only utilized a drone to collect hyperspectral imagery in heterogeneous plant communities but also incorporated species-specific phenology into these methods for a more robust attempt to develop effective detection algorithms. Plant phenology can be a useful tool in invasive species detection, as species vary in their timing of leaf-out, flowering, and fall senescence, and invasive species also tend to have longer growing seasons than native species. In answering the following questions on how to accurately detect these species of interest, I provide a methodological foundation for their detection and management, as well as further the understanding of their spatial and temporal patterns on the landscape:

1. When in the growing season are *A. altissima*, *E. umbellata*, and *R. davurica* most differentiable from other species in fine-scale hyperspectral imagery collected by UAV?
2. What are the spectral features that allow for differentiation of *A. altissima*, *E. umbellata*, and *R. davurica* individuals over the growing season?
3. Do *A. altissima*, *E. umbellata*, and *R. davurica* have consistent spectral features that allow for their detection across the growing season?

2. Methods

2.1 Study site

Data were collected at the ~280 ha biological field station Blandy Experimental Farm (BEF) in northwestern Virginia (39.06°N, 78.07°W). Aerial images were collected over three 1-ha fields in early- to mid-successional stages (approximately 20 to 30 years following last disturbance), based on their abundance of the invasive plant species of interest, *A. altissima*, *E. umbellata*, and *R. davurica* (Huelsman et al. 2023).



Figure 1. Locations of fields in which hyperspectral data were collected during the 2020 growing season. A field in early secondary succession, an intermediate early-to-mid successional field, and a mid-successional field, shown in green, blue, and purple, respectively (aerial image from Google Maps satellite view).

2.2 Data collection and image post-processing

Hyperspectral images were collected during the 2020 growing season using a DJI Matrice 600 Pro drone equipped with a high-precision GPS system and a VNIR imaging spectrometer (Nano-Hyperspec, Headwall Photonics, Bolton, MA) with a spectral range of 400 to 1000 nm and a spectral resolution of 2-3 nm (a total of 270 spectral bands). Images were collected by the Nano-Hyperspec imaging spectrometer on the UAV, programmed to capture images using HyperSpec III software (Headwall Photonics, Bolton, MA) over consistent, straight flightlines at 48 m altitude. Flights were planned using Universal Ground Control Software (UgCS), resulting in images with spatial resolution of about 3 cm.

Images were collected as weather permitted from early season leaf-out through fall senescence approximately every four weeks: DOY 106 (April 15), DOY 134 (May 13), DOY 160 (June 8), DOY 178 (June 26), DOY 249 (September 6), DOY 276 (October 2), DOY 309 (November 4). To reduce bidirectional reflectance distribution function (BRDF) effects, images were collected midday between 10h and 15h, under consistent sky conditions, and from nadir to a 10.55 degree viewing angle (the total field of view of the sensor was 21.1 degrees). A mosaic of multiple images was created with SpectralView software (Headwall Photonics, Bolton, MA) after images were adjusted for incoming and scattered solar radiation using a dark reference and grey-scale tarp, and terrain and perspective effects were removed via orthorectification (Huelsman et al. 2023).

2.3 Image sampling & data cleaning

Vegetation surveys were conducted in each field to determine common species and develop a robust spectral dataset of vegetation representing the variety and complexity of plant communities.

Up to eight individuals of 15 different species, genera, or plant type across trees, shrubs, forbs, and graminoids (*A. altissima*, *E. umbellata*, *Gleditsia triacanthos*, *Galium verum*, *Maclura pomifera*, *Juglans nigra*, *Juniperus virginiana*, *Lonicera japonica*, *Lonicera maackii*, *Pinus virginiana*, *Rhamnus davurica*, *Rubus spp.*, *Solidago altissima*, *Symphoricarpos orbiculatus*, and graminoids) were identified in each field using a high-precision Trimble GPS (measurement accuracy of 0.5 m) and used to identify and catalogue individuals in images. In cases where fewer than eight individuals were present, as many as were present were sampled. Some species that were common in the training fields were included for robustness of the training algorithm but were not present in the testing field images (e.g. *G. verum* and *P. virginiana*; Table 1). From each catalogued individual plant in images from each of the seven dates, 15 well-lit pixels were selected to provide reflectance data.

To remove outliers, the mean reflectance across all wavelengths for each pixel and canopy were compared for each data collection date. Any pixel within a canopy that differed more than 25% from the canopy mean was removed from the dataset, as it was assumed the given reflectance spectra was not representative (Huelsenman et al. 2023). This threshold was chosen for two reasons: first, it was equal to a difference of about 2 standard deviations from the mean and removed approximately 5% of pixels from the entire growing season dataset, with balanced representation of overall lower and higher reflectance; and second, it was approximately equal to the “saturation point” of pixels removed, above which, few additional pixels would be removed (Figure S1). Canopies that included but were not dominated by secondary liana (vine) species, such as *C. orbiculatus* or *L. japonica*, were also removed from analysis to focus on purer pixels. Pixels sampled from images with changes in light conditions were also removed, as these impacted the magnitude of reflectances measured.

Table 1. Number of individuals of each species visible in hyperspectral images collected and from which 15 well-lit and representative pixels were sampled to then be used for training and testing. Species of interest are presented in bold.

Species	Growth Form	Training Individuals	Testing Individuals
<i>A. altissima</i>	Tree	10	3
<i>E. umbellata</i>	Shrub	9	8
<i>G. verum</i>	Forb	7	0
<i>G. triacanthos</i>	Tree	7	5
Graminoid <i>spp.</i>	Graminoid	6	1
<i>J. nigra</i>	Tree	8	1
<i>J. virginiana</i>	Tree	6	4
<i>L. japonica</i>	Vine	5	3
<i>L. maackii</i>	Shrub	9	8
<i>M. pomifera</i>	Tree	4	7
<i>P. virginiana</i>	Tree	3	0
<i>R. davurica</i>	Shrub	16	8
<i>Rubus spp.</i>	Shrub	8	8
<i>S. altissima</i>	Forb	3	0
<i>S. orbiculatus</i>	Vine	8	3

2.4 Analysis and classification

To determine when during the growing season *A. altissima*, *E. umbellata*, and *R. davurica* are most differentiable from other plant species, I used a Partial Least Squares Discriminant Analysis (PLS-DA) model to classify individual trees and shrubs using the mixOmics package in R (Rohart et al., 2016). PLS-DA is a machine learning tool, which handles large datasets and collinearity well, two features inherent to spectral data. It applies the statistical tool of PLS to feature selection and classification scenarios (Nguyen & Rocke, 2002; Pérez-Enciso & Tenenhaus, 2003). A PLS-DA was performed for each date of image collection for each species of interest. Data sampled from all fields and all dates were first recoded as a species of interest (*A. altissima*, *E. umbellata*, or *R. davurica*) or as “other” species in each image. Spectral signatures collected from the images of the two training fields were randomly split into 70% and 30% portions for calibration and validation, respectively. A PLS-DA classification model was generated based on the training calibration dataset, and then applied to the remaining 30% of validation training data to classify each pixel within a canopy. Because each canopy included 15 pixels, each with a classification, each canopy was classified as a unit, based on the percentage of pixels classified as the species of interest or “other.” In other words, even though a pixel-based classification was used in the first step, the classification of each pixel was combined for a single object-based classification for each individual tree or shrub.

Rather than assuming a majority of pixels (>50%) as the best threshold for classification of an individual canopy, I searched for a “threshold percentage,” or the percentage of pixels in a canopy (out of 15) needed to be classified as a species of interest to maximize overall classification accuracy. User and producer accuracies were calculated for each species of interest using thresholds of 10 to 90% of pixels in a canopy. A threshold set too low or high increased the

probability of false positives and negatives, respectively. Thresholds of 35, 25, and 40% were selected for *A. altissima*, *E. umbellata*, and *R. davurica*, as they balanced false negatives and positives in the validation portion of the training dataset. The fact that all thresholds were below 50% demonstrates that this approach is helpful to incorporate in classification methodology, particularly for invasive plant detection.

After determining the optimal threshold of percent of pixels, all pixels in the training dataset were used to create a classification model to detect each species of interest on each of the seven dates in the testing dataset (the third field over which images were collected). Each of the 15 pixels of each plant canopy in the testing field was classified. If the percentage of pixels in a canopy was greater than the threshold for each species of interest (35, 25, and 40% for *A. altissima*, *E. umbellata*, or *R. davurica*, respectively), that individual was classified as the species of interest. The classification of each of the 59 individual canopies in the testing field was compared to its true, field-referenced identity (Figure 2). User Accuracy, Producer Accuracy, Omission Error, and Commission Error were calculated for each species on each date.

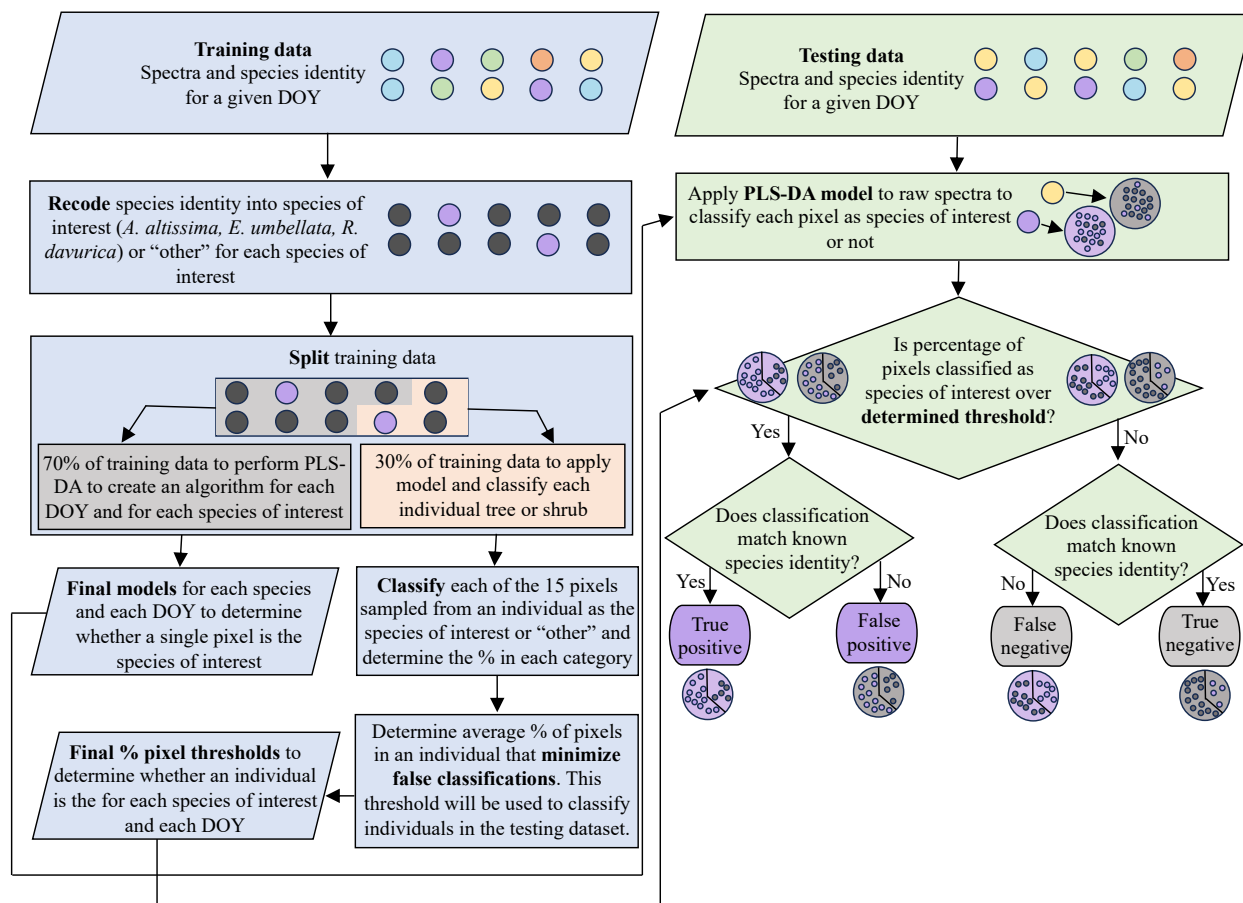


Figure 2. Workflow for models to answer research questions. This process will be utilized for each species of interest (*A. altissima*, *E. umbellata*, and *R. davurica*) for each date in the growing season. This will allow for the assessment of which time(s) in the growing season are best for the detection of these plants in a heterogeneous field as well as what features allow for detection.

2.5 Assessing the importance of spectral features in detection

The PLS-DA model not only serves to differentiate *Ailanthus*, *Elaeagnus*, and *Rhamnus* from other species via classification, but it also serves to determine what spectral features are important in their differentiation over the growing season. Wavelengths that loaded heavily (i.e. wavelengths with greater absolute magnitude loading factors) were most important in differentiating a species of interest from the others (Liland et al., 2022). Though PLS-DA is prone to overfitting (i.e. a model can misinterpret noise as relevant information), the classification accuracy of each PLS-DA model approximates model goodness. Key spectral regions seen in algorithms with detection accuracy >75% were examined to assess the importance of spectral features at given points in the growing season (phenology) and their consistency across the growing season. To assess the questions of important spectral regions on each date with good detection accuracy (>75%), loading values were smoothed using a 20 nm rolling window in the R zoo package (Zeileis & Grothendieck, 2005).

To determine which spectral regions were consistently important, smoothed loading factors were used to rank bands for each species of interest, date, and PLS-DA component. I ranked bands within each component separately, as components tend to complement each other due to the orthogonal nature of PLS-DA. Then ranks >180 were selected and averaged across components for each species of interest on each date. Because there are 225 total bands considered in each component of each algorithm, ranking bands by loading value, then considering any bands with mean ranks >180 focuses on the top 45 (or top 20% of) bands in each component. There could theoretically be 45 bands with mean ranks >180 in each component over the growing season, which would necessitate that each band be consistently among the 45 top-loading bands. The less frequently a band is among the 45 top-loading bands, the less likely it is to have a mean rank >180.

Thus, more bands with mean rank >180 implies greater consistency across algorithms, whereas fewer bands implies less consistency.

3. Results

3.1 Phenology of spectral features

Trait differences, as well as phenological differences, are apparent in the spectral data. Spectral differences among the three species of interest were more apparent in different parts of the reflectance spectra and at different points in the growing season. Over much of the growing season, *E. umbellata* had greater reflectance in blue and red spectral regions than *R. davurica* and *A. altissima*, with the greatest differences among them occurring around June 26 (DOY 178). The green reflectance peak on June 26 was similar for *E. umbellata* and *R. davurica* individuals, whereas it was lower in *A. altissima*. *A. altissima* and *E. umbellata* had similar reflectance at the green peak on June 8 and September 5 (DOY 160 and 249), while it was greater and lower in *R. davurica* individuals on each respective date. The most differentiable feature for *A. altissima* in the visible wavelengths occurred on October 2 (DOY 276), when reflectance in green to red wavelengths were greater than the other two species. *A. altissima* had greater reflectances in the NIR spectral region than *R. davurica* and *E. umbellata*, and *R. davurica* demonstrated the greatest decrease in NIR reflectances late in the growing season (Figure 3).

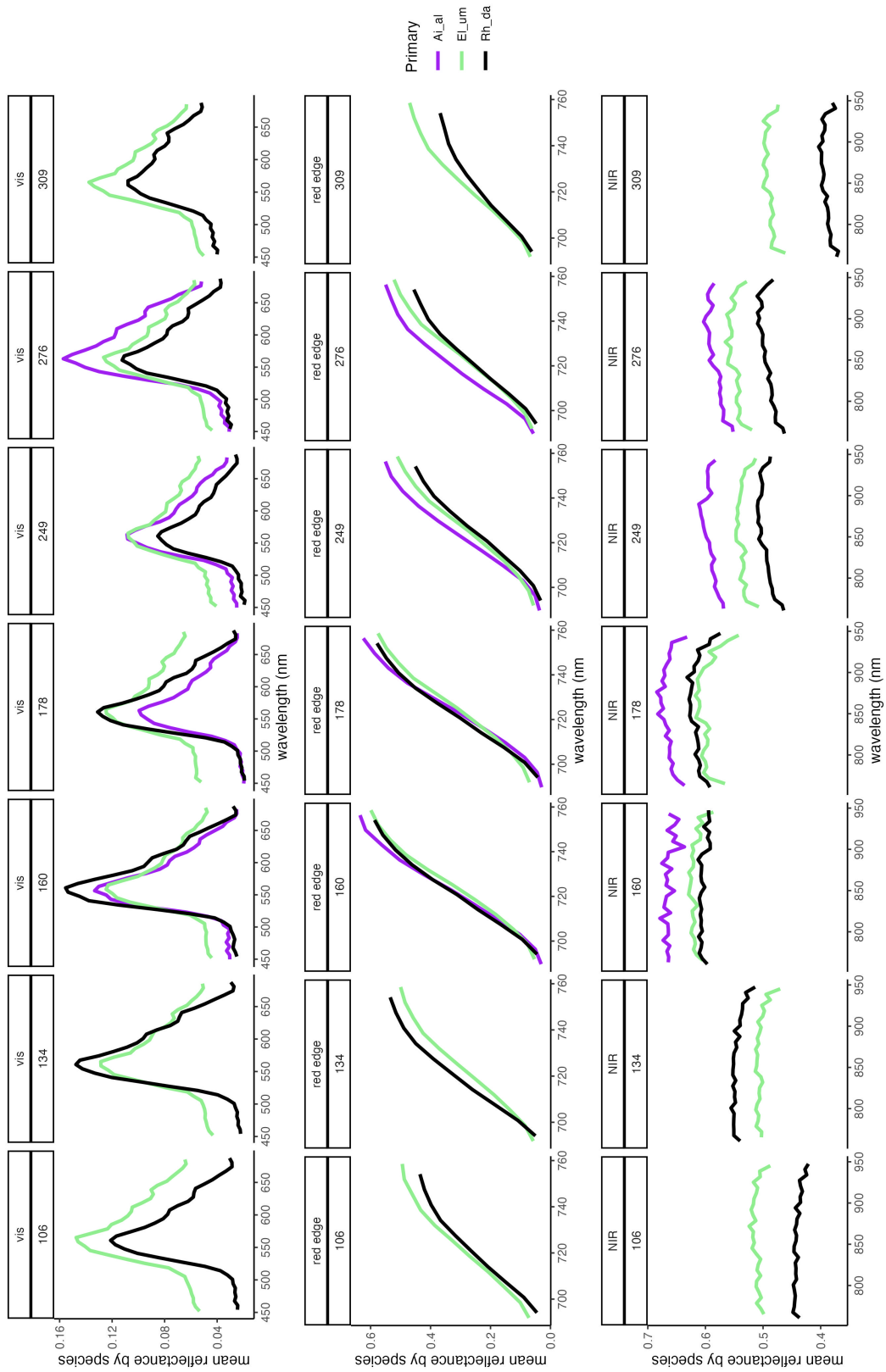


Figure 3. Full reflectance spectra of the three species of interest: *A. altissima* (Ai_al), *E. umbellata* (EL_um), and *R. davurica* (Rh_da) over the growing season. Spectra were split into visible, red edge, and NIR (seen top to bottom) regions to highlight details. From left to right, each panel is the date of data collection, beginning with early April and ending with November.

3.2 Seasonality of detection of invasive plant species of interest

3.2.1 Detecting *A. altissima*

All *A. altissima* individuals were correctly classified using PLS-DA models based on June 26 and October 2 images (DOY 178 and 276, respectively), with the greatest overall accuracy in October (91% and 100% user and producer accuracy, respectively; Table S1). Though the detection rate of *A. altissima* in late June images was 100%, the commission error (false positive) rate of the PLS-DA classification was 34%, compared to only 9% in late season images from October. The two PLS-DA components used to differentiate *A. altissima* from all other species in October images explained a total of 71% of variability in the data (63% and 8% in components 1 and 2, respectively). Reflectances in the blue, yellow-orange, and red edge spectral regions (approximately 450 to 515, 560 to 630 nm, and 700 to 720 nm) loaded heavily in the October PLS-DA classification, with positive associations with yellow-orange and red edge (i.e. greater reflectances in those regions were associated with greater classification probability) and negative associations with blue spectral regions (i.e. lower reflectances in that regions were associated with greater classification probability; Figure S2).

Reflectances in the NIR spectral region, which were greater in *A. altissima* than in the other two species of interest (Figure 3), were important (loading values > 0.05) to algorithms over the growing season, though algorithms that accentuated the contributions of NIR reflectance performed less well (e.g. early June and September). The most accurate algorithm (October) had greater contributions of several spectral regions outside of the NIR (blue, yellow-orange, and red edge). The late June algorithm, which highlighted the yellow-orange spectral region (~570-600) also had good detection accuracy (Figure 4).

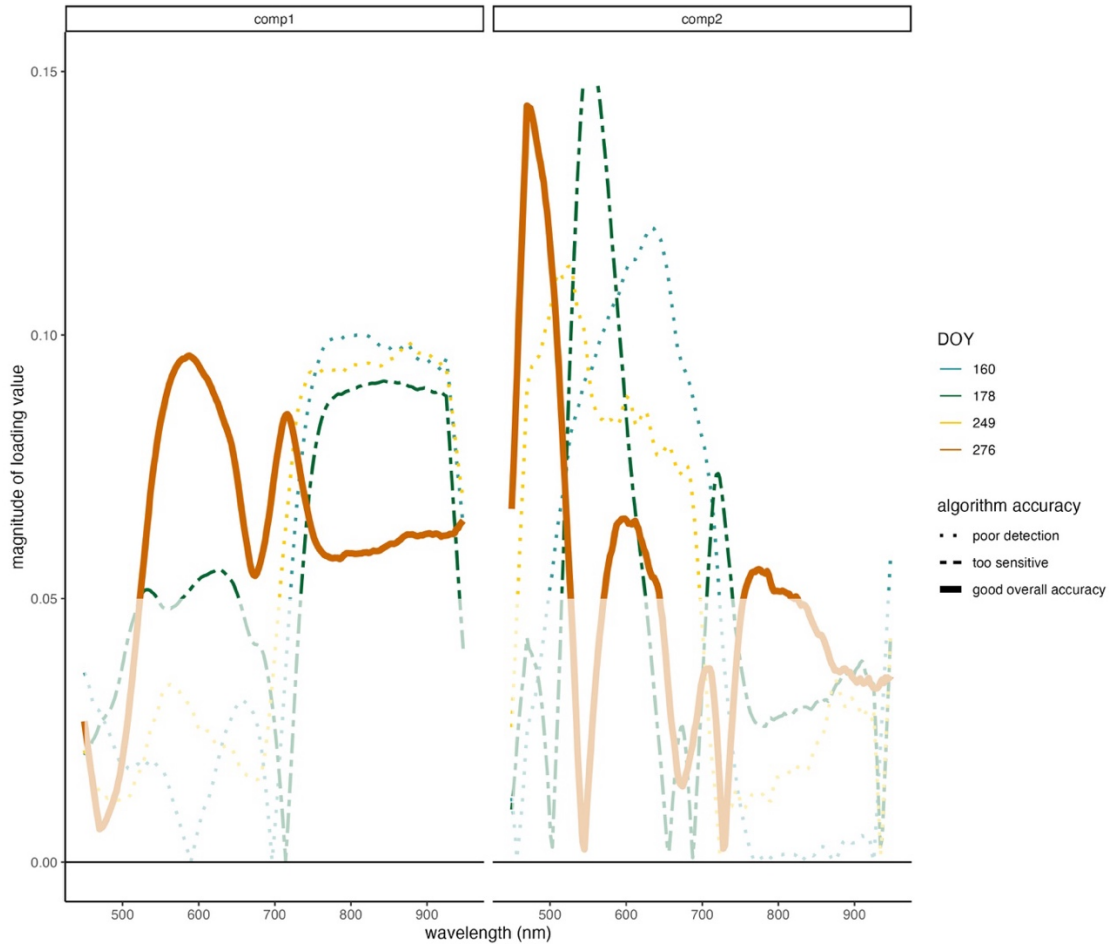


Figure 4. Magnitude of loading factors (the importance in separation) over all wavelengths for components 1 and 2 (left and right panels, respectively) in a partial least squares discriminant analysis (PLS-DA) to separate *A. altissima* from all other species over the course of its growing season. A 20 nm moving window was used to average and smooth the loading factors to remove noise and for digestibility. Wavelengths that are more important (loading values > 0.05) are in full color, while less important wavelengths are lighter in color. The prominence of each curve depicts the accuracy of each algorithm: dates with good overall accuracy (both user and producer accuracies > 75%) are solid, bold lines; dates with good detection but more than 25% false positives (labeled as “too sensitive”) are depicted with dashed lines; and dates with poor detection (< 75%) are dotted.

3.2.2 Detecting *E. umbellata*

All *E. umbellata* individuals were correctly classified using a PLS-DA based on June 8 and 26 and September 5 (DOY 160, 178, and 249, respectively) imagery, each with 100% accuracy. Its classification was also more consistently accurate than the other two species of interest, with the greatest omission error rates (indicating the lowest detection rates) seen early in the growing season (25% and 38% omission error rates on April 15 and May 13) and late in the growing season (25% omission error rate on November 4; Table S1). The two PLS-DA components used to differentiate *E. umbellata* from all other species explained a total of 72% of variability in the data (46% and 26% in components 1 and 2, respectively).

Reflectances in the blue to blue-green, green-yellow, red, and red edge (approximately 450 to 510, 530 to 585, 660 to 690, and 705 to 725 nm) loaded heavily in the late June PLS-DA classification, with positive associations with blue-green and red reflectance and negative associations with green-yellow and red edge reflectance (Figure S3). Loading values followed a similar pattern in algorithms based on adjacent sampling dates (e.g. June 8, June 26, and September 5; Figure 5). Loading value results are consistent with spectral differences, in which *E. umbellata* had greater reflectance in blue-green (450 to 525 nm) and red spectral regions than *R. davurica* and *A. altissima*, with the greatest differences among them occurring around DOY 178 (Figure 3). The PLS-DA classification algorithms generated from earlier and later in the growing season (e.g. DOY 106 and 309) to detect *E. umbellata*, which had lower classification accuracies, had notable differences from those with greater classification accuracies; for example, the more accurate detection algorithms had lower loading values in the yellow-orange spectral region in component 1 but greater loading values in component 2 (Figure 5).

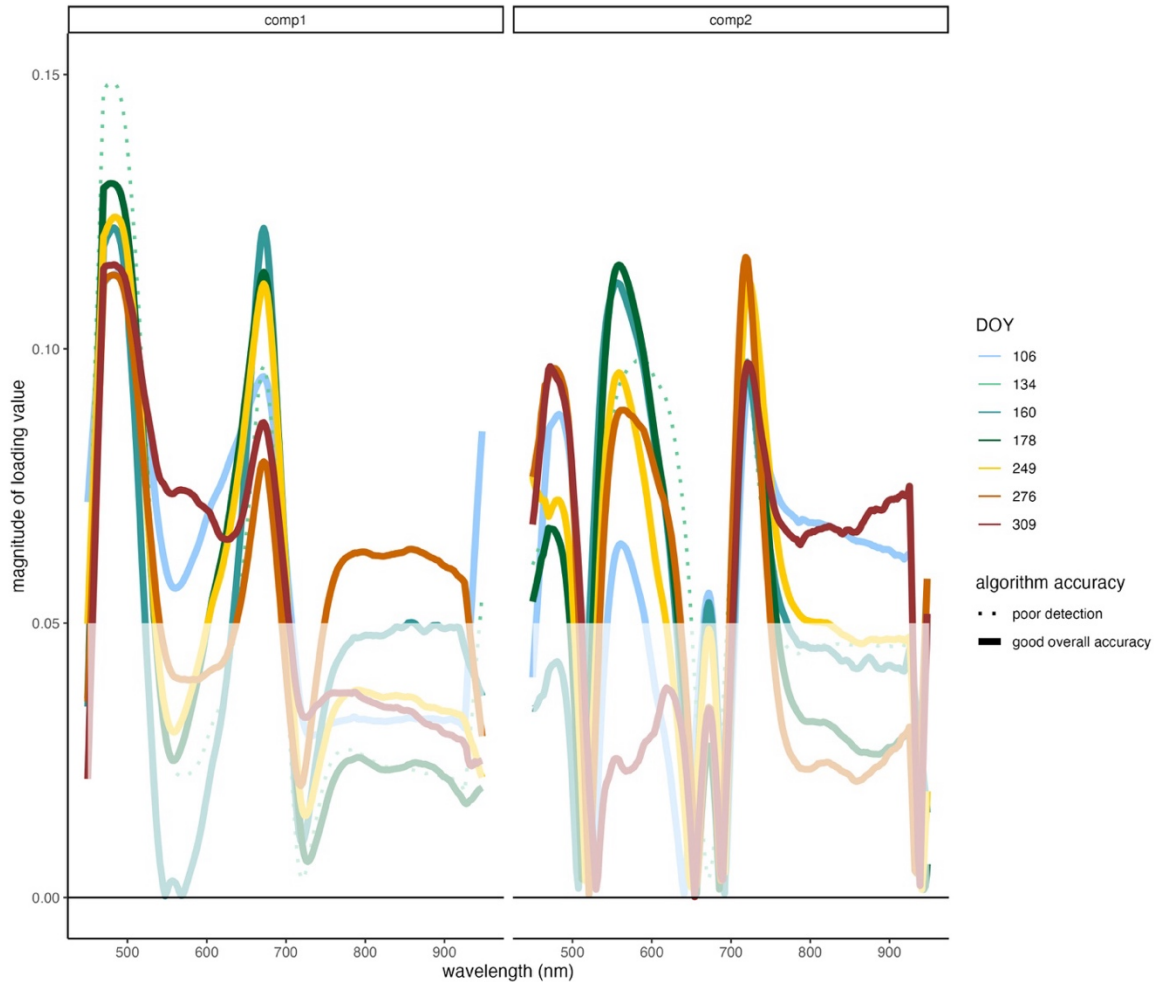


Figure 5. Magnitude of loading factors (the importance in separation) over all wavelengths for components 1 and 2 (left and right panels, respectively) in a partial least squares discriminant analysis (PLS-DA) to separate *E. umbellata* from all other species over the course of its growing season. A 20 nm moving window was used to average and smooth the loading factors to remove noise and for digestibility. Wavelengths that are more important (loading values > 0.05) are in full color, while less important wavelengths are lighter in color. The prominence of each curve depicts the accuracy of each algorithm: dates with good overall accuracy (both user and producer accuracies > 75%) are solid, bold lines; dates with good detection but more than 25% false positives (labeled as “too sensitive”) are depicted with dashed lines; and dates with poor detection (< 75%) are dotted.

3.2.3 Detecting *R. davurica*

The PLS-DA models used for each date to separate *R. davurica* from other species had the greatest accuracy mid-growing season (June 8 and 26), with 88% and 75% producer accuracies (detection rates). Algorithms from early (April and May) and late (October and November) in the growing season had low producer accuracies, ranging from 38% to 50% (Table S1). The two PLS-DA components used to differentiate *R. davurica* from all other species explained a total of 76% of variability in the data (47% and 29% in components 1 and 2, respectively).

Reflectances in the blue-green, green-yellow, red edge minimum, and NIR spectral regions (approximately 450 to 515, 540 to 580, 670 to 695, and 710 to 940 nm) loaded heavily in the early June PLS-DA, with positive relationships between probability of classification as *R. davurica* and reflectances in green-yellow and NIR, and negative relationships between probability of classification as *R. davurica* and reflectances in blue-green and red edge minimum (Figure S4). Loading values followed a similar pattern in the classification algorithm based on late June images (Figure 6). Loading value results are consistent with spectral differences (Figure 3), in which *R. davurica* had greater reflectance than *A. altissima* and *E. umbellata* at the green peak in June.

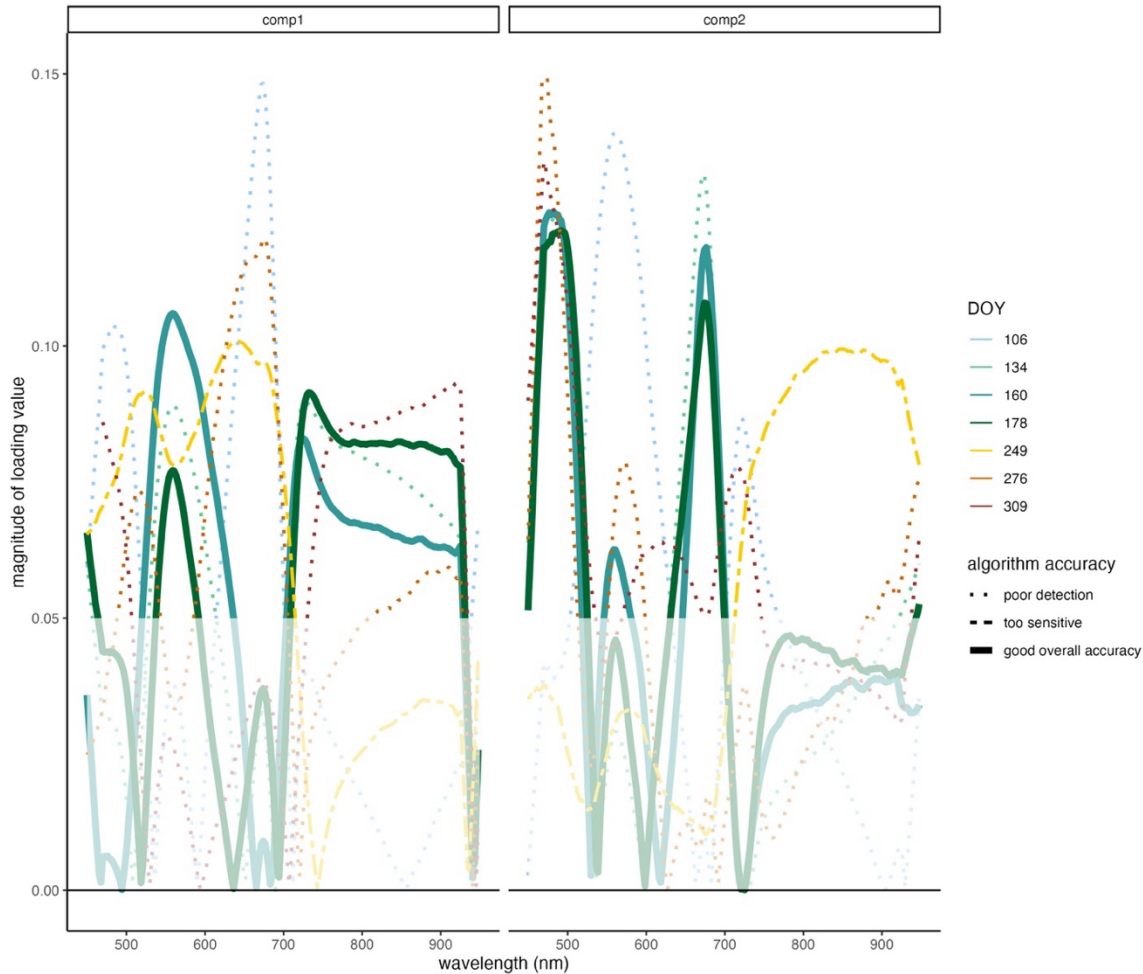


Figure 6. Magnitude of loading factors (the importance in separation) over all wavelengths for components 1 and 2 (left and right panels, respectively) in a partial least squares discriminant analysis (PLS-DA) to separate *R. davurica* from all other species over the course of its growing season. A 20 nm moving window was used to average and smooth the loading factors to remove noise and for digestibility. Wavelengths that are more important (loading values > 0.05) are in full color, while less important wavelengths are lighter in color. The prominence of each curve depicts the accuracy of each algorithm: dates with good overall accuracy (both user and producer accuracies > 75%) are solid, bold lines; dates with good detection but more than 25% false positives (labeled as “too sensitive”) are depicted with dashed lines; and dates with poor detection (< 75%) are dotted.

3.3 Consistent features used for detection

The mean rank of loading factors in detection algorithms from different points in the growing season with producer accuracies >75% (a total of 2, 6, and 3 algorithms for *A. altissima*, *E. umbellata*, and *R. davurica*, respectively) summarizes how consistently a band is important across multiple algorithms. A total of 28, 58, and 6 bands had mean ranks >180 in *A. altissima*, *E. umbellata*, and *R. davurica* detection algorithms, respectively. Of the 28 bands consistently found to be important across reasonably accurate *A. altissima* algorithms, several were in blue, yellow, and red edge spectral regions. *E. umbellata* had the greatest number of bands found to be consistently important across reasonably accurate detection algorithms, which were seen in blue, green, red, and red edge spectral regions. Only a few bands in blue-green spectral region were consistently important in accurate *R. davurica* detection algorithms.

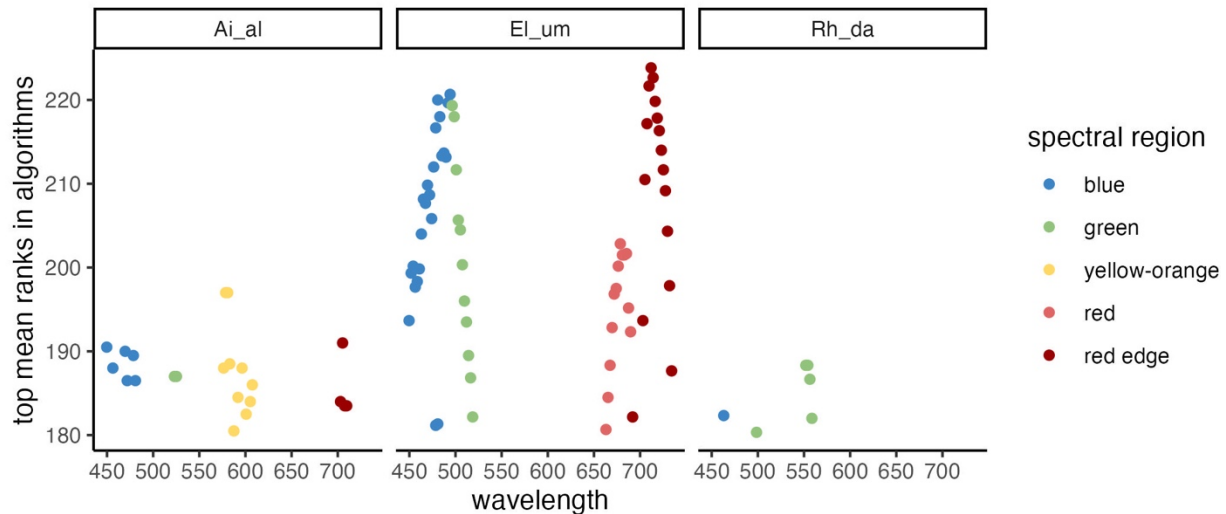


Figure 7. Mean rank of loading factors over all wavelengths from PLS-DA detection algorithms for each species of interest, *A. altissima* (Ai_al), *E. umbellata* (El_um), and *R. davurica* (Rh_da), across the 2020 growing season with good (>75%) producer (detection) accuracies.

4. Discussion

4.1 The importance of phenology in detection

Detection algorithms for *A. altissima*, *E. umbellata*, and *R. davurica* are likely driven by species-specific differences in leaf traits as well as the timing of changes in those traits over a growing season. The temporal and spectral differences seen in Figure 3 indicate not only the potential to use hyperspectral images for detection but also the importance of incorporating phenological features. Hyperspectral remote sensing studies in temperate broadleaf forests found that biochemical traits such as pigment and nutrient concentrations are associated with the visible and red edge spectral regions, while structural traits such as leaf type, LMA, and canopy structure are associated with the NIR spectral region (Hoepfner et al., 2020; Muraoka et al., 2013; J. Wang et al., 2016; Z. Wang et al., 2020; Yang et al., 2016). Thus, the spectral regions included in accurate detection algorithms likely indicate differences in traits at a given time in the growing season.

4.1.1 *A. altissima*

A. altissima, with a shorter growing season than the other two invasive plant species of interest, was best detected in June and October using the visible and red edge (450 to 515, 560 to 630, and 700 to 720 nm). Despite greater reflectances in the NIR spectral region of *A. altissima* than the other species of interest and its high loading values in detection algorithms across the growing season, the most accurate algorithms highlighted spectral regions outside of the NIR.

There is some overlap between the spectral regions I found to be important and those that others found. Burkholder et al. (2010) were able to identify *Ailanthus* using the red edge and NIR (as well as SWIR regions, which the spectrometer did not measure) from laboratory spectra in July. Aneece and Epstein (2017) also had success with classifying *Ailanthus* (75% accurate identification) using a handheld field spectrometer and found that bands in the ranges of 500-549

nm and 700-749 nm were important for differentiation. Though the visible and red edge spectral regions were found to be important across studies, the importance of NIR in detection was not shared. This could be due to differences in platforms and therefore differences in viewing angle (in the case of handheld field spectrometer) or the incorporation of canopy architecture features (in the case of laboratory spectra).

These results illustrate the importance of leaf characteristics in differentiating *A. altissima* from a variety of native and nonnative plants during the mid- and late-growing season, however, leaf characteristics were not consistently important. *A. altissima* had only 28 bands (out of 90 possible) with mean ranks over 180 from the two algorithms with decent detection accuracies (June 8 and October 2), which indicates a lack of consistency. More importantly, these results illustrate the benefit of including dates outside of peak greenness in data collection and algorithm generation to incorporate species-specific phenological traits.

Because female *A. altissima* trees are prolific seed producers, seed pods are highly visible in images due to their clumped nature. The fine resolution images allowed for a focus on foliar spectral signals with little to no interference from seed pods, however, coarser scale imagery may contain mixed pixels of foliage and seed pods, which will impact spectral signals. While the addition of the spectral signal from seed pods may improve differentiation, it is also possible it would hinder accuracy due to the phenology and variability of seed pod characteristics.

4.1.2 *Elaeagnus umbellata*

E. umbellata was detected with accuracies of at least 60% over the entire growing season, with 100% accuracy mid-growing season using the visible and red edge spectral regions (450 to 510, 530 to 585, 660 to 690, and 705 to 725 nm). The main driver appeared to be greater reflectances in blue to blue-green (450 to 510) and red (660 to 690) wavelengths than other species.

Because chlorophyll b creates an absorbance feature near 450 nm, the greater blue reflectances and their importance in *E. umbellata* detection suggests lower chlorophyll b as a driver. Other species in the *Elaeagnus* genus had 45% higher concentrations of foliar chlorophyll a than chlorophyll b, which supports this finding (Carradori et al., 2020). The addition of reflectances in green-yellow (530 to 585 nm) and red edge (705 to 725 nm) in detection algorithms imply that foliar carotenoid concentration (with a maximum absorbance feature near 560 nm) and foliar N content are also important in *E. umbellata* detection in summer months.

E. umbellata had the greatest number of bands (58 out of 90 possible) found to be consistently important across its six reasonably accurate detection algorithms. The spectral regions that were consistently important were blue, green, red, and red edge spectral regions. This indicates that timing may be less important for its detection, as the traits that allow for differentiation (pigments and nutrients) appear to be consistently different from other species over the growing season.

4.1.3 *Rhamnus davurica*

R. davurica was best detected mid-growing season using the visible and red edge spectral regions (450 to 515, 540 to 580, 670 to 695, and 710 to 940 nm), suggesting that both biochemical and structural traits are important to differentiating *R. davurica* at this time. The importance of NIR is consistent with the spectral range (900 to 999 nm) that Aneece and Epstein (2017) found most useful for differentiating *R. davurica* from other species using laboratory foliar spectra. The visible and red edge spectral regions were not found to be important in that study, possibly due to differences in platforms. *R. davurica* had only 6 bands (out of 90 possible) with mean ranks over 180 from the two algorithms with decent detection accuracies, which indicates the greatest lack of consistency in differentiating spectral features across the growing season.

The low accuracies early and late in the growing season could be due to intraspecific foliar variability during leaf out and senescence. It is also possible that berry production late in the season on female plants is causing spectral differences among individuals, as *R. davurica* is a prolific producer of berries, which would impact the spectral signal.

4.2 Conclusions and Implications

The first two goals of this study were to determine when in the growing season *A. altissima*, *E. umbellata*, and *R. davurica* are most differentiable from other species in fine-scale hyperspectral imagery collected by UAV and which spectral features enabled their detection. Overall, *A. altissima*, *E. umbellata*, and *R. davurica* could be accurately detected in June. The detection algorithms for all three species of interest in June shared importance of blue-green, green-yellow, and red edge spectral regions (450 to 510, 560 to 580, and 710 to 720 nm), but each had additional important bands. In addition to detection in June, *A. altissima* was most accurately detected in early October, with fewer false positives. The yellow-orange spectral region was key to detection in June, and in October the yellow-orange spectral region was again important, in addition to the blue and red edge spectral regions. *E. umbellata* was most accurately detected in early and late June and September with 100% accuracy. Reflectances in the blue to blue-green, green-yellow, red, and red edge were important to the accurate detection of individuals. *R. davurica* was most accurately detected in both early and late June, and reflectances in the blue-green, green-yellow, red edge minimum, and NIR spectral regions were important.

These results illustrate the usefulness of flexible sampling time, which incorporates phenological features into detection algorithms. For times when accuracy of detection is high (resulting in few false positives and negatives), such as June, single classification results can be

used independently with good results, however, the flexible sampling and multi-month nature of the drone-based dataset has the potential to improve accuracy by combining classifications across times. For example, classification in October could be used to complement results for *A. altissima* but not *E. umbellata* or *R. davurica*.

My third goal was to determine how consistently spectral features allowed for detection across the growing season to elucidate the temporal flexibility of detection in this setting. The blue, yellow, and red edge spectral regions were consistently important to *A. altissima* detection. *E. umbellata* had the greatest number of bands found to be consistently important across reasonably accurate detection algorithms, which were in blue, green, red, and red edge spectral regions. Only a few bands in blue-green spectral region were consistently important in accurate *R. davurica* detection algorithms. The lack of consistency in algorithms across the growing season for *A. altissima* and *R. davurica* suggests that *in situ* or date-specific detection algorithms may be more useful than a standard algorithm across the entire growing season, though a standard algorithm may be applicable for *E. umbellata* detection.

These results demonstrate that UAV hyperspectral imagery can be a useful tool in detecting and monitoring ecosystems invaded by *A. altissima*, *R. davurica*, and *E. umbellata*. These species are not only issues in Virginia, but across the U.S. Rather than attempting to classify all three species in concert with one another, I chose to detect each species of interest individually to create robust and more widely applicable algorithms that can be used in vegetation communities that do not necessarily include all three species.

These methods can also be extended to other regions, ecosystems, and species. A large portion of natural resource management budgets are consumed by invasive species detection and control programs, for which there is high demand for technological innovations that increase

efficiency and reduce cost (Kirk et al., 2019; Martinez et al., 2020). Drone-based hyperspectral images can provide information about how much and where invasive plants have established in communities, including new occurrences and non-dominant populations. In cases where multi-year data collection is possible, information on the rate of expansion of invasion can increase the usefulness of this UAV-based approach. These results demonstrate the potential usefulness of this tool for land managers and communities to prioritize invasive plant species management approaches.

These methods can also be used to improve understanding of the ecological impact of invasive plants on vegetation communities, as high-resolution monitoring is key to assessing dynamics of modern-day ecosystems experiencing climate change and drastic biodiversity changes (Besson et al., 2022). Hyperspectral remote sensing provides the foundation to not only determine species composition of plant communities but also their structure and function (Dietze et al., 2018; Petchey et al., 2015).

There are potentially broad-reaching benefits, including expanding the techniques to larger spatial extents, which would enhance regional strategies for invasive plant management far beyond what can be done with ground surveys alone. Successful applications using hyperspectral data collected by the National Ecological Observatory Network's Airborne Observation Platform would increase spatial extent. Satellite sensors such as the ESA EnMap and NASA's Surface Biology and Geology (SBG), which have potentially challenging coarser resolutions but the added benefit of frequent observations, can allow users to incorporate phenology into detection. Both the methodology and results of this study have important implications for ecology and environmental sciences, forest and park management, and individual landowners managing invasive species on their properties.

Chapter 3: Scaling fine-resolution drone-based hyperspectral algorithms to the landscape scale: A case study in invasive plant species detection

Abstract

Reducing the spread of invasive plants to minimize their ecological impacts requires extensive ecosystem monitoring. Different approaches to monitoring, from field-based to remote sensing observations, have trade-offs in terms of the details provided, spatial extent, and frequency of visits that can be accomplished. Because of these trade-offs, different approaches may be better suited for different applications, and different approaches may be able to complement each other.

With the aim of assessing interoperability and scalability between platforms with different spatial resolutions, as well as the interannual variability in detection algorithms, I assessed how well a variety of detection algorithms could detect three invasive species of interest, *Ailanthus altissima*, *Elaeagnus umbellata*, and *Rhamnus davurica* in four years of aerial images in heterogeneous fields in northwestern Virginia. Detection algorithms were created for each species of interest based on three different training datasets, 1) reflectances from very fine (~3 cm) resolution and 2) coarser (~1 m) resolution drone images collected in 2020, and 3) reflectances from 1 m resolution fixed-wing aircraft images collected in a single year by the National Ecological Observatory Network (NEON) in the same locations but across different years. Each training dataset was then applied to each year's NEON image to assess accuracy of each approach. Both drone-based and NEON-based

approaches accurately detected each species of interest, with greater accuracy from NEON-based algorithms, as they eliminated temporal and scale differences among platforms. Transforming and resampling both increased the number of important spectral regions in detection algorithms, though neither guaranteed an increase in detection accuracy. Spectral features important to the accurate detection of *A. altissima* were consistent within each platform but not across platforms, which suggests that its spectral features are not universal across time and/or space. Spectral features key to the accurate detection *E. umbellata* were inconsistent, which suggested that they are resolution dependent. *R. davurica* had the most consistency in features that allowed for its detection at every level, although the features changed, which suggests at least some variability associated with time and space. This analysis of the inconsistencies across detection algorithms, however, also elucidates the importance of considering time and space, not only in the detection of invasive plant species, but also in answering ecological questions.

1. Introduction

Reducing the spread of invasive plant species and minimizing their impacts on biodiversity is a high conservation priority. Understanding where invasions are under way requires extensive ecosystem monitoring, for which there are several viable approaches, however, each has caveats (Table 1). Satellite- and ground-based observations have traditionally been used for ecosystem monitoring. Satellite imagery provides information with large spatial extents but often with resolutions greater than the size of individual plants (Pettorelli et al., 2018). Ground-based observations can be used to detect individual plants, but the time and energy required for surveys make this approach cost-prohibitive for large spatial extents (Kays et al., 2015; Pimm et al., 2015). Fixed-wing aircrafts have also been used to survey landscapes to detect invasive plant species (Gregory P. Asner et al., 2008). Because of the proximity to the ground, this approach to monitoring provides finer resolution than satellites, often fine enough to detect individual plants. This approach, however, is also cost-prohibitive (Giordan et al., 2018). Unoccupied aerial vehicles (UAVs) or drones have become increasingly accessible to users as an additional approach to ecosystem monitoring (Sun & Scanlon, 2019). They provide very fine spatial resolution, high continuous coverage within the spatial extent, and are affordable and flexible to operate (Alvarez-Vanhard et al., 2021). The high spatial resolution, at which spectral variability does not impede the detection of invasive plants (Huelsman et al., 2023), facilitates the detection of plants early in an invasion, increasing the possibility for mitigation of impacts (Reaser et al., 2020). Despite the benefits of high spatial resolution, it often means a lower spatial extent, which may not be ideal for mapping and monitoring invasive plants at the landscape scale (Royimani et al., 2018).

Table 1. A comparison of the strengths and limitations of four common approaches to ecosystem observation: satellite, ground surveys, fixed-wing aircraft, and drone (UAV). Spatial resolution (pixel size), level of continuous coverage within the spatial extent, spatial extent, and capacity for repeat visits are all considered.

	Spatial resolution	Continuous coverage	Spatial extent	Cost to researchers	Capacity for repeat visits
Satellite	Low	High	High (global)	Low	High
Ground surveys	High	Low	Low (local)	High	Low
Fixed-wing aircraft	Intermediate	High	Intermediate (regional landscape)	High	Low
Drone	High	High	Low (local)	Low	High

Spectroscopy, or hyperspectral imaging, can be used in concert with these approaches. Hyperspectral imaging includes reflectance information from many adjacent and narrow (< 10 nm in width) bands (Chance et al., 2016; Kaufmann et al., 2008). It provides spectral information driven by the biochemical and structural traits of plants (Matongera et al., 2016; Z. Wang et al., 2020; Yang et al., 2016). Pigments, proteins, and structural molecules interact with light and impact spectra (Homolova et al., 2013). Thus, an “electromagnetic signature” provides information on a variety of functional and plant structural traits (Gregory P. Asner et al., 2015; Hill et al., 2019; Homolova et al., 2013). Because traits vary across plant species, individual species exhibit different spectra, which allows for species differentiation using spectroscopy (M. Clark et al., 2005; Cochrane, 2000). Plant species with different evolutionary histories will differ more greatly in traits (and therefore spectra), which supports the differentiation of invasive plants from native plants.

Drone-based spectroscopy has been used to successfully detect invasive plant species in plant communities (e.g. Diruit et al., 2022; Dmitriev et al., 2022; Gao et al., 2023; Papp et al., 2021; Sabat-Tomala et al., 2020). In drone-based images, pixels can be about the size of a leaf (on the scale of a few cm, e.g., Huelsman et al. 2023), meaning they are “purer” (providing information about a single object) than coarser pixels. Thus, the fine resolution of this approach benefits the detection of invasive plants. This approach is also affordable to repeatedly operate, further supporting its use in invasive plant detection efforts (Singh et al., 2024). The limited spatial extent of UAV-based observation, however, suggests an intermediate spatial resolution (i.e., via fixed-wing aircraft platforms) may improve monitoring efforts at the landscape scale.

Within a single species, however, traits can vary across space and time, which can impact spectra (Ustin & Gamon, 2010). Additionally, linking canopy spectra to biochemical and structural traits is not as straightforward as doing so using spectra collected in an ideal laboratory setting (i.e., perpendicular to a single leaf in a controlled light environment). Scaling to the canopy level incorporates not only biochemical traits into spectra but also canopy structural traits and solar illumination (Gregory P. Asner, 1998) (also Goel 1988). Additionally, the spectral signals driven by leaf-level trait differences are amplified at the canopy level by 3D canopy architecture (Horn, 1971, 1975). Although viewing angle, canopy geometry, and scale all impact spectra, hyperspectral signatures are linked with biochemical pigments at both leaf level and canopy level (Ewald et al., 2018; Zarco-Tejada et al., 2004), supporting the use of aerial remote sensing for invasive plant species detection.

Hyperspectral sensors on fixed-wing aircraft platforms such as NASA's Airborne Visible/InfraRed Imaging Spectrometer (AVIRIS), the Global Airborne Observatory (GAO; formerly Carnegie AO), and the National Ecological Network's (NEON) Airborne Observatory

Platform (AOP) provide opportunities for regional invasive plant detection and monitoring. The coarser spatial resolution of images collected by fixed-wing aircraft (on the scale of meter(s), e.g. Marconi et al., 2022), however, results in pixels about the size of a branch or even an entire canopy. Branch-sized pixels are “mixed,” incorporating the spectral signatures of multiple leaves in addition to shadows in the canopy (Ewald et al., 2018; Zarco-Tejada et al., 2004). Despite the potential impacts of mixed pixels on detection, others have used hyperspectral images with moderate spatial resolutions to detect general assemblages of plants (Hochberg et al., 2015; Sanchez-Azofeifa et al., 2013; Schmidt & Skidmore, 2003).

The extent of monitoring required for the regional detection and management of invasive plant species suggests the utilization of imagery with intermediate spatial resolution. Operating regional-scale platforms (e.g. fixed-wing aircrafts) is more costly and inflexible than operating a drone. A potential option for detection and management applications may combine both approaches: fine-scale drone-based imagery that is flexible and affordable to collect can be used to generate detection algorithms, and those algorithms can be applied to coarser-scale imagery with greater spatial extents. This scaling approach is theoretically possible; UAV survey data have been successfully scaled up and applied to 30 m resolution Landsat data to determine percent cover of plants (He et al., 2021). However, the spectral variability of individual species over space and time, in addition to scale-based spectral differences, may impede detection.

I evaluate the effectiveness of this combined fine- and intermediate-resolution approach to invasive plant species detection by answering the following questions:

1. How do mean spectral signatures of species differ in images collected by drone and by fixed-wing aircraft?

2. To what extent can detection algorithms created using fine-resolution drone imagery be used to accurately detect invasive plants species in coarser resolution images collected by the NEON AOP?
3. To what extent can detection algorithms created using NEON AOP imagery be used to accurately detect invasive plants species within the same images?
4. What features are used in each algorithm, and how do they differ with respect to detection accuracy?

2. Methods

2.1 Study site and aerial image data collection

Aerial hyperspectral images were collected by fixed-wing aircraft and UAV at Blandy Experimental Farm (BEF) in northwestern Virginia, United States (39.06°N, 78.07°W). NEON collects data on a near-annual basis during times with at least 90% maximum greenness using their AOP, weather and logistics permitting. Peak greenness on average at BEF occurs on DOY 150 (approx.. late May or early June). Images collected by NEON's AOP were available for 2016, 2017, 2019, and 2021. Drone-based images were collected using a DJI Matrice 600 Pro equipped with a Headwall HyperSpec imaging spectrometer (Nano-Hyperspec, Headwall Photonics, Bolton, MA) on June 26, 2020 (DOY 178) to approximate the date of NEON's AOP data collection.

NEON corrects their reflectance data for atmospheric and illumination effects caused by solar angle and atmospheric conditions using Atmospheric and Topographic Correction (ATCOR) and provides 1 km² stitched tile images that have been orthorectified to a UTM projection, with 1 m spatial resolution.

2.2 Image sampling

Reflectances from 149 individuals of 15 different species, genera, or plant type across trees, shrubs, forbs, and graminoids (*A. altissima*, *E. umbellata*, *Gleditsia triacanthos*, *Galium verum*, *Maclura pomifera*, *Juglans nigra*, *Juniperus virginiana*, *Lonicera japonica*, *Lonicera maackii*, *Pinus virginiana*, *Rhamnus davurica*, *Rubus spp.*, *Solidago altissima*, *Symphoricarpos orbiculatus*, and graminoids) were extracted from drone images. Spectral data cubes were downloaded from NEON’s Application Programming Interface using the neonUtilities R package (Lunch et al., 2024) for locations that overlapped with areas where drone data were collected at BEF. Reflectance data were extracted from data cubes using the rhdf5 R package (Fischer et al., 2023). Non-vegetation and shadow pixels were removed from the images (51% of pixels). To reduce computing requirements, locations of 79 individual tree and shrub canopies, were extracted from each image, which would later be used to assess accuracy. Each canopy was approximated based on plant size (trees and shrubs with canopies of ~5 m and ~3 m diameters, respectively). Canopy sizes translated to polygons with 9 or 25 pixels centered on the coordinates of each individual location (Table 2).

Table 2. Species identities of the 79 individual tree and shrub canopies considered in algorithm development and classification, including the number of each, the estimated size of each canopy, and number of pixels considered and extracted from NEON images.

Species	Number of individuals	Simulated canopy diameter (m)	Number of pixels in a canopy
<i>Ailanthus altissima</i>	9	5	25

<i>Elaeagnus umbellata</i>	9	3	9
<i>Rhamnus davurica</i>	10	3	9
<i>Gleditsia triacanthos</i>	9	5	25
<i>Juglans nigra</i>	9	5	25
<i>Juniperus virginiana</i>	7	5	25
<i>Lonicera maackii</i>	10	3	9
<i>Maclura pomifera</i>	11	5	25

2.3 Harmonizing and comparing data from different platforms

Spectra sampled from NEON images were restricted to bands in the VNIR and resampled to match bands of drone-based data using the `prospectr` R package (Stevens & Ramirez-Lopez, 2022). Because NEON imagery has coarser spatial resolution than the drone-based imagery (1 m compared to ~3 cm), spectral signatures were also extracted from drone images in ENVI using 25 x 25 pixel squares to better match NEON’s coarser spatial resolution. Up to three squares were sampled from each canopy to serve as replicates.

In addition to adjusting methods to harmonize the spatial and spectral resolution of the two platforms, all data were transformed with a convex hull continuum removal using the `prospectr` R package. Convex hull continuum removal is a common transformation applied to remotely sensed data to eliminate lighting effects. The approach creates a convex hull around a spectral signature by connecting local maxima with interpolated line segments, then normalizes the spectral signature relative to the convex hull (Stevens & Ramirez-Lopez, 2022). To evaluate the spectral similarities of the two platforms, the difference in reflectance of each band between the two platforms was

calculated. Spectral regions that differed least, with at least 75% of bands differing less than 0.01 in at least two different years, were noted.

2.4 Algorithm development and accuracy assessment

Algorithms to detect each species of interest (*A. altissima*, *E. umbellata*, and *R. davurica*) were created by applying a two-component Partial Least Squares Discriminant Analysis (PLS-DA) to the drone-based data. Algorithms were developed using both the original, untransformed reflectances as well as a convex hull continuum removal-transformed version of both fine- and coarse-scale data, for a total of four approaches for each species of interest. Appropriate models (untransformed and transformed, respectively) were then applied to untransformed and transformed pixels extracted from each NEON image (2016, 2017, 2019, and 2021).

Each model provided a classification for each PLS-DA component for each pixel in NEON images. This provided an opportunity to consider two approaches to pixel and canopy classification with different levels of “strictness.” A more lenient algorithm would allow a pixel to be classified as the species of interest with classification in only one PLS-DA component, whereas a stricter algorithm would require a pixel to be classified as the species of interest with classification in both components. Once pixels were classified at either level of strictness, canopies would also be classified. A more lenient canopy classification approach would allow a canopy to be classified as the species of interest with a minimum of two pixels, whereas a stricter approach would require a majority (>50%) of pixels to be classified as the species of interest (Table 3). Each approach to detection strictness was used to evaluate the accuracy of each classification model for each species of interest, as the detection of each species of interest may benefit from different approaches. The combination of two different resolutions of drone images, two transformations, four years of

NEON data, and four strictness levels resulted in the evaluation of 64 different approaches for each species of interest.

Table 3: The four categories of “strictness of detection” (most lenient, moderately lenient, moderately strict, and most strict) were based on the number of components (“components”) required in a PLS-DA for classification of a single pixel and the number of pixels required in a canopy for classification (“pixels”).

Components	Pixels	Strictness of detection
1	1 or more	Most lenient
1	Majority of pixels in canopy	Moderately lenient
2	1 or more	Moderately strict
2	Majority of pixels in canopy	Most strict

In addition to creating algorithms using reflectances in drone images, algorithms were also created using NEON images to detect each species of interest in each NEON image. A randomly selected 30% subset of untransformed and transformed data from each image was used to train each algorithm by applying a two-component PLS-DA. Each algorithm was then applied to the remaining 70% of data to evaluate the accuracy, using the same levels of strictness. The combination of two transformations, four years of NEON data, and four strictness levels resulted in evaluation of 32 different approaches for each species of interest. Last, the classification of each canopy was compared to its ground-truthed identity for each of the 79 individuals, allowing for the calculation of accuracy statistics for each of the 64 drone-based algorithms and 32 NEON-based algorithms: user and producer accuracy, commission and omission error.

2.5 Assessment of spectral features

The various PLS-DA models not only serve to differentiate each species of interest from other species, but they also determine what spectral features are important in their differentiation across time and scale. Wavelengths that loaded heavily (those with greater magnitude) were most important in differentiating a species of interest from the others (Liland et al., 2022). Though PLS-DA is prone to overfitting (i.e. a model can misinterpret noise as relevant information), the classification accuracy of each PLS-DA model approximates model goodness. Therefore, key spectral regions in algorithms with both user and producer accuracies >50% were examined to assess the importance of spectral features for different platforms, scales, and time.

Loading values of accurate algorithms were ranked by band for each component, and ranks >180 (out of 225 bands) were selected to focus on bands within the top 20% of loading values. For each species of interest, loading value ranks were averaged across all accurate detection algorithms and within each platform for each species of interest. This was done to evaluate the importance of time, platform, and resolution in species detection. Similarities across all accurate algorithms would indicate that spectral signals key to the detection of a species are consistent across time and space, and that algorithms are more likely to be applicable across time (e.g. across growing seasons) and space (e.g. resolution and viewing angle). Within drone-based algorithms, only those that used reflectances from both original fine-resolution drone images and those resampled to a coarser resolution were compared. Similarities across different resolutions within drone-based algorithms would suggest that differentiating spectral features are not resolution-dependent. Similarities across NEON-based algorithms would suggest that spectral features are not time-dependent.

3. Results

3.1 Spectral differences between platforms

3.1.1 Original drone data vs. NEON data

Reflectances in fine-scale drone images were most consistently similar (across multiple years) to NEON images in the untransformed data. Across all eight species, reflectances in images from the two platforms were most consistently similar in spectral regions associated with chlorophyll absorption (blue and red). Reflectances of *A. altissima* and *R. davurica* were most consistently similar in images from the two platforms in the blue spectral region. Reflectances of *E. umbellata* were not consistently similar in any spectral regions between fine-scale drone images and NEON images. The greatest differences in reflectance of all eight species, *A. altissima*, *E. umbellata*, and *R. davurica* in fine-scale drone images and NEON images occurred in the red edge minimum and high NIR spectral regions. Transforming reflectances increased the number of spectral regions that differed most between the two platforms to include green (all 8 species, and *R. davurica*) and blue (all 8 species, *A. altissima*) in addition to the red edge minimum and high NIR (Figure 1).

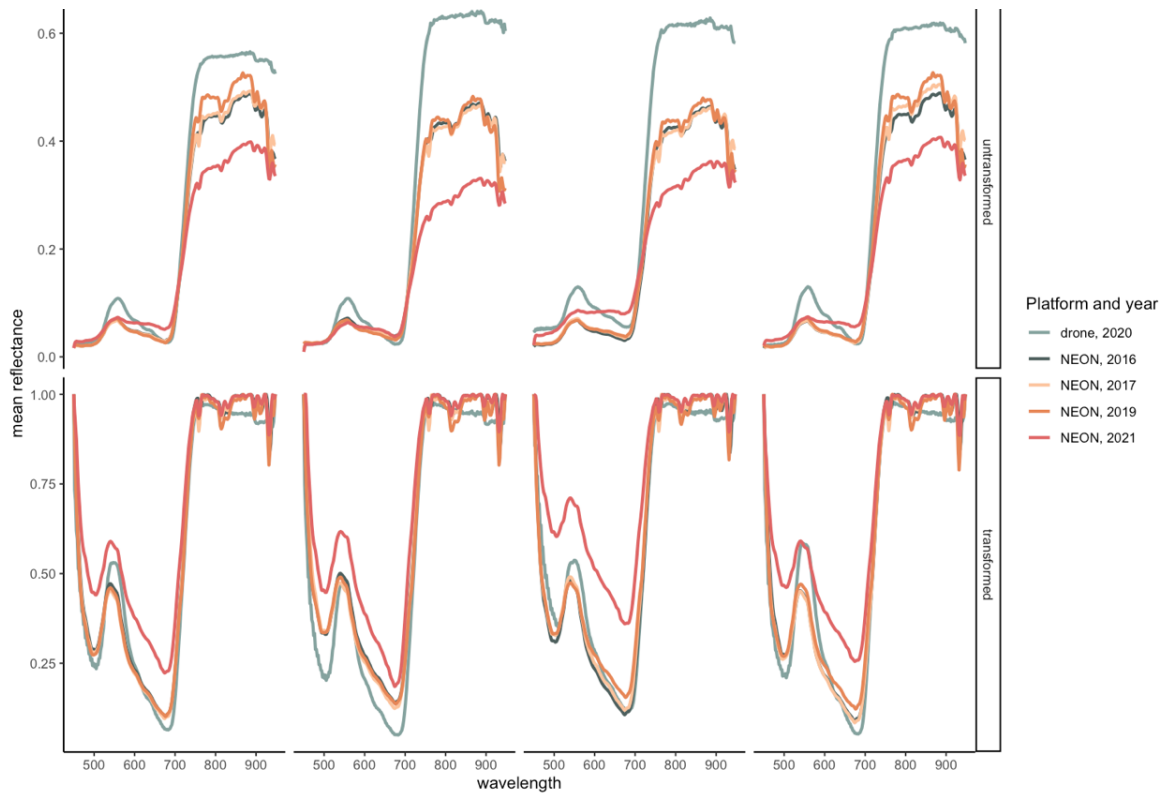


Figure 1. A) Mean reflectances of original, fine-scale drone data and NEON data. Columns left to right include all species in images, *A. altissima*, *E. umbellata*, and *R. davurica*, and rows top to bottom are for untransformed and transformed data.

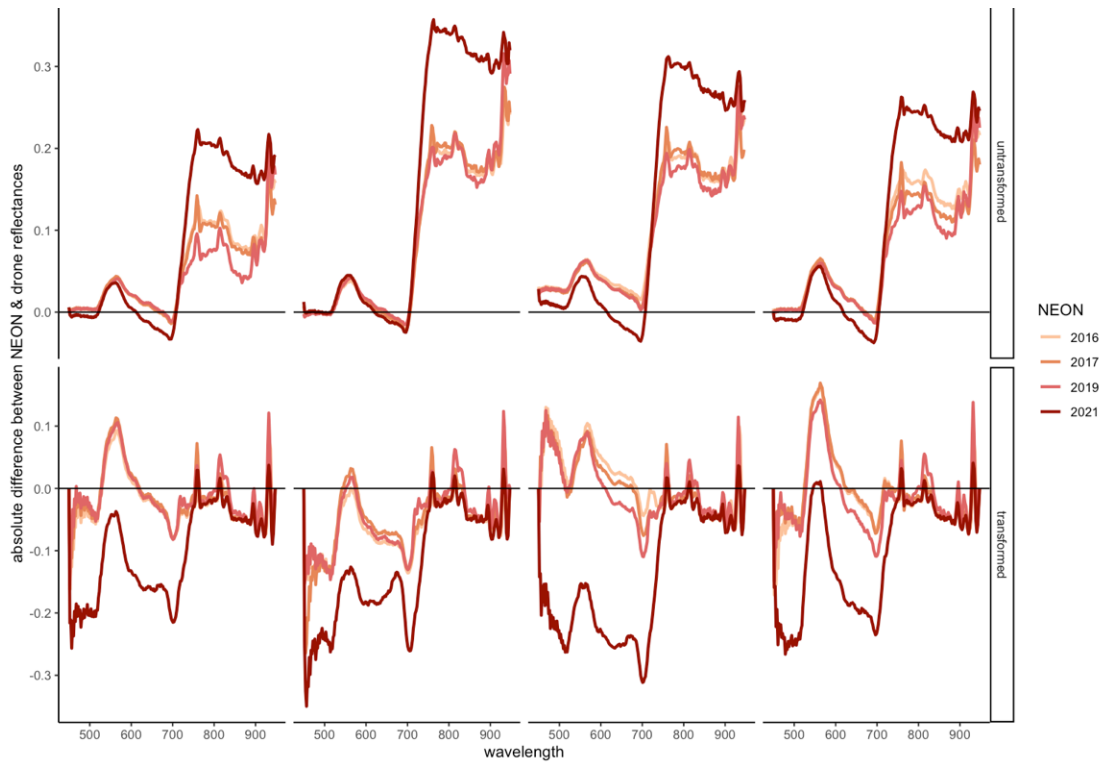


Figure 1.B) Mean differences between reflectances in original, fine-scale drone and NEON images. Columns left to right include all species in images, *A. altissima*, *E. umbellata*, and *R. davurica*, and rows top to bottom are for untransformed and transformed data.

3.1.2 Resampled drone data vs. NEON data

As in the fine-scale drone images, reflectances in resampled, coarser-resolution drone images were most consistently similar to NEON images (across multiple years) in untransformed data. Because resampling to a coarser resolution creates pixels that included shadows, the number of spectral regions with similar reflectances across platforms increased when drone images were resampled (Figure 2A).

Across all eight species, reflectances in images from the two platforms were most consistently similar in blue, green, yellow, and orange spectral regions (rather than just blue and red for the finer-scale data). Resampling drone data to a coarser resolution changed reflectances in the blue and red spectral regions in *E. umbellata* and *R. davurica* more than they did in *A. altissima*, whereas resampling changed reflectances in the green more in *A. altissima* (Figure 2A). Reflectances of *A. altissima* were more similar in coarser-scale drone and NEON images in the green, yellow, and orange spectral regions; *E. umbellata* in the blue, orange, and red spectral regions; and *R. davurica* in the blue, orange, red, and low NIR spectral regions. The greatest differences in reflectances of all eight species, *A. altissima*, *E. umbellata*, and *R. davurica* in coarser-scale drone images and NEON images occurred in the red edge minimum and high NIR spectral regions, as they did in fine-scale drone images. Transforming reflectances increased the differences between reflectances of the two platforms in the blue spectral region. Transformed reflectances of *E. umbellata* differed most in the red edge minimum rather than the blue spectral region (Figure 2).

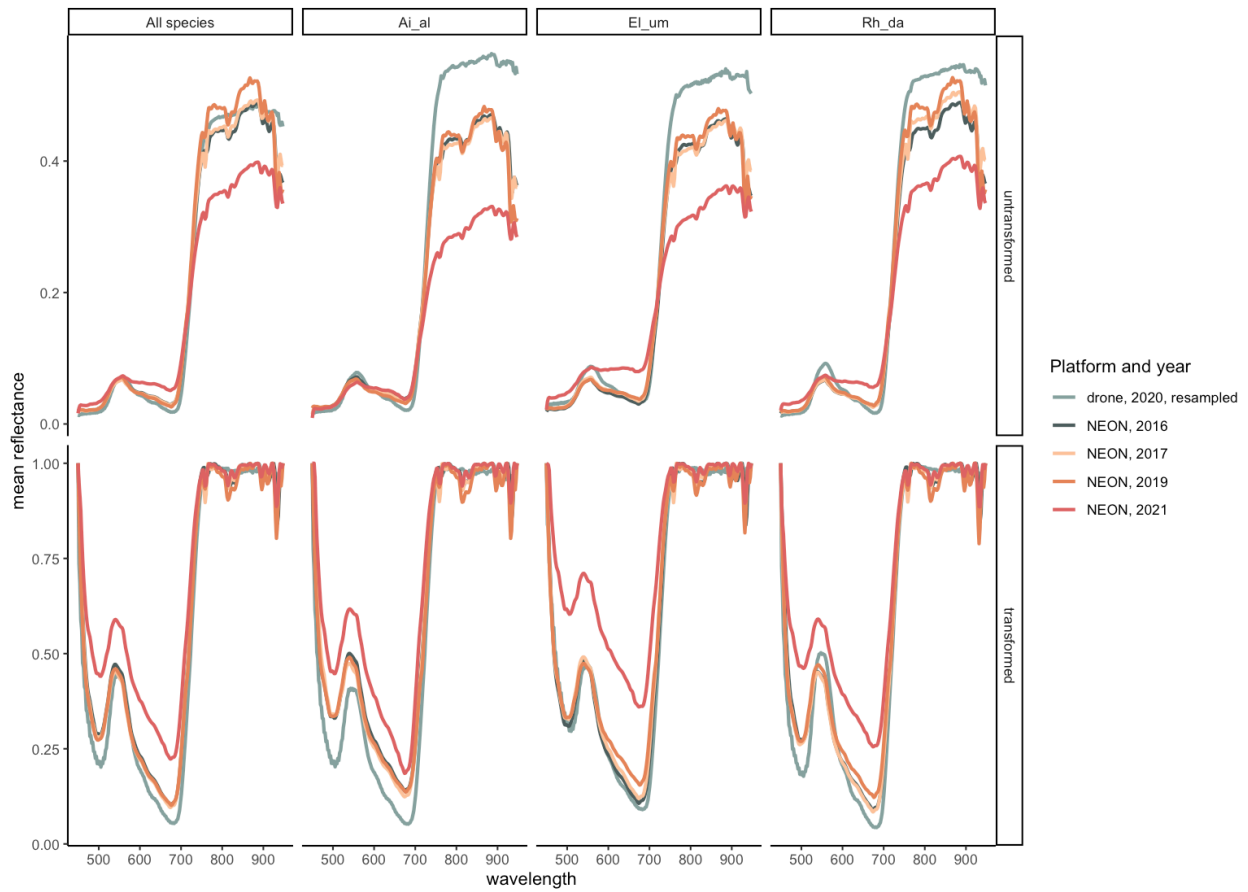


Figure 2. A) Mean reflectances of resampled, coarser-scale drone data and NEON data and B) differences between reflectances in resampled, coarser-scale drone and NEON images. Columns left to right include all species in images, *A. altissima*, *E. umbellata*, and *R. davurica*, and rows top to bottom are for untransformed and transformed data.

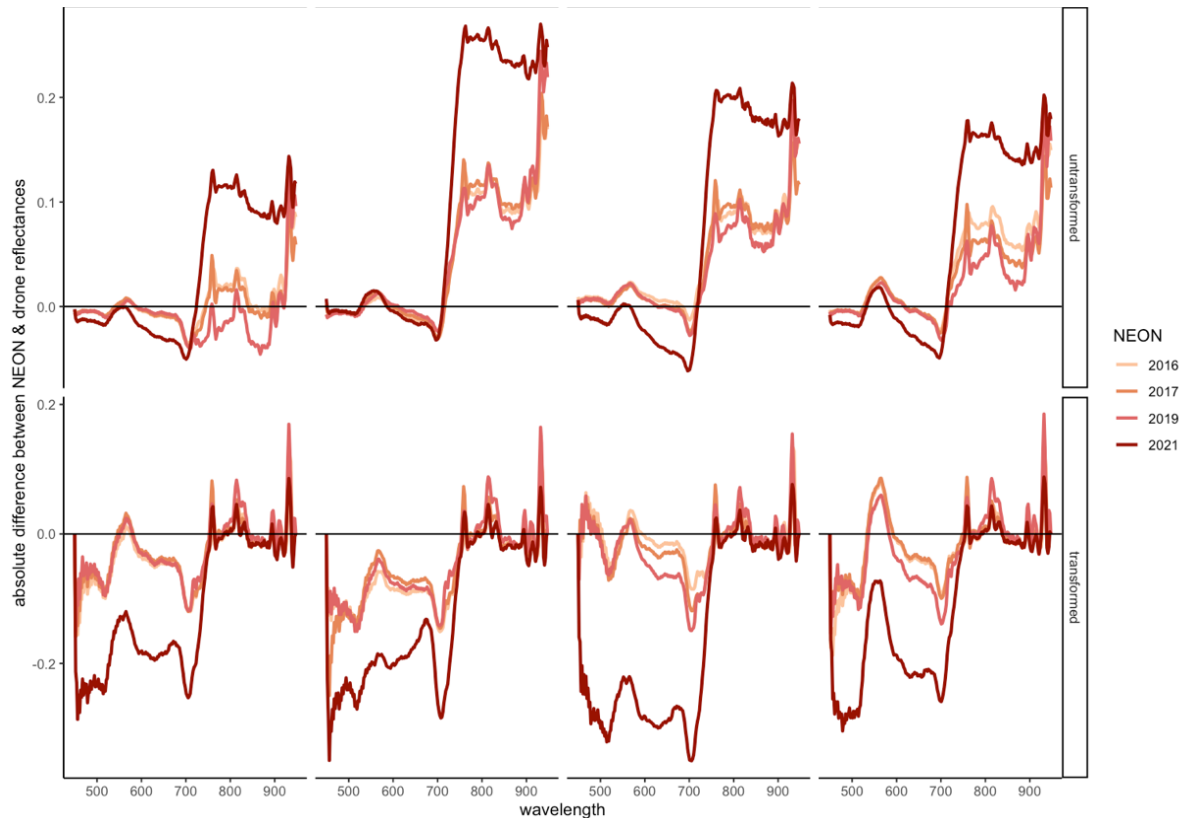


Figure 2. B) Mean differences between reflectances in resampled, coarser-scale drone and NEON images. Columns left to right include all species in images, *A. altissima*, *E. umbellata*, and *R. davurica*, and rows top to bottom are for untransformed and transformed data.

3.2 Accurately detecting each species of interest using drone-based algorithms

Using detection algorithms trained on drone imagery allowed for the accurate detection (>50% user and producer accuracy) of each species of interest in at least two years of NEON images. Overall, reflectances from fine resolution drone images were used more than those resampled to a coarser resolution (seven compared to five, of the 12 accurate algorithms). Untransformed reflectances were also used more than transformed reflectances (seven compared to five algorithms). Untransformed and transformed reflectances from original drone data were

used in three and four accurate algorithms, respectively. Untransformed and transformed reflectances from resampled drone data were used in four and one algorithm(s), respectively.

A. altissima was accurately detected in three different years (2016, 2017, and 2021) using four different approaches (out of the 64 total approaches). Most (three of the four) accurate approaches used the most lenient detection standards, whereas one used moderately strict detection. Most (three of the four) used resampled, coarser-resolution drone data. Transformed and untransformed data were equally effective (each in two algorithms). All *A. altissima* detection algorithms used green and yellow spectral regions, regardless of resolution and transformation. The most accurate algorithm used transformed fine-resolution drone reflectances and had 100% producer accuracy (sensitivity) and 58% user accuracy (specificity) when used to detect *A. altissima* in transformed 2021 NEON imagery.

E. umbellata was accurately detected twice (in 2017 and 2021 NEON images). Both algorithms used the original, fine-resolution drone data, and both used the strictest detection standard. Transformed and untransformed drone data were each used. The algorithm based on untransformed reflectances highlighted the blue, green, and red edge slope spectral regions. The algorithm based on transformed reflectances, which detected *E. umbellata* with the greatest accuracy, highlighted the blue, green, yellow, red, red edge minimum, and red edge slope. This algorithm had 86% producer accuracy (sensitivity) and 51% user accuracy (specificity) when used to detect *E. umbellata* in 2017 transformed NEON imagery.

R. davurica was accurately detected in two different years (2017 and 2019) using six different approaches. Several exhibited equally good producer accuracies (67%) paired with varying degrees of user accuracies. Of the six approaches, four used untransformed drone data, and two used transformed data; four used the original, fine resolution drone data, and two used

drone data resampled to a coarser resolution. None of the accurate algorithms used the most lenient detection standard, and the other strictness levels were used equally. The blue spectral region was important in algorithms based on the original, fine-resolution and untransformed drone data. More spectral regions were important in the algorithm based on transformed fine-resolution drone data: blue, green, yellow, orange, and red edge slope all loaded heavily. When applied to transformed reflectances from 2019 NEON images, this was the most accurate algorithm to detect *R. davurica*, with 67% producer accuracy (sensitivity) and 88% user accuracy (specificity) (Table S1).

3.3 Accurately detecting each species of interest using NEON-based algorithms

A. altissima was accurately detected using NEON-based algorithms in three different years using 19 different approaches (out of the 32 total approaches), most of which used transformed reflectances (11 of the 19). More lenient approaches were used more frequently than stricter approaches, with 12 of the 19 algorithms using either moderately lenient or most lenient. The spectral regions that loaded heavily in accurate algorithms varied across years and transformations: in 2017 detection algorithms a combination of visible (both untransformed and transformed data) and high NIR (transformed data only) loaded heavily; in 2019 detection algorithms, the red edge (both untransformed and transformed data) and green (untransformed data only) loaded heavily; and in 2021 the red edge to low NIR loaded heavily. *A. altissima* was best detected (an accuracy of 98%) in transformed 2021 NEON images.

E. umbellata was accurately detected using NEON-based algorithms in three different years using 14 different approaches, with approximately equal use of untransformed and transformed reflectances (six and eight, respectively). Stricter approaches were used more frequently to accurately detect *E. umbellata* (11 of the 14 approaches). When untransformed data

were used, the red edge minimum (in both 2016 and 2017) and red edge slope (2017 only) loaded heavily in accurate *E. umbellata* detection algorithms. When transformed data were used, combinations of spectral regions that loaded heavily varied more across years: in one algorithm the red edge slope and high NIR loaded heavily, while in the most accurate algorithm (using the 2016 NEON images, with an accuracy of 77%) the green and red edge shoulder loaded heavily.

R. davurica was accurately detected in two different years using 13 different approaches, with approximately equal use of untransformed and transformed reflectances (six and seven, respectively). Accurate detection of *R. davurica* was equally possible in all but the most lenient approach, and other levels of strictness were used equally. The spectral regions that loaded heavily in accurate algorithms varied across years and transformations: in 2017, reflectances in the blue, green, yellow, and red edge minimum spectral regions loaded heavily when untransformed data were used, whereas high NIR loaded heavily when transformed data were used; in 2019, the shorter wavelengths of the red edge loaded heavily in untransformed data, whereas the longer red edge wavelengths loaded heavily in transformed data. When untransformed data were used, the blue, green, yellow, and red edge minimum were important in 2017, and the red edge minimum and red edge slope were important in 2019. When transformed data were used, high NIR was important to detection in 2017, and the red edge slope and shoulder were important to detection in 2019. The most accurate detection algorithm (95%) for *R. davurica* used 2019 NEON images, in which the red edge region loaded heavily (Table S2)

3.4 Comparing drone-based and NEON-based detection algorithms

3.4.1 Detection accuracy

Across the three species of interest, drone-based algorithms had lower accuracy and were less frequently accurate than NEON-based algorithms. Accurate drone-based algorithms (with user and producer accuracies $> 50\%$) had a mean accuracy of $65 \pm 1\%$ and a mean maximum accuracy of $75 \pm 3\%$ across the three species, whereas accurate NEON-based algorithms had a mean accuracy of $77 \pm 4\%$ and a mean maximum accuracy of $90 \pm 7\%$ across the three species.

On average, accurate detection algorithms of *A. altissima* based on drone and NEON data, respectively, had mean accuracies of $62 \pm 6\%$ and $80 \pm 4\%$. The best detection accuracies of *A. altissima* were 79% and 98% in drone-based and NEON-based algorithms, respectively. On average, accurate detection algorithms of *E. umbellata* based on drone and NEON data, respectively, had mean accuracies of $67 \pm 1\%$ and $70 \pm 1\%$, and the best detections were 68% and 77%, respectively. *R. davurica* was accurately detected using drone and NEON images with mean accuracies of $66 \pm 3\%$ and $80 \pm 2\%$, respectively, and maximum accuracies of 78% and 95%, respectively.

3.4.2 Temporal sensitivity, strictness, and key spectral features

A. altissima could be accurately detected in three different years using either drone-based or NEON-based algorithms. Accurate drone-based algorithms were less flexible in approach (transformation, resampling, and detection strictness standards) than NEON-based algorithms; only four drone-based approaches were accurate, whereas 19 NEON-based approaches were accurate. More lenient standards were better than stricter standards for accurate *A. altissima* detection. Transformed reflectances were used slightly more often than untransformed reflectances in NEON-based algorithms (Figure 3, bottom panel).

The only spectral region that was important for accurate *A. altissima* detection across platforms was the green region. Spectral regions important in accurate drone-based detection algorithms were yellow and green (in both transformations and resolutions). More spectral regions were important in accurate NEON-based detection algorithms: the green, orange, red, and red edge minimum and slope in untransformed data, and the blue, green, red, red edge slope and shoulder, low and high NIR (Figure 3, Table 4).

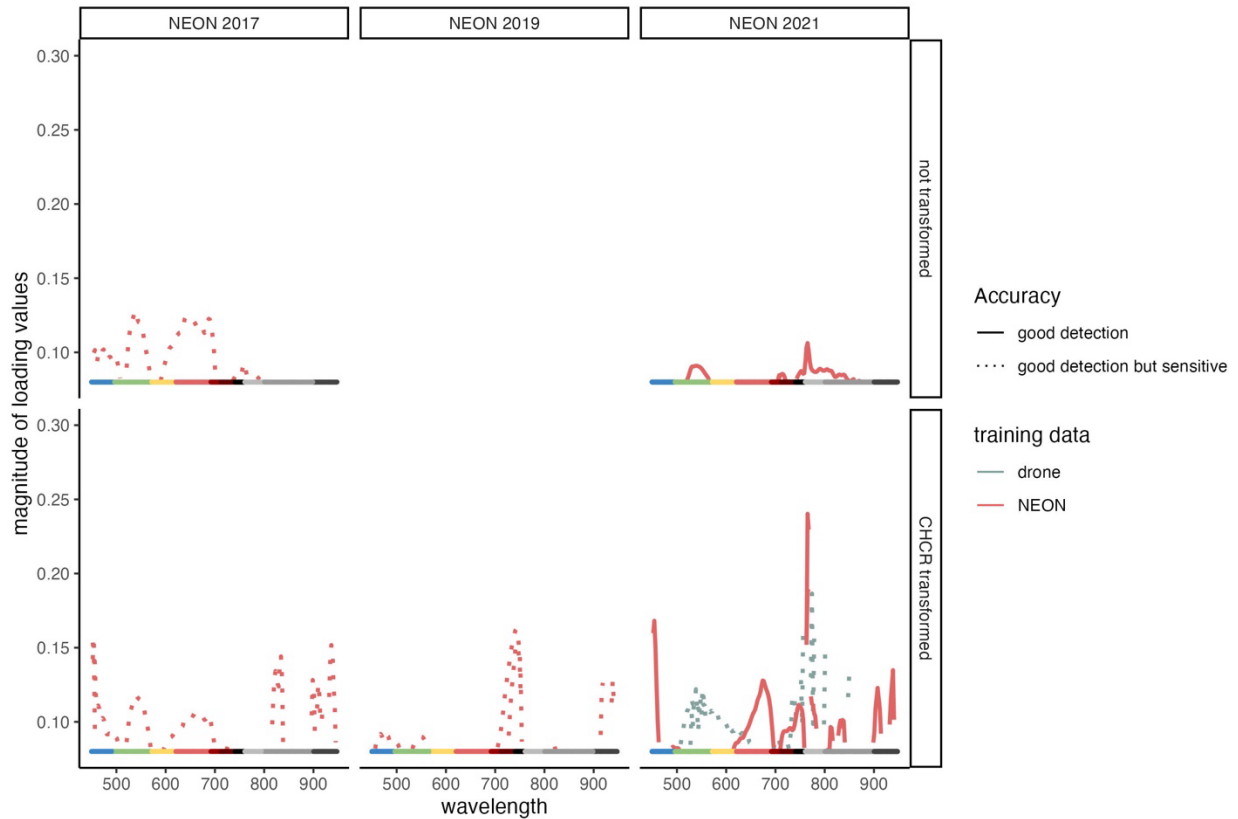


Figure 3. Magnitudes of top (>0.1) loading values for the most accurate detection algorithms for *A. altissima* across all training and testing datasets. The top and bottom panels represent algorithms that used untransformed and transformed data, respectively. Each panel from left to right includes years of NEON images with good detection accuracies (>70%). Lines in each panel are colored by training data (fine-resolution drone image or each year’s NEON image) and are solid for algorithms with good detection (>70% user and producer accuracies) or dotted for algorithms with good detection (>70%) but higher than ideal false positive rates (between 30% and 50%). Algorithms with <70% accuracies were not included to simplify the figure. To aid in interpretability, the band at the bottom is colored by spectral regions, where blue, green, yellow/orange, and red are colored according to identity, the red edge is dark red, and the NIR is shades of grey.

Table 4. Training datasets (reflectances extracted from fine- or coarser-resolution drone images or NEON images) that most accurately detected *A. altissima*, to what degree (best user accuracy, UA, and producer accuracy, PA, across all strictness approaches), and the spectral regions that were important in each algorithm. For more details, see tables S1 and S2.

Training	Transformation	Spectral regions	UA	PA
NEON 2017	not transformed	green, orange, red	69%	75%
NEON 2017	transformed	blue, green, red, high NIR	69%	100%
NEON 2019	not transformed	green, red edge minimum, red edge slope	69%	60%
NEON 2019	transformed	red edge slope, red edge shoulder	93%	100%
NEON 2021	transformed	red, red edge shoulder	97%	100%
drone coarse res	not transformed	green, yellow	56%	60%
drone coarse res	transformed	green, yellow	53%	60%
drone fine res	transformed	green, yellow	58%	100%

NEON-based algorithms for *E. umbellata* detection were also much more flexible than drone-based algorithms; only two drone-based approaches accurately detected *E. umbellata*, whereas 14 different NEON-based approaches did. In accurate algorithms developed from both platforms, untransformed and transformed reflectances were used equally, and stricter standards were better. Reflectance in the red edge slope was most consistently used across accurate drone-based and NEON-based *E. umbellata* detection algorithms, followed by the green. Reflectance in the blue spectral region was key to detection in drone-based algorithms but not as frequently in NEON-based algorithms. Yellow and red were more important in transformed drone-based algorithms than in transformed NEON-based algorithms (Figure 4, Table 5).

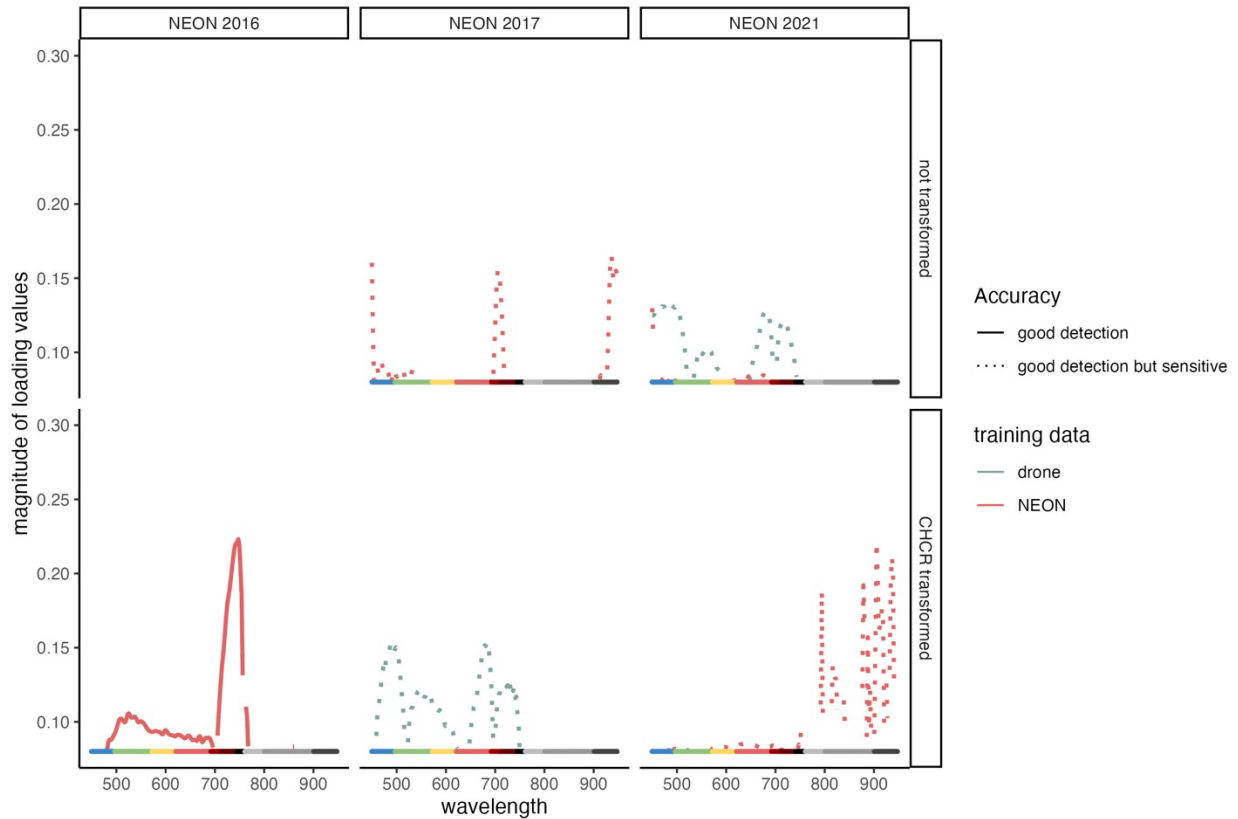


Figure 4. Magnitudes of top (>0.1) loading values for the most accurate detection algorithms for *E. umbellata* across all training and testing datasets. The top and bottom panels represent algorithms that used untransformed and transformed data, respectively. Each panel from left to right includes years of NEON images with good detection accuracies (>70%). Lines in each panel are colored by training data (fine-resolution drone image or each year’s NEON image) and are solid for algorithms with good detection (>70% user and producer accuracies) or dotted for algorithms with good detection (>70%) but higher than ideal false positive rates (between 30% and 50%). Algorithms with <70% detection accuracies were not included to simplify the figure. To aid in interpretability, the band at the bottom is colored by spectral regions, where blue, green, yellow/orange, and red are colored according to identity, the red edge is dark red, and the NIR is shades of grey.

Table 5. Training datasets (reflectances extracted from fine- or coarser-resolution drone images or NEON images) that most accurately detected *E. umbellata*, to what degree (best user accuracy, UA, and producer accuracy, PA, across all strictness approaches), and the spectral regions that were important in each algorithm. For more details, see tables S1 and S2.

Training	Transformation	Spectral regions	UA	PA
NEON 2016	not transformed	red edge minimum, red edge slope	81%	67%
NEON 2016	transformed	green, red edge slope, red edge shoulder	82%	80%
NEON 2017	not transformed	red edge minimum	79%	80%
NEON 2017	transformed	red edge slope, high NIR	83%	67%
NEON 2021	transformed	high NIR	69%	75%
drone fine res	not transformed	blue, red edge slope	59%	71%
drone fine res	transformed	blue, green, yellow, red, red edge slope	51%	86%

R. davurica could be accurately detected in two different years using drone-based or NEON-based algorithms. Fewer approaches allowed for its accurate detection in drone-based algorithms (six compared to 13 with NEON-based). Accurate drone-based algorithms used untransformed reflectances slightly more often than transformed reflectances, whereas NEON-based algorithms used them more equally. All but the strictest detection standard accurately detected *R. davurica* in drone-based approaches, whereas all but the most lenient detection standard resulted in accurate detection in NEON-based approaches.

Untransformed reflectance in the blue spectral region was important in both accurate drone-based and NEON-based *R. davurica* detection algorithms, though NEON-based algorithms incorporated several other spectral regions (green, yellow, and red edge minimum and slope). Transformed reflectance in the red edge slope was important in both drone-based and NEON-based algorithms, but drone-based algorithms incorporated several visible spectral regions (blue, green, yellow, orange), whereas NEON-based algorithms incorporated the red edge shoulder and high NIR (Figure 5, Table 6).

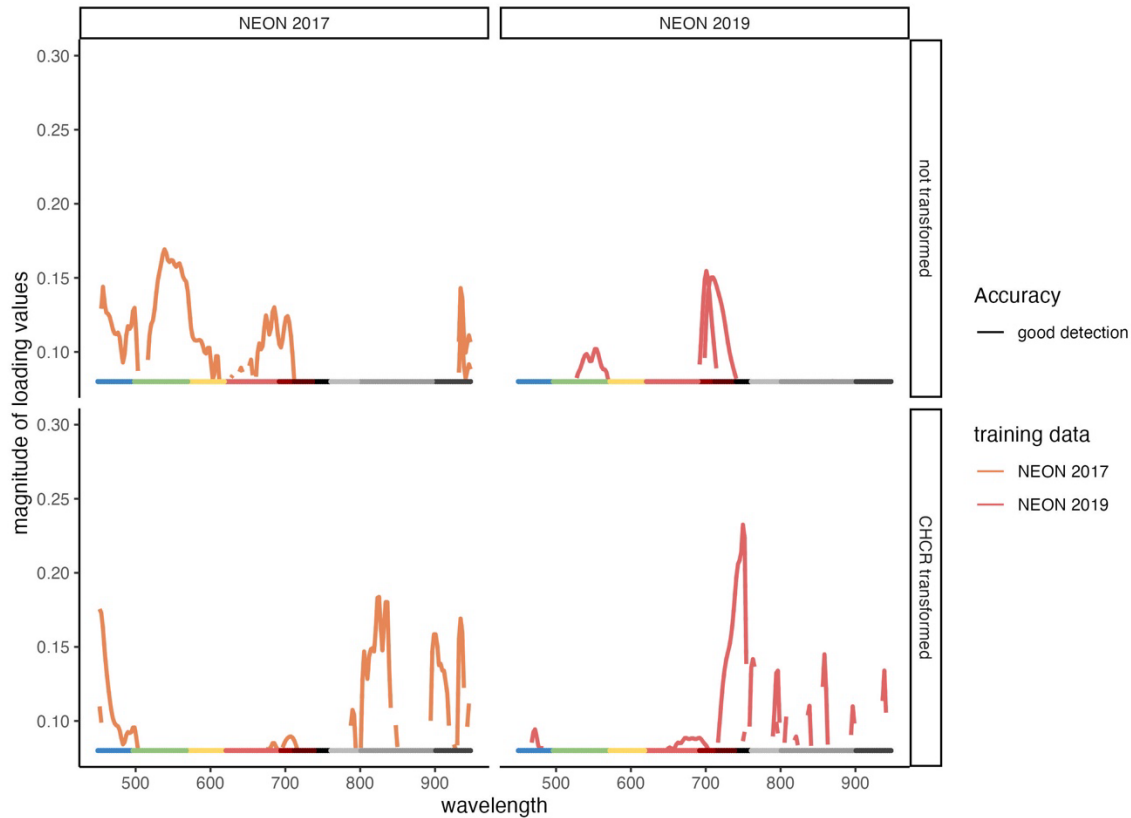


Figure 5. Magnitudes of top (>0.1) loading values for the most accurate detection algorithms for *R. davurica* across all training and testing datasets. The top and bottom panels represent algorithms that used untransformed and transformed data, respectively. Each panel from left to right includes years of NEON images with good detection accuracies (>70%). Lines in each panel are colored by training data (each year's NEON image) and are solid for algorithms with good detection (>70% user and producer accuracies). Although there were algorithms with good detection (>70%) and false positive rates between 30% and 50%, their loading factors did not exceed 0.1. Algorithms with <70% detection accuracies were not included to simplify the figure. To aid in interpretability, the band at the bottom is colored by spectral regions, where blue, green, yellow/orange, and red are colored according to identity, the red edge is dark red, and the NIR is shades of grey.

Table 6. Training datasets (reflectances extracted from fine- or coarser-resolution drone images or NEON images) that most accurately detected *E. umbellata*, to what degree (best user accuracy, UA, and producer accuracy, PA, across all strictness approaches), and the spectral regions that were important in each algorithm. For more details, see tables S1 and S2.

Training	Transformation	Spectral regions	UA	PA
NEON 2017	not transformed	blue, green, yellow, red edge minimum	80%	100%
NEON 2017	transformed	high NIR	85%	75%
NEON 2019	not transformed	red edge minimum, red edge slope	89%	100%
NEON 2019	transformed	red edge slope, red edge shoulder	80%	100%
drone coarse res	not transformed	blue, red edge slope	62%	67%
drone fine res	not transformed	blue	65%	67%
drone fine res	transformed	blue, yellow, orange, red edge slope	88%	67%

3.4.2 Consistency of important spectral features across algorithms

When ranks of loading values were averaged across all accurate detection algorithms (across all four years of NEON data and the two resolutions of drone data) for each species of interest, those that used untransformed data had more bands with means > 180 (or in the top 20%). *A. altissima* had 15 bands with mean ranks > 180 (17% of the maximum possible), all of which were in the green spectral region. *E. umbellata* had 11 bands (12%) with mean ranks > 180 , most of which were in the red edge. *R. davurica* had the greatest number of bands (29, or 32%) with mean ranks > 180 , a majority of which were in the green and red edge minimum spectral regions.

There were only two cases in which both resolutions of drone-based algorithms accurately detected a species of interest (*A. altissima* using transformed data, and *R. davurica* using

untransformed data). When ranks of loading values from each accurate drone-based algorithm were averaged across the two resolutions, *A. altissima* had 17 bands (19%) with mean ranks > 180, a majority of which were in the red edge slope. *R. davurica* had 72 bands (80%) with mean ranks > 180, with several bands in the blue, green, red, red edge slope and red edge shoulder.

When ranks of loading values were averaged across all accurate NEON-based detection algorithms (across all four years of NEON data), *E. umbellata* had the fewest bands with mean ranks > 180 (10, or 11%). *A. altissima* had 25 bands (28%) with mean ranks > 180 for untransformed data, a majority of which were in the low NIR spectral region, and 37 bands (41%) with mean ranks > 180 for transformed data, which were mostly in the green and red spectral regions. *R. davurica* had 39 bands (43%) with mean ranks > 180 for untransformed data, most of which were in the green and red edge minimum, and 41 bands (46%) for transformed data, which were in the red, red edge minimum, and high NIR.

4. Discussion

4.1 Spectral differences between platforms

4.1.1 Original drone data

Untransformed reflectances in both fine- and coarser-resolution drone images were more similar to reflectances in NEON images than transformed reflectances for either resolution. The purpose of the transformation was to highlight certain wavelengths that I thought would lead to greater similarity between the platforms, however it increased the differences between them. Algorithms based on transformed fine-scale reflectances in drone images did, however, tend to include more spectral regions in algorithms than untransformed fine-scale reflectances.

4.1.2 Resampled drone data

Resampling drone images from a fine-scale resolution to a coarser-scale resolution led to greater similarities in reflectances between the two platforms overall and to the greatest extent in the green, yellow, and orange spectral regions (across all eight species on average). This change in differences in reflectances between drone and NEON images most illustrates how resolution impacts reflectance values; in resampled images, mixed pixels incorporate shade, which reduces reflectances in drone images to better match reflectances in NEON images. Further supporting this harmonization of drone and NEON images through resampling is the impact that resampling had on accurate algorithms. Similar to how transforming reflectances of fine-scale drone images increased the number of spectral regions included in accurate algorithms, resampling to a coarser resolution had the same effect. Accurate algorithms that used untransformed reflectances from drone images resampled to a coarser resolution included blue, green, yellow, and orange, whereas those that used untransformed reflectances from fine-scale drone images only used blue and red reflectances.

4.2 Accurately detecting each species using drone-based algorithms

4.2.1 Implications of transforming and resampling drone data

The balance of the disadvantage of transforming drone-based data (increasing differences in reflectances from NEON images) and the advantage (increasing the number of spectral features that may help detect individual species of interest) is illustrated by the fact that untransformed and transformed fine-scale drone reflectances were used in the same number of accurate detection algorithms for both *A. altissima* and *E. umbellata*. So even if reflectances differ more from the NEON data, transforming may accentuate these species differences in the visible spectrum,

increasing their differentiability from other species. For *R. davurica*, however, only two accurate algorithms used transformed data, whereas four used untransformed data. The better alignment between untransformed drone and NEON images (compared to transformed drone and NEON images) is confirmed by the consistency of accurate algorithms across all platforms that used untransformed data.

Detection of *A. altissima* benefited from resampling drone-based images. Resampling to a coarser resolution changed reflectances most in the green spectral region, likely due to the incorporation of shade into the spectral signature. Resampling also increased the number of spectral regions with similar reflectances to NEON data to include the green, yellow, and orange. As a result, *A. altissima* was accurately detected using drone-based images three out of four times (two of which were untransformed reflectances). *A. altissima* was the only species of interest accurately detected in NEON images using a combination of resampled drone images and transformed reflectances.

Although resampling drone images made reflectances of *E. umbellata* in the blue, orange, and red spectral regions approximately equal to those in NEON images, algorithms that used reflectances from resampled drone images did not accurately detect it in any of the NEON images. *E. umbellata* was instead only detected using fine-resolution drone images. The increase in similarity of reflectances in the blue spectral region to NEON images may be caused by a “dampening” of (or reducing the reflectance in) the blue spectral signal. *E. umbellata* had greater reflectances in the blue spectral region than other species in drone-based images, which would imply its importance in its differentiation. If that spectral feature is lost through a dampening via resampling, it would explain the decreased detection accuracy.

Resampling drone images also changed reflectances of *R. davurica* most in the blue and red spectral regions and increased the number of spectral regions with similar reflectances to NEON images from only blue to blue, orange, red, and low NIR. Despite more similar reflectances in resampled data, *R. davurica* was accurately detected by twice as many algorithms using fine-resolution drone data than resampled drone data. Similar to what was seen in *E. umbellata*, the spectral features that allowed for differentiation of *R. davurica* from other species are likely dampened with resampling, which reduces the possibility of detection.

4.2.2 Implications of detection strictness

Stricter detection approaches were used more often when applying drone-based algorithms to accurately detect species of interest in NEON images. This overall pattern can be explained by species-specific patterns. *A. altissima* benefitted from more lenient approaches, whereas *E. umbellata* and *R. davurica* tended toward stricter approaches (with *E. umbellata* only using the strictest, and *R. davurica* using all but the most lenient approach).

This result is notable for two reasons; first, canopy size likely contributed to these patterns, and second, spectral characteristics of each species of interest also contributed. *A. altissima*, a tree species with a larger canopy than the shrub species, would require more pixels for accurate identification using stricter standards than with more lenient standards (i.e., half of the well-lit pixels classified in a canopy, compared to just one pixel). Therefore, its accurate detection benefitted from the requirement of fewer pixels for classification. The two shrub species, *E. umbellata* and *R. davurica*, had smaller canopies, which potentially resulted in the evaluation of additional, neighboring pixels or mixed pixels at the boundary of each canopy in NEON images. Therefore, accurate detection of the shrub species benefitted from the requirement of more pixels for classification, decreasing the possibility of false negatives. Canopies of female *A. altissima*

trees also include a high density of seed pods, which could make the spectral signatures of entire canopies more variable, as some pixels may include a signal from seed pods, and some may not. Therefore, accurate detection of *A. altissima* also likely benefitted from more lenient approaches, as fewer pixels would need to resemble the characteristics in each algorithm.

4.3 Accurately detecting each species using NEON-based algorithms

Reflectances in all aerial remotely sensed imagery are impacted by biological features in addition to features of the platform and sensor. Platform and sensor differences can impact spectra due to different spatial and spectral resolutions, viewing angles due to footprint differences, and atmospheric interference caused by water or gas absorption bands, depending on the elevation of image collection. Plant biochemical traits, which are not constant over either space or time, also impact spectra. Additionally, long- and short-term changes in canopy structure, including canopy architecture and leaf angle, can also interact with reflected light and therefore spectra. Thus, the greater number of accurate NEON-based algorithms and their greater accuracy were to be expected, as their use eliminates differences between training and testing data, in terms of space (resolution, viewing angle, differences in atmospheric depth) and time (across years).

4.4 Key spectral features and sensitivity to scale and time

Accurate algorithms for the detection of *A. altissima* were somewhat consistent within each platform (drone or NEON) but not across all platforms (drone and NEON). The greatest overlap in important spectral features was among accurate NEON-based algorithms that used transformed data (41% overlap), which highlighted the green and red spectral regions. Because transformed reflectances accentuate absorption features, and those features were consistently important in NEON-based algorithms across years, this suggests a lack of temporal variability in those features key to detecting *A. altissima*. Although there were considerable similarities in key spectral regions across accurate NEON-based algorithms using transformed data, there was no similarity across algorithms from all platforms (NEON- and drone-based algorithms) using transformed data. This misalignment between features key to NEON- and drone-based detection is confirmed by the overlap between accurate transformed drone-based algorithms, which highlighted the red edge slope.

E. umbellata had the least consistent algorithms both within each platform and across platforms. Unlike *A. altissima* and *R. davurica*, it was not accurately detected using resampled drone imagery. This suggests that reflectances of *E. umbellata*, and therefore spectral features key to its detection, are heavily resolution-dependent, as resampling to a coarser resolution tended to dampen the blue and red spectral signals in fine-scale drone imagery, which were key to its detection in drone-based algorithms. This is also supported by the lower number of accurate drone-based algorithms, as well as their lower accuracy, compared to drone-based algorithms of the other two species of interest.

Accurate *R. davurica* detection algorithms that used untransformed data had the most consistency across all algorithms (32%), across NEON-based algorithms (43%), and especially

across the two resolutions of untransformed drone-based algorithms (80%). The green and red edge minimum spectral regions were both important across all algorithms and all NEON-based algorithms, whereas the blue, green, red, and red edge slope and shoulder spectral regions were important in the drone-based algorithms. The red edge minimum was less important among the two resolutions of drone-based algorithms compared to the NEON-based algorithms. The consistency in important spectral regions among accurate NEON-based algorithms (46% overlap that highlighted the red, red edge minimum, and high NIR) that used transformed reflectances did not translate to overall consistency across all approaches.

4.5 Conclusion

The first question I explored in this study was how spectral signatures differed in drone-based images and NEON images. Reflectances in fine-scale drone-based images were generally most consistently similar to those in NEON images in blue and red spectral regions across all species, except for *E. umbellata*. When drone images were resampled to a coarser resolution, reflectances were most similar in blue, green, yellow, and orange spectral regions. Reflectances were most different between the two platforms in the red edge and high NIR spectral regions. Transforming reflectances increased differences between the two platforms.

I then examined how well invasive plants could be detected in coarse resolution images collected by the NEON AOP, first using detection algorithms created using fine-resolution drone imagery, then using detection algorithms created using NEON AOP imagery. Accurate drone-based algorithms (with user and producer accuracies > 50%) had a mean accuracy of $65 \pm 1\%$ and a mean maximum accuracy of $75 \pm 3\%$ across the three species, whereas accurate NEON-based algorithms had a mean accuracy of $77 \pm 4\%$ and a mean maximum accuracy of $90 \pm 7\%$ across the

three species. NEON-based algorithms detected each with greater accuracy, as it eliminated both temporal and scale differences among platforms.

The last goal of this study was to determine the most useful spectral features in detection. The green spectral region was important for accurate *A. altissima* detection across all platforms. Drone-based algorithms also included yellow, and NEON-based algorithms included blue, orange, red, and red edge, and NIR. Reflectance in the red edge slope was most consistently used across accurate drone-based and NEON-based *E. umbellata* detection algorithms, followed by the green. Reflectance in the blue spectral region was key to detection in drone-based algorithms but not as frequently in NEON-based algorithms. Untransformed reflectance in the blue spectral region and transformed reflectance in the red edge slope were important in both accurate drone-based and NEON-based *R. davurica* detection algorithms.

The consistency of drone- and NEON-based algorithms can elucidate the importance of time or space; consistency among algorithms within each platform suggests that resolution and temporal variability, respectively, may not be issues, but that features of each platform (e.g. viewing angle) may affect applications across both. Spectral features that allowed for the accurate detection of *A. altissima* were consistent within each platform but not across platforms, which suggests that its spectral features are not universal across time and/or space. Spectral features that were key to accurately detecting *E. umbellata* were inconsistent, which suggested that they are resolution dependent. *R. davurica* had the most consistency in features that allowed for its detection at every level, although the features changed, which suggests at least some variability associated with time and space.

Differences in reflectance signatures between fine and coarse resolution drone images, as well as the similarity of their accurate detection algorithms, highlight the importance of

observational scale. The similarities among accurate NEON-based detection algorithms across years can inform how temporally stable the spectral features are that allow for detection. The similarities among accurate detection algorithms across platforms can be used to assess their interoperability. Although the two platforms are not perfectly interoperable, due to variability across time and space, they nevertheless allowed for the detection of each invasive plant species. This analysis of the inconsistencies across detection algorithms, however, also elucidates the importance of considering time and space, not only in the detection of invasive plant species, but also in answering ecological questions.

Chapter 4: Fine-scale ecological organization contributes substantively to spectral variability in Virginia successional forests

Abstract

Due to the relationship between biochemical and structural plant traits and spectra, greater spectral variation is associated with trait and thus species variation. The positive relationship between spectral variation and species richness, known as the spectral variation hypothesis (SVH), is supported in some cases but may not be consistent across ecosystems, time, and organizational scales (leaf, individual canopy, and community). To further elucidate potential temporal and scale-based exceptions to the SVH, I utilized fine-scale (3 cm) hyperspectral images collected by an unoccupied aerial vehicle (UAV) equipped with a Nano-Hyperspec imager during early, mid-, and late growing season (DOY 134, 178, and 249, respectively). Spectral signatures of eight tree and shrub species were extracted from pixels within images of three 1-ha fields. I examined species-specific intra-annual trends in spectral variability at different organizational scales: within individual canopies, among individual canopies of the same species, among species, and among communities. I found that variability among species was greatest early in the growing season, supporting the SVH. Among-species variability in some spectral regions increased then decreased over the growing season, suggesting divergence in photosynthetic pigments among species earlier in the growing season and convergence later in the growing season. As the growing season

progressed, both within-individual and among-individual spectral variability increasingly exceeded among-species variability in more spectral regions and to a greater degree, which suggests that more traits become increasingly variable at finer organizational scales as leaves mature. The contribution of among-community spectral variation suggests that some observed species-specific among-individual spectral variability was likely caused by spatial heterogeneity. Later in the growing season, the total within- and among-individual spectral variability contributed to over half of the total observed spectral variability in spectral regions associated with biochemical traits, and among-individual variability was also >30% in spectral regions associated with canopy structure. These results suggest that differences within individual canopies and among individuals of a species are greater than differences among species, particularly in biochemical traits, from mid-growing season and into the start of fall senescence. Therefore, species-based assumptions about traits in mid- to late growing season may neglect considerable variability among individuals within species and within individuals. As functional traits can be used to make generalizable predictions across organizational and spatial scales, understanding trait variation at different scales and times can facilitate answering major questions in community ecology to further the understanding of plant communities and ecosystems. Spectroscopy can be used to this end and will benefit from increasingly available hyperspectral airborne data and new satellite missions.

1. Introduction

Hyperspectral imaging, which includes a large number of narrow, contiguous bands, provides detailed spectral information (Chance et al., 2016; Kaufmann et al., 2008). Canopy reflectance spectra are strongly related to certain biochemical and structural plant traits and physiological responses to the environment (Jacquemoud et al., 2009; Kattenborn et al., 2019; Matongera et al., 2016; Ollinger, 2011; Z. Wang et al., 2020; Yang et al., 2016), including: pigments (Mahlein et al., 2010; Xiao et al., 2014), such as chlorophyll (Gregory P. Asner & Martin, 2008b; Chance et al., 2016; Thenkabail et al., 2014), anthocyanins, and carotenoids (Blackburn, 2007); leaf N, P, and K (Gregory P. Asner & Martin, 2008b; Chance et al., 2016; Mutanga et al., 2004; Thenkabail et al., 2014); and plant water and vegetation stress (Thenkabail et al., 2014). These characteristics impact spectra, as they create wavelength-specific absorption or reflectance features (Gregory P. Asner, 1998; Grant, 1987; D. A. Roberts et al., 2004; Woolley, 1971).

Because spectral reflectance from vegetation is a function of physiological, biochemical, and structural differences, spectra should differ more among distantly related groups than among close relatives (Cavender-Bares et al., 2016; McManus et al., 2016; Schweiger et al., 2018). The positive relationship between spectral variability and species diversity, known as the spectral variation hypothesis (SVH; Palmer et al., 2002), is grounded in functional variation, with the assumption that functions and therefore spectra differ most among species. Though the SVH has been supported by positive relationships between spectral variation and species richness, in some cases, it has also been refuted (Aneece & Epstein, 2017; Schmidtlein & Fasnacht, 2017). Exceptions to the SVH are grounded in the concept of the phenotype, which is the physical expression of the combination of genetic and environmental information. A spectral signature is one form of phenotypic expression, the “spectral phenotype.”

The SVH is not consistent across ecosystems (Fassnacht et al., 2022; Schmidtlein & Fassnacht, 2017; Schweiger et al., 2018), seasons (Fassnacht et al., 2022; Rocchini et al., 2010; Schmidtlein & Fassnacht, 2017), or scales (Marks, 2007; Messier et al., 2010), as both time and space impact the balance of variability within and among species. Phenology, which impacts traits and thus spectral signatures, can increase spectral variability within and among species at certain points in a single growing season (Fassnacht et al., 2022). Trait variability within a species is sometimes similar to or greater than it is among species (Auger & Shipley, 2013; Jung et al., 2010; Messier et al., 2010; Siefert et al., 2015), particularly in leaf chemical traits (e.g. chlorophyll and N), which tend to vary more within species than leaf morphological traits (e.g. thickness). Trait variability also becomes more pronounced at certain scales. Canopy level traits are more sensitive to environmental conditions and thus more variable within species due to genetic adaptation and phenotypic plasticity, whereas leaf level traits tend to be conserved at the species level and vary more across species (Marks, 2007).

Despite the clear evidence supporting considerable variability within species as well as its interesting implications, comparisons among species often focus on mean functional trait values with little to no attention to trait variation (Albert et al., 2010; McGill et al., 2006). According to Messier et al. (2010), functional trait variability within and among species are often examined independently of each other and not across spatial and temporal scales. Examining and quantifying spectral variability and placing it in an ecological context can reveal which spatial and temporal scales are most variable and most appropriate to answer questions about plant ecology and biodiversity (McGill et al., 2006; Schweiger et al., 2018). The very fine spectral resolution of hyperspectral imagery allows for the examination of spectral regions associated with leaf-level biochemical and structural characteristics of terrestrial vegetation. Using this technology in concert

with an unoccupied aerial vehicle (UAV), which collects very fine spatial resolution images over a continuous area, allows for the examination of variability at multiple organizational scales: within individual canopies, among individuals of the same species, and among species. Because UAV flights can take place readily at multiple points in the growing season, phenological differences in these features can be detected (Castro-Esau et al., 2006).

Relating observed spectral variability to plant traits is less straightforward in aerial images than it is in a laboratory setting. Although canopy structure influences spectral signatures and is considered a potentially confounding factor in estimating traits based on reflectances in aerial imagery, architecture and biochemistry do tend to covary (Kokaly et al., 2009; Ollinger, 2011; Townsend et al., 2013; Wright et al., 2004). Therefore frequently observed correlations between traits and reflectances should not be dismissed (Townsend et al., 2013). To increase confidence in the ecological context in which these results would be placed, I examined trait modeling studies with similar attributes (e.g. hyperspectral aerial remote sensing of temperate broadleaf forests; Table 1).

The range of blue-green bands from 460 nm to 540 nm and orange-red bands 600 nm to 690 nm are associated with canopy chlorophyll in temperate forests (Hoepfner et al., 2020; J. Wang et al., 2016). The range of green-yellow bands from 550 nm to 600 nm and red edge bands from ~690 nm to ~760 nm are associated with chlorophyll, in addition to carotenoids and nitrogen (Hoepfner et al., 2020; Muraoka et al., 2013; J. Wang et al., 2016; Z. Wang et al., 2020; Yang et al., 2016). This observed relationship between chlorophyll and N (and therefore overlap in relevant spectral regions) is also supported by several existing vegetation indices (Daughtry et al., 2000; Oppelt & Mauser, 2004). The red edge is particularly useful in estimating chlorophyll content, because it is less affected by leaf and canopy structure than other spectral regions (Sims & Gamon,

2002). Whereas the visible and red edge spectral regions can be used to model vegetation pigments and nutrients, the NIR spectral region is associated with vegetation structure. NIR bands from 800 nm to 850 nm are linked to canopy structure (J. Wang et al., 2016) and near 940 nm to leaf mass per area (LMA) (Wang et al., 2020; Table 1).

Table 1. Biochemical and structural traits that have been accurately modeled in temperate, broadleaf forests using spectral regions in aerial remotely sensed hyperspectral imagery were used to place variability results seen in this study in an ecological context.

Spectral region	Linked trait	General trait	Reference
460-540 nm	Chlorophyll, N	Pigments nutrients	& Hoepfner et al. 2020; Wang et al. 2016 Hoepfner et al. 2020
550-600 nm	Chlorophyll, carotenoids, N (a)	Pigments nutrients	& Yang et al. 2016 Wang et al. 2016 Wang et al. 2020
600-690	Chlorophyll	Pigments nutrients	& Hoepfner et al. 2020 Hoepfner et al. 2020
690-760 nm	Chlorophyll, carotenoids, N (b)	Pigments nutrients	& Yang et al. 2016 Wang et al. 2016 Wang et al. 2020 Muraoka et al. 2012
800-850	Canopy structure	Leaf & canopy structure	Wang et al. 2016
940	Leaf mass per area (LMA)	Leaf & canopy structure	Wang et al. 2020

As young leaves are low in chlorophyll, phenological differences among species (e.g. timing of leaf out and therefore variable timing in increasing chlorophyll concentrations) will likely result in greater differences among species in spectral regions associated with chlorophyll, N, and other pigments (460-540 nm, 550-600, and 690-760 nm) early in the growing season. Because chlorophyll concentrations can be more variable within than across species (M. L. Clark et al., 2005), variability at finer organizational scales (within individuals and among individuals within a species) can be expected to increase once leaves have matured. Schweiger et al. (2018) found local maxima of the coefficient of variation (CV) among 17 species aligned closely with chlorophyll and carotenoid absorption features, which further supports this hypothesis. Young leaves are also thinner, resulting in a lower near-infrared (NIR) reflectance, compared to mature, thicker leaves (Buschmann & Nagel, 1993; Neuwirthová et al., 2021; Rapaport et al., 2014; Slaton et al., 2001). Leaf aging may depress or enhance species-level differences (D. A. Roberts et al., 2004). As with anticipated changes in variability in pigment-associated spectral regions, variability will likely be greatest among species early in the growing season due to variable phenology but may increase over the growing season at finer organizational scales.

To elucidate temporal (phenological) patterns in spectral variability at different organizational scales, I examine spectral variability within individuals, among individuals within a species, among species, and among communities at different points in the growing season and answer the following questions:

1. In what spectral regions and at what times in a growing season does variability within individuals and among individuals within a species exceed variability among species?

2. How does the total spectral variability partition across organizational scales (within individuals, among individuals of a species, among species, and among communities) for all wavelengths over a single growing season?
3. What is the biological significance of spectral variability at different organizational scales over the growing season?

2. Materials and Methods

2.1 Study site

Blandy Experimental Farm (BEF), a biological field station owned by the University of Virginia, is in the Shenandoah Valley in northwestern Virginia (39.06°N, 78.07°W). At 190 m elevation, BEF has a mean annual precipitation of 975 mm, a mean annual temperature of 12°C, and a mean July maximum temperature of 31.5°C. It contains 80 ha of old fields in various stages of succession (Bowers, 1997).

Aerial hyperspectral data collection took place over three 1-ha fields at BEF. The fields are in early to mid-successional stages and are approximately 20, 25, and 30 years in age (Figure 1A; green, blue, and purple polygons, respectively). Each field is located on low-relief topography. The early successional field (E; green polygon in Figure 1a, Figure 1b) contains abundant non-native invasive shrubs, including *Elaeagnus umbellata* (autumn olive) and *Rhamnus davurica* (Dahurian buckthorn) within a heterogeneous matrix of forbs, graminoids, shrubs, and trees. Commonly occurring tree species include *Maclura pomifera* (Osage orange) and *Gleditsia triacanthos* (honey locust). The 25-year-old early-to-mid-successional field (EM; blue polygon in Figure 1a, Figure 1c) contains abundant invasive shrubs, including *E. umbellata*, *R. davurica*, *Lonicera maackii* (bush or Amur honeysuckle) within a heterogeneous matrix of forbs, grasses,

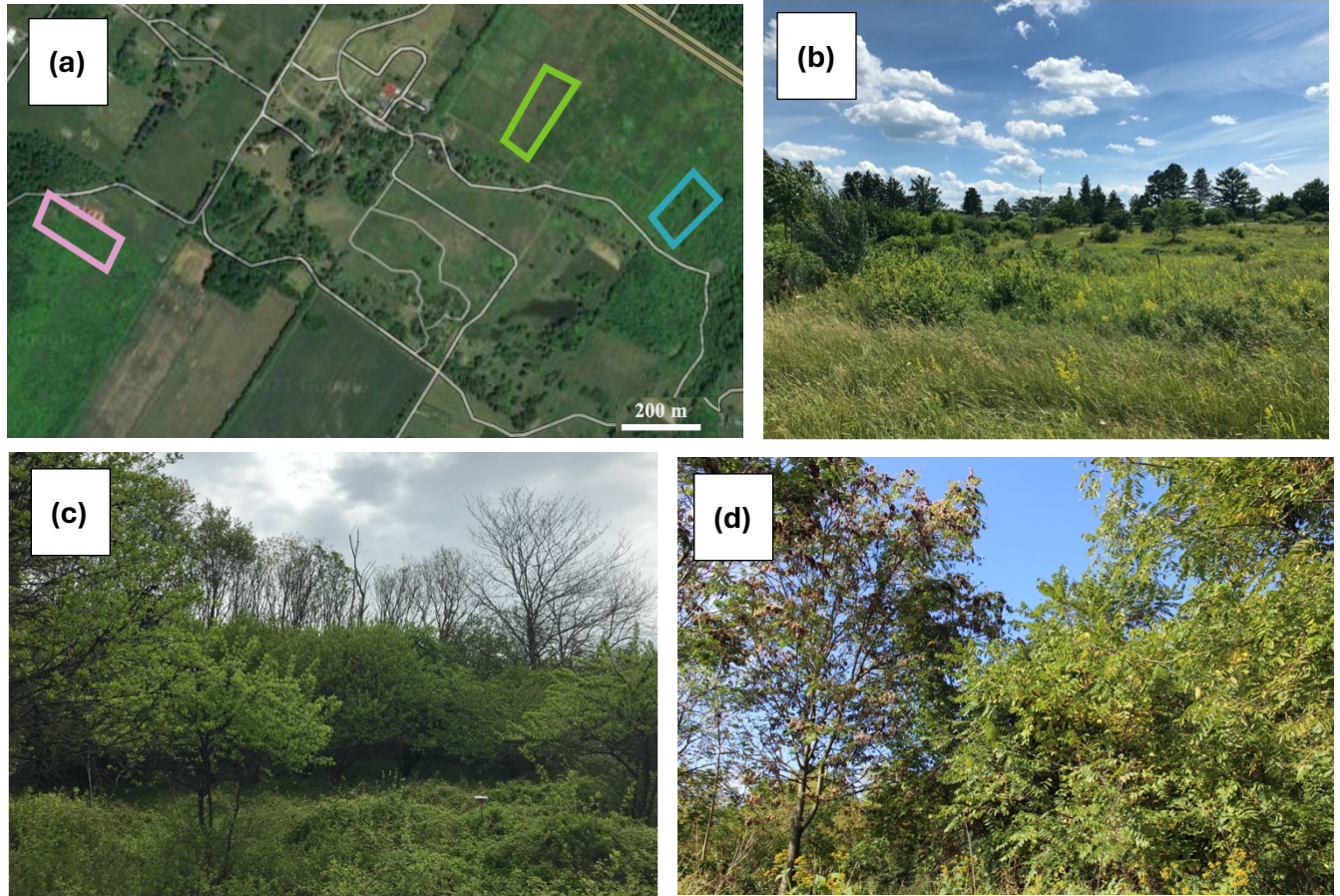


Figure 1. a) Locations of fields in which hyperspectral data were collected during the 2020 growing season. A field in early secondary succession, an intermediate early-to-mid successional field, and a mid-successional field, shown in green, blue, and purple, respectively. b) The early successional field, which is about 20 years in age and contains abundant invasive shrubs, including *E. umbellata* and *R. davurica*. c) The early-to-mid successional field (EM), which is about 25 years in age and contains abundant invasive shrubs, including *E. umbellata*, *R. davurica*, and *Lonicera maackii*. d) The mid-successional field (M), which is about 30 years in age and contains abundant invasive shrubs, including *R. davurica*, and *L. maackii*, along with *A. altissima*.

shrubs, and trees, but with more prevalent trees and shrubs than the early successional field. Commonly occurring tree species include *M. pomifera*, *G. triacanthos*, *Juniperus virginiana* (eastern red cedar), and *Ailanthus altissima* (tree of heaven). The mid-successional field (M; purple polygon in Figure 1a, Figure 1d) contains abundant invasive shrubs, including *R. davurica* and *L. maackii*, along with abundant *A. altissima* and *Juglans nigra* (black walnut) among forbs.

2.2 Hyperspectral data collection and image post-processing

Spectroscopic images were collected using a DJI Matrice 600 Pro equipped with a high-precision GPS system (nominal geolocation accuracy of 1 m) and an imaging spectrometer (Nano-Hyperspec, Headwall Photonics, Bolton, MA). The imaging spectrometer has a spectral range of 400 to 1000 nm, with a spectral resolution of 2 to 3 nm and 270 spectral bands. Flight plans over each field were created using Universal Ground Control Software (UgCS), in which the UAV would fly in straight lines at a consistent height of 48 m above the ground (an average of about 42 m above vegetation) to obtain images with 3 cm pixels (ground level, or 2.6 cm pixels on sampled vegetation) that could later be pieced together to form a larger image. The imaging spectrometer was programmed to capture images along the flight plan using HyperSpec III software (Headwall Photonics, Bolton, MA).

Images were collected at three points during the 2020 growing season: early (DOY 134; May 13), mid (DOY 178; June 26), and late (DOY 249; September 5), midday between 10h and 15h to reduce the impacts of bidirectional reflectance distribution function (BRDF) effects and under a consistent clear sky, sunny conditions. Dates of data collection were chosen to capture seasonal variability and phenological characteristics but after leaves of all species had emerged and prior to the end of season senescence.

Reflectance was calculated for collected spectroscopic images by adjusting for incoming and scattered solar radiation using a sampled dark reference at the time of flight and a gray-scale reference tarp with known reflectance located in the flight scene using SpectralView software. Terrain and perspective effects were also removed using SpectralView software with a digital elevation model provided by the U.S. Geological Survey, and mosaics of multiple images in single rows were created. Though the bidirectional data collection lines on preplanned flights had 40% overlap, the images did not perfectly overlap due to prevailing winds, so only every other row in images was sampled.

2.3 Image sampling

Spectral signatures were collected from 3-cm resolution hyperspectral images for individuals of eight tree and shrub species (*A. altissima*, *R. davurica*, *E. umbellata*, *G. triacanthos*, *M. pomifera*, *J. nigra*, *L. maackii*, and *J. virginiana*) from the three fields (E, EM, and M) where present (Table 2). Individuals were identified in the field using a high-precision GPS and then catalogued within the imagery. If a given species was present in images of a field, up to five individuals were selected for analysis for each of the three dates. In cases where fewer than five individuals were present, as many as were present were sampled.

From each collection date, 15 well-lit and representative pixels were selected for spectral sampling from each individual. To ensure 15 pixels adequately captured variability, I analyzed the variance of sequential sample sizes up to 15 and found that variance saturates with fewer than 15 pixels (~8-10 pixels). To ensure that interpreted spectral variability was not due to sensor noise, I resampled and smoothed reflectances using 5 nm, 10 nm, and 15 nm moving windows.

Table 2. Total number (N) of each invasive (marked with *) and non-invasive shrub or tree species sampled from hyperspectral images for each date (early, mid- and late growing season) across all three fields, where present.

Species	Growth form	N
<i>E. umbellata</i> *	Shrub	10
<i>R. davurica</i> *	Shrub	13
<i>L. maackii</i> *	Shrub	7
<i>A. altissima</i> *	Tree	10
<i>G. triacanthos</i>	Tree	8
<i>M. pomifera</i>	Tree	9
<i>J. nigra</i>	Tree	5
<i>J. virginiana</i>	Tree	9

2.4 Spectral analysis and biological significance

Absolute and relative spectral variability were quantified using the standard deviation (SD) and coefficient of variation (CV; standard deviation divided by mean reflectance), which were calculated across all wavelengths, on each of the three dates, at four scales: within individual canopies, among individuals of a species, among species, and among communities. Variability was quantified using the original reflectance dataset as well as each of the three smoothed datasets. Within-individual spectral variability was calculated across all wavelengths for each individual on each of the three dates, and then a mean was taken across individuals of each of the eight species. Spectral variability among individuals of each species was calculated. Last, spectral variability among species was calculated.

To determine at which times and over which spectral regions variability within canopies and among individuals of a species exceeded variability among species, a ratio of variability at finer organizational scales (within individual canopies and among individuals of the same species) compared to among species was calculated by dividing the CV or SD for each wavelength at each scale by the among-species CV or SD, using the original and three smoothed datasets. Ratios of spectral variability were very similar for both CV and SD ratios in the 5 nm and 10 nm smoothed datasets, which increased confidence in interpreting a single metric (CV or SD ratio) in a single smoothed dataset (5 nm or 10 nm).

To examine the composition of spectral variability, I used linear mixed-effects models with random intercepts for field, species, and individual to partition the variance into four different levels: among the plant communities across fields, among the species, among individuals within a species, and among the pixels within an individual canopy. A mixed-effects model was run for each wavelength on each date. Linear mixed-effects models do not require balanced groups and are ideal for nested data such as these.

To associate spectral variability with spectral regions and biologically meaningful traits, I examined the patterns in variability in key spectral regions (blue, 450 to 495 nm; green, 495 to 570 nm; yellow-orange, 570 to 620 nm; red 620 to 690 nm; red edge 690 to 760 nm; and NIR 760 to 950 nm) and in spectral regions found to be important in empirical studies using aerial hyperspectral remote sensing to model traits in temperate, broadleaf forests (Table 1).

3. Results

3.1 Comparing spectral variability at finer organizational scales to among-species variability

3.1.1 Within individuals

Variability within individuals exceeded variability among species increasingly as the growing season progressed: for more species, in more spectral regions, and to a greater extent. Early in the growing season (DOY 134, top panel in Figure 2), only one species (*J. virginiana*) exhibited spectral variability among individuals that exceeded spectral variability among species, most of which was in the yellow-orange spectral region. The maximum CV ratio (1.1) occurred at 694 nm. During mid-growing season (DOY 178, second panel in Figure 3), all but two species (*E. umbellata* and *R. davurica*) exhibited greater spectral variability among individuals than among species, most of which was in the green and yellow-orange spectral regions, and some of which was in the red edge. The maximum CV ratio (1.4) occurred at 703 nm in *L. maackii*. In late summer (DOY 249, bottom panel in Figure 2), spectral variability among individuals exceeded spectral variability among species in all eight species. Most of the variability was in the green, yellow-orange, and red edge spectral regions, with fewer in the red region. The maximum CV ratio (1.7) occurred at 707 nm in *A. altissima*.

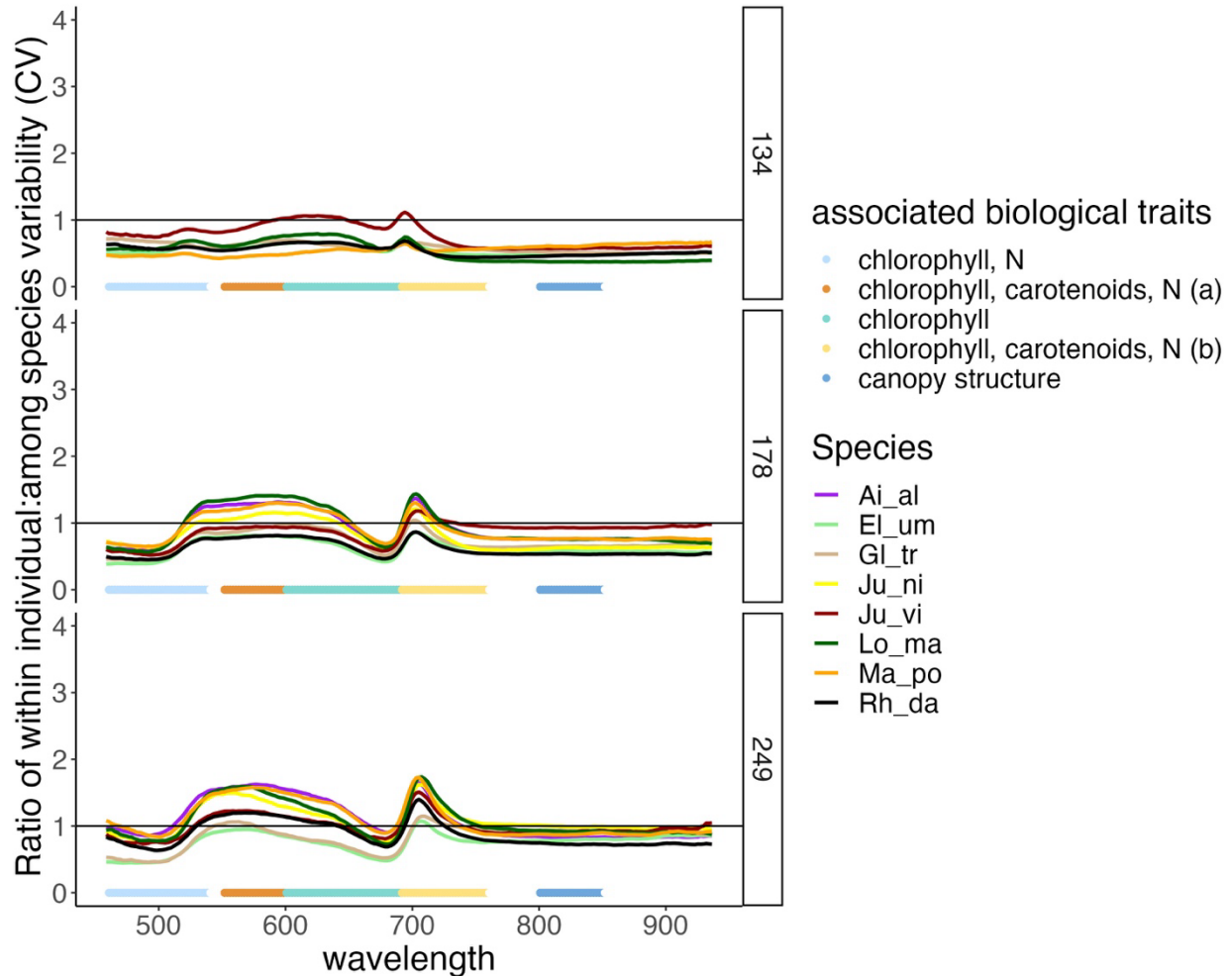


Figure 2. Ratio of within-individual to interspecific variability, averaged by species, quantified as ratios of CV (standard deviation normalized by the mean) over all wavelengths, 450 to 950 nm. Values >1 (marked with a solid black line) indicate greater variability within individuals than among species for a given wavelength. Each figure contains three rows, which represent early, mid- and late growing season. Each curve is for a single species: *A. altissima* (Ai_al), *G. triacanthos* (Gl_tr), *J. virginiana* (Ju_vi), *M. pomifera* (Ma_po), *E. umbellata* (El_um), *J. nigra* (Ju_ni), *L. maackii* (Lo_ma), and *R. davurica* (Rh_da). To aid in digestibility and interpretability, ratios were calculated using smoothed reflectances from the 10 nm window, and the band at the bottom is colored by biologically meaningful spectral regions. See Figure S1 for more details.

3.1.2 Among individuals (within a species)

Variability among individuals of a species also exceeded variability among species increasingly as the growing season progressed: for more species, in more spectral regions, and to a greater extent. Early in the growing season (DOY 134, top panel in Figure 4), only three species (*G. triacanthos*, *J. virginiana*, and *L. maackii*) had greater spectral variability among individuals than among species, most of which occurred in the yellow-orange spectral region. The greatest CV ratio (1.3) occurred at 696 nm in *J. virginiana*. Mid-growing season (DOY 178, second panel in Figure 4), five species (*A. altissima*, *G. triacanthos*, *J. nigra*, *J. virginiana*, and *M. pomifera*) exhibited greater spectral variability among individuals than among species, most of which was in the green, yellow-orange, and red edge spectral regions. The greatest CV ratio (2.0) occurred at 705 nm in *J. virginiana*. In late summer (DOY 249, bottom panel in Figure 4), all but two species (*E. umbellata* and *J. nigra*) exhibited spectral variability among individuals that exceeded spectral variability among species, most of which was in the blue, green, yellow-orange, red, and red edge spectral regions, and some of which was in the NIR spectral region. The greatest CV ratio (2.8) occurred at 707 nm in *A. altissima*.

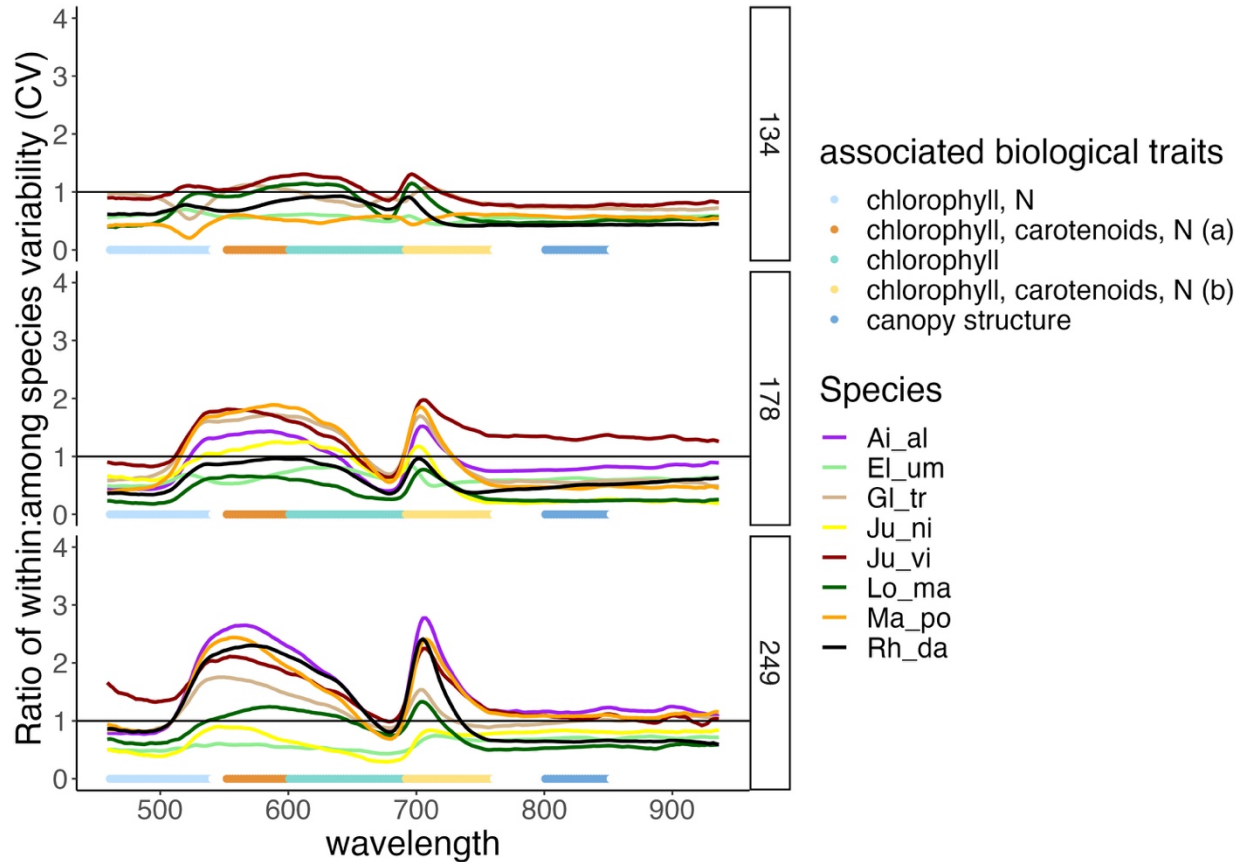


Figure 3. Ratio of within-species (among individuals of a species) to among-species variability, quantified as ratios of CV (standard deviation normalized by the mean) over all wavelengths, 450 to 950 nm. Values >1, which is marked with a solid black line, indicate greater variability within individuals than among species for a given wavelength. Each figure contains three rows, which represent early, mid- and late growing season (DOY 134, 178, and 249 respectively). Each curve is for a single species: *A. altissima* (Ai_al), *G. triacanthos* (Gl_tr), *J. virginiana* (Ju_vi), *M. pomifera* (Ma_po), *E. umbellata* (El_um), *J. nigra* (Ju_ni), *L. maackii* (Lo_ma), and *R. davurica* (Rh_da). To aid in digestibility and interpretability, ratios were calculated using smoothed reflectances from the 10 nm window, and the band at the bottom is colored by biologically meaningful spectral regions. See Figure S1 and Table S1 for a summary of species with greater variability at finer organizational scales.

3.1.3 Biological significance of variable spectral regions

Within- and among-individual variability were greatest and often exceeded among-species variability in spectral regions that correspond with biochemical traits, and that have been used widely to accurately predict chlorophyll, carotenoids, and N (Hoeppepner et al., 2020; J. Wang et al., 2016; Z. Wang et al., 2020; Yang et al., 2016). Among-individual variability within some species exceeded among-species variability in spectral regions associated with biochemical traits, even early in the growing season. As the growing season progressed, additional spectral regions associated with chlorophyll, carotenoids, and N also became more variable, and spectral regions associated with canopy structure (Wang et al. 2016) also were more variable mid- and late growing season among individuals.

3.2 Partitioning spectral variance

The relative contribution of the four levels of organizational scale (among plant communities across fields, among species, among the individuals within a species, and among the pixels within an individual canopy) to total variance differed over time and across wavelengths. Early in the growing season (DOY 134), spectral variability among species was greater than spectral variability among communities, among individuals of a species, and within individuals across all wavelengths. Variability within individuals and species contributed approximately equal parts of the total variance (ranging from ~15 to 25%), although variability among individuals was greater in green and NIR regions, whereas variability within individuals was greater in the blue and red edge (Figure 7, left panel).

Mid-growing season (DOY 178), the contribution of within-individual variability to total variability exceeded variability among species in yellow-orange, red, and red edge spectral regions (~580-645 and ~695-705 nm), with a maximum contribution of 30% to total variability

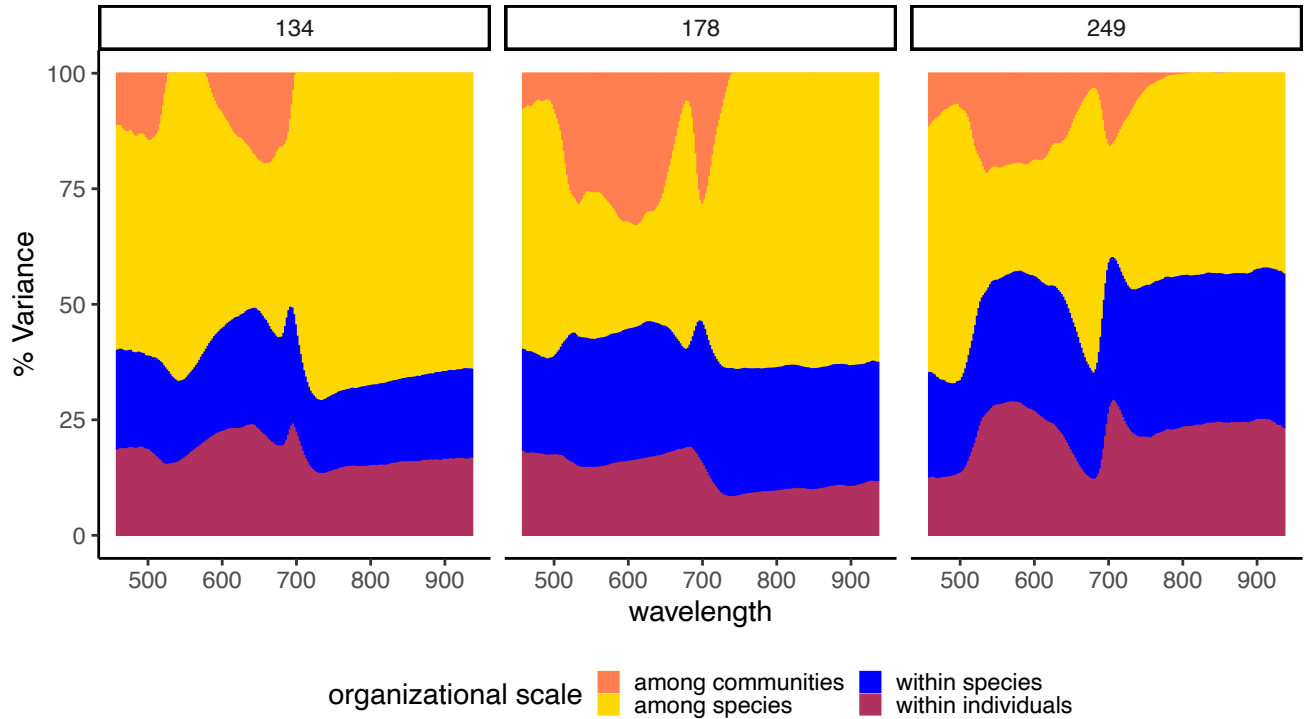


Figure 4. Contribution of intra-individual, intraspecific, interspecific, and inter-community variance to total variance over all wavelengths, 450 to 950 nm. Each panel, left to right, represents each date.

in the red edge at 700 nm. For all wavelengths, variability within individuals comprised more of the total variability (ranging from 20 to 30%) than variability among individuals did (ranging from 9 to 19%) across all wavelengths. Variability among the communities also exceeded variability among species in the same regions, with a maximum contribution of 33% to total variability in yellow-orange bands at 610 nm (Figure 7, center panel).

Late in the growing season (DOY 249), the contribution of among-species variability was greatest in the red bands ~680 nm (~62% contribution to total variance), but it was exceeded by both finer organizational scales in some other spectral regions. Variability within individuals ranged from 19 to 33% of the total variability, and exceeded variability among species in green, yellow-orange, and red edge spectral regions (~535 to 620 and 700 to 715 nm). Variability among individuals ranged from 12 to 30% across all bands and exceeded variability among species in the same spectral regions (~535 to 605 and 700 to 710 nm), with the greatest contribution to total variance in the red edge at 707 nm (Figure 7, right panel).

4. Discussion

4.1 Overview

Both within-individual and among-individual spectral variability increasingly exceeded among-species variability as the growing season progressed. The finer organizational scales (within and among individual canopies) demonstrated similar temporal trends in spectral variability; the number of species with greater variability at fine scales, the number of bands with greater variability at fine scales, and the magnitude of the variability all increased from early to late in the growing season. This suggests that more traits become more variable at finer organizational scales as leaves mature from mid- to late growing season. The spectral regions in which the greatest variability occurred also exhibited similar trends for both organizational scales, shifting from shorter wavelengths to longer wavelengths in the red edge (695 nm to 707 nm). This shift in maximum variability could be linked to the shift in the red edge slope, caused by broadening (or narrowing) of the chlorophyll absorption feature ~680 nm as the growing season progresses (Boochs et al., 1990; Buschmann & Nagel, 1993; T. P. Dawson & Curran, 1998).

The large increase in variability within individuals from early to mid-growing season in spectral regions associated with biochemical traits suggests that canopies become more heterogeneous in N and photosynthetic pigments during the first half of the growing season. Although among-species variability was greatest compared to variability at finer organizational scales early in the growing season, due to phenological differences among species, photosynthetic pigments and canopy structure likely become more homogeneous among species toward mid-growing season and peak greenness and biomass. The increased spectral variability at finer resolutions from mid- to late growing season was partly driven by a decrease in among-species variability in blue and red spectral regions, suggesting species did indeed become more homogeneous in some traits.

Although the two organizational scales exhibited a similar overall increase in variability, which species and which spectral regions exhibiting those increases varied, as did the magnitude of variability. Generally, among-individual spectral variability exceeded among-species variability in more species, in more spectral regions (including canopy structural traits), and to a greater degree than within-individual spectral variability did. This is a logical extension of the spectral phenotype; individuals across a landscape are subjected to greater differences in conditions and resource availability compared to within a single canopy. The CV ratios suggest that chlorophyll, carotenoids, and N can vary nearly twice as much (1.7) within individuals as they do among species and nearly three times as much (2.8) among individuals.

Canopy structure can also vary more among individuals within a species than among species in mid- and late growing season, though not to the same extent as biochemical traits (CV ratios of ~1.1 to 1.3). These results align with Siefert et al. (2015), who found that spectra associated with leaf nutrient concentrations tended to vary more among individuals, while those

associated with morphology tended to be more stable. This pattern of greater variability in leaf nutrient concentrations than morphology was also found in traits themselves (Kazakou et al., 2014; Rozendaal et al., 2006).

4.2 Species-specific patterns in variability at finer organizational scales

Early in the growing season, interspecific differences were expected to be greatest due to phenological differences among species, which result in differences in the timing of chlorophyll concentration increases. Although this was the case for most species and most spectral regions, both within-individual and among-individual variability in *J. virginiana* exceeded among-species variability in yellow-orange bands by up to ~10% and 30% (CV ratios of 1.1 and 1.3). As the only coniferous species in the plant community, this could potentially be explained by its evergreen traits and therefore a lack of young leaves and differing phenology compared to the other species. Two additional species also exhibited slightly greater (~10%) spectral variability among individuals across the landscape, *G. triacanthos* and *L. maackii*. The spectral variability observed among *G. triacanthos* individuals could be due to low leaf area index (LAI), which could lead to spectral interference from neighboring or understory plants, especially as its leaves emerge relatively late and may have not fully matured by the date of data collection. Although *L. maackii* leaves emerge much earlier, interference from neighboring or overstory plants may have led to the slightly elevated among-individual variability.

Mid-growing season, spectral variability within and among individuals exceeded among-species variability in some spectral regions for a majority of the species, however, two invasive shrub species, *E. umbellata* and *R. davurica*, exhibited less spectral variability at both finer organizational scales. A third invasive shrub species, *L. maackii* also exhibited less spectral

variability among individuals (although not within individuals). As invasive plants tend to be more tolerant of a wide range of conditions, their similarities among individuals across the landscape suggest that they may respond to environmental changes less than other species will (Treurnicht et al., 2020). The high intraspecific variabilities of *A. altissima* and *M. pomifera* relative to interspecific variability suggest these individuals are more variable across a landscape. These results make sense in the context that leaves emerge in *A. altissima* and *M. pomifera* later than most other species in these communities, and there is greater heterogeneity in leaf pigments in young leaves.

Late growing season, all but *E. umbellata* and *J. nigra* exhibited greater spectral variability within individuals than among species in spectral regions associated with biochemical traits, and all eight species exhibited greater variability among individuals in spectral regions associated with biochemical traits and structural traits. As a canopy-level trait, canopy structure is more sensitive to environmental conditions than leaf-level traits. The increased variability in spectral regions associated with canopy structure among individuals within a species is expected due to phenotypic plasticity (Marks, 2007).

4.2 Partitioning variability among organizational scales

When among-community variability was incorporated into the analysis (through variance partitioning), spectral variability among species was greater than variability at all other organizational scales across all wavelengths early in the growing season. This suggests that the slightly greater spectral variability observed among individuals within *J. virginiana*, *G. triacanthos*, and *L. maackii* had a spatial component and was caused by variability among communities. The contributions of variability within and among individuals to total variance were

approximately equal, which implies that processes at each of these scales are equally important in determining trait values (Messier et al., 2010).

Despite approximately equal contributions to total variance early in the growing season, there were differences in magnitudes of variability across bands. Blue and red regions were more variable within individuals, whereas green and NIR were more variable among individuals. This suggests that within-individual variability was caused by differences in chlorophyll content among leaves within canopies, whereas variability in structure also contributed to variability among individuals. These results elucidate functional variation at different ecological scales, which is a critical component of biodiversity research (Schweiger et al., 2018). Nevertheless, the spectral variabilities at each of these fine organizational scales were less than that of among-species early in the growing season. These results of overall greater among-species variability are consistent with the SVH and with those of Roberts et al. (2004), who also found low spectral variance within species in May.

When mid-growing season variances were partitioned across organizational scales, and variability among communities was also considered, variability within individuals was greater than variability among individuals across all wavelengths. This suggests that leaf-level traits are more variable than canopy-level traits overall. It also suggests that the greater variability observed within individual species, especially in yellow-orange bands, was driven by environmental differences across the landscape. Because variability among communities did not contribute to total variance in the NIR, the structural differences observed among individuals of a species can be assumed to be driven by canopy-level traits rather than spatial variability in conditions.

Later in the growing season, within-individual and among-individual spectral variability contributed to over half of the total observed spectral variation in the green, yellow-orange, and

red edge spectral regions, which are associated with biochemical traits. Additionally, among-individual variability was very high in the NIR spectral region, which is associated with structure. The contribution of variability among species was greatest in blue and red spectral regions (~60% of total variability) but was otherwise exceeded by variability at finer organizational scales.

The results of greater variability in some trait-associated spectral regions are aligned with those of others; Jónsdóttir et al. (2022) found that intraspecific trait variability ranged from 30 to 71% of total trait variation. Globally, intraspecific trait variation accounts for ~25% of plant community trait variation (Siefert et al. 2015), with greater variation seen locally (Messier et al. 2017; Thomas et al. 2020). This makes a strong case for trait-based rather than species-based approaches to ecological modeling, as intra-individual and intraspecific variability in leaf chemical traits have implications for ecosystem functions such as primary productivity, nutrient cycling, and decomposition rates (Quested et al. 2007; Cornwell et al. 2008).

4.3 Potential issues and future work

Roberts et al. (2004) found that interspecific variability was driven mostly by differences between broadleaf and conifer species. Because the common species occurring in these studied plant communities only included one conifer species (*J. virginiana*), interspecific variability may be lower than in other communities. Because the interspecific variability is not small, this indicates that there is strong variability, even in a largely broadleaf species community.

Spectral signatures in aerial images are subject to the influence of several factors: illumination and viewing geometry impact absorption, reflectance, light-scattering, and shadows. These factors can be minimized but not entirely avoided. Viewing geometry variation is likely not a serious issue in this study, as the total field of view of the sensor was only 21.1 degrees (viewing

zenith angle of 10.55 degrees), and the data were collected within two hours of solar noon. Biochemical absorption features are accentuated by photon scattering among leaves, which changes with crown architecture. Therefore, biochemical properties may be differentially impacted across species, depending on canopy structure. Because of this possible confounding factor, using empirical spectra-trait relationships based on aerial hyperspectral remote sensing of temperate, broadleaf forests was key to examining the ecological implications of the ways in which variability was partitioned over the growing season. Future work could further examine the crown structure, its impacts on viewing geometry, and subsequent spectral patterns, as leaf arrangement in canopies may be driving some observed variability.

5. Conclusion

The first two goals of this study were to determine the times in the growing season and spectral regions in which variability within and among individuals exceeded variability among species, serving as exceptions to the SVH. I found that among-species variability was greatest early in the growing season, supporting the SVH, but as the growing season progressed, both within-individual and among-individual spectral variability increasingly exceeded among-species variability in several spectral regions.

The third goal was to assess the biological significance of spectral variability at different organizational scales. The number of species and number of bands with greater variability at fine scales, as well as the magnitude of the variability, all increased from early to late in the growing season, which suggests that more traits become more variable at finer organizational scales as leaves mature from mid- to late growing season. The large increase in variability within individuals from early to mid-growing season in spectral regions associated with biochemical traits suggests

that canopies become more heterogeneous in N and photosynthetic pigments during the first half of the growing season. Phenological differences among species likely drove the greater variability among species early in the growing season, however, photosynthetic pigments and canopy structure likely become more homogeneous among species toward mid-growing season and peak greenness and biomass. Canopy structure also varied more among individuals within a species than among species in mid- and late growing season, though not to the same extent as biochemical traits, which is in agreement with more stable morphological traits.

Understanding intra-individual and intraspecific trait variation can facilitate answering major questions in community ecology (Siefert et al., 2015), in which functional traits are used to make generalizable predictions across organizational and spatial scales (Adler et al., 2013). These results support that leaf-level and canopy-level traits are sensitive to variable environmental conditions across a landscape for most species. This work provides an additional framework for trait-based functioning by examining functional variability via spectroscopy at various ecological scales and at different times intra-annually. Spectral variability can serve as a novel lens through which to examine varied species responses to environmental changes (Bolnick et al., 2003; Milla et al., 2009; Vellend & Geber, 2005).

I thus provide information regarding spectral phenotypes, the combination of genetic information and response to the environment of the plant over the course of its lifetime. The spectral phenotype varies among and within individuals, within a growing season, and over longer time periods. By identifying the importance of within-canopy and among canopy variation in visible and NIR wavelengths, particularly as the growing season progresses, I further highlight the importance of functional traits as opposed to species-based traits for ecosystem analyses.

Chapter 5: Spectral variability and biodiversity across scales in an early successional plant community

Abstract

The spectral variation hypothesis (SVH) is a logical connection between species and spectral diversity, by way of trait diversity. The SVH is, however, not universally supported, as both phenotypic plasticity and variability inherent to remote sensing affect spectral signals. Alpha and beta spectral and biological diversity can clarify the applicability of the SVH and elucidate ecosystem dynamics, including trait and functional diversity, community stability, habitat heterogeneity, and invasion. Spectral diversity is rarely compared to explicit biodiversity data at multiple scales, but the abundantly available biodiversity and spectral data provide the opportunity to do so. Linking spectral and biological diversity data also would improve their interoperability and complementary use to fill data gaps. I found that spectral variability within plots was greater in biochemical traits than in structural traits, but greater in structural traits than biochemical traits among plots. Overall, this invaded early successional plant community did not exhibit patterns consistent with the SVH. Invaded plots agreed with the SVH less often than non-invaded plots did. The lack of agreement in invaded plots was linked to a combination of misaligned biodiversity metrics (e.g. higher evenness with few species or low evenness with many species) and the low spectral diversity that tends to be seen in invaded plots. The two non-invaded plots that did not

agree with the SVH appeared to exhibit phenotypic plasticity (within canopy spectral variability) and scale exceptions. Despite the overall lack of agreement with the SVH at this scale in this early successional plant community, plot-specific patterns provide context for the lack of agreement. These methods also provide a framework through which the SVH can be evaluated and assessed across times and scales to improve applications.

1. Introduction

Preserving plant biodiversity is a conservation priority, as its loss decreases ecosystem functioning and stability (Cardinale, 2011). Biodiversity preservation requires extensive ecosystem monitoring across the globe to identify conservation priorities (Barnosky et al., 2011). Ecosystem monitoring can be done on the ground or remotely from the air; each approach has its own benefits and limitations. Aerial imagery can provide information with large spatial extents but often with resolutions greater than the size of individual plants (Pettorelli et al., 2018). Ground-based observations can be used to detect individual plants, but the time and energy required for large-scale surveys makes it cost-prohibitive for large spatial extents (Kays et al., 2015; Pimm et al., 2015). Imaging spectroscopy or hyperspectral remote sensing has become increasingly popular in aerial observations of ecosystems (Féret & Asner, 2014; R. Wang & Gamon, 2019). Hyperspectral remote sensing provides a unique opportunity to measure plant properties and gain better understanding of plant communities over large areas (G. P. Asner et al., 2017; Jetz et al., 2016). Thus, a remote sensing approach to monitor biodiversity at the global level is a promising avenue (Geller et al., 2020; Pereira et al., 2013; Scholes et al., 2012; Turner, 2014)

The long-term evolutionary history of a plant species, including the historical climate and disturbance regimes of its environment, are preserved through the genotype, which includes biochemical and structural properties that shape hyperspectral signatures. For example, traits associated with the leaf economic spectrum (Wright et al., 2004), such as specific leaf area or foliar N can be estimated with reasonable accuracy using hyperspectral remote sensing (Gregory P. Asner & Martin, 2008b; Azadnia et al., 2023; Chance et al., 2016; Ely et al., 2019; Kothari et al., 2023; Mahlein et al., 2010; Mutanga et al., 2004; Serbin et al., 2014; Thenkabail et al., 2014; Xiao et al., 2014), which allows for the differentiation between fast-growing, opportunistic plant species and

slower-growing, conservative and competitive plant species (Cavender-Bares et al., 2020; Díaz et al., 2016; Reich, 2014). The Spectral Variation Hypothesis (SVH) argues that spectral diversity is correlated with trait diversity and is thus also correlated with species diversity (Palmer et al., 2002). A slightly different framing of the SVH is that spectral heterogeneity implies a greater number of available ecological niches and greater species diversity (Rocchini et al., 2004). Spectral diversity may indicate high diversity areas (high alpha biodiversity) or heterogeneous areas (high beta biodiversity), which are both useful criteria in assigning ecological value (Laliberté et al., 2020).

Although genetics shape the spectral signatures of vegetation, other factors do as well. Short-term environmental drivers, such as changes in resource availability or species interactions, can also change characteristics, which then change signatures (Laliberté et al., 2020; Z. Wang et al., 2020). The physical expression of the genotype through spectroscopy, shaped by environmental conditions, is referred to as the spectral phenotype. Phenotypic plasticity, or varying phenotypes for a single genotype (Bradshaw, 1965; Marais et al., 2013; Scheiner, 1993), can occur across many temporal and spatial scales, e.g. over a growing season, across multiple growing seasons, within a single canopy, across multiple biomes, and globally (Dronova et al., 2021; J. Wang et al., 2023). Physical factors can also affect how vegetation reflects incoming solar radiation and how that reflected radiation is then perceived by a sensor. Varying illumination and sensor viewing geometry can both affect a spectral signature. The spatial resolution (pixel size) also affects a spectral signature (Huelsenman et al. 2024, in preparation).

The SVH is a logical connection between species diversity and spectral diversity, by way of trait diversity, and it has been supported over broad regions (Bush et al., 2017; Pereira et al., 2013; Turner, 2014). The SVH is true if alpha spectral diversity and biodiversity are correlated in communities or ecosystems. Phenotypic plasticity and physical characteristics of remotely sensed

imagery suggest that the relationship between spectral variability and biodiversity is not universal, and exceptions to the SVH occur (Fassnacht et al., 2022; Marks, 2007; Rocchini et al., 2010; Schmidtlein & Fassnacht, 2017; Schweiger et al., 2018). Exceptions could include cases where characteristics differ more within a species than among species (i.e. phenotypic plasticity), the spatial resolution is greater than the size of individual plant canopies, or if the spatial resolution is greater than the grain size at which biological diversity varies (i.e. physical characteristics of images; Marconi et al., 2022).

Alpha and beta spectral diversity and biodiversity can inform not only our understanding of the applicability of the SVH but also of ecosystem dynamics (Adler et al., 2013). In plant communities that adhere to the SVH, high alpha spectral diversity paired with high alpha biodiversity suggests trait or functional diversity, species diversity, and long-term coexistence (Adler et al., 2013; Rocchini et al., 2021). This is a spectral extension of the classic concept of niche partitioning, or the variability in traits and resource use within a community that minimize competitive forces (Chesson, 2000). Low alpha spectral diversity paired with low alpha biodiversity suggests plots may be dominated by a few plant species with similar traits (Rocchini et al., 2021). As invasive plants tend to dominate plant communities due to their competitive traits, which also impact spectra, this could be a sign of invasion (Cavender-Bares et al., 2020; Matongera et al., 2016). In cases where spectral diversity is not correlated with biodiversity, spectral variability both within plots (alpha) and among plots (beta) can still indicate details about community assembly and ecosystem functioning (Cadotte et al., 2009; C. M. Clark et al., 2012; Cornwell et al., 2006; Laliberté et al., 2020). For example, high spectral diversity paired with low biodiversity suggests within-species variability or phenotypic plasticity. Low alpha spectral

diversity paired with high alpha biodiversity suggests more functionally similar plant communities that may be less stable due to overlap in strategies (e.g. traits and resource use).

Although the magnitudes of alpha and beta spectral diversity cannot be directly compared, the variability of spectral regions relative to each other within each level can be compared. Greater beta spectral diversity in a spectral region suggests greater heterogeneity across the landscape in the associated trait (Jost, 2007; Whittaker, 1972). Trait heterogeneity can be considered in the context of heterogeneity of abiotic landscape conditions (e.g. differences in soil moisture and sunlight due to slight variations in topography and aspect, which would be very slight in this case, as these sites at BEF are on low-relief topography) or in the context of biodiversity.

Spectral diversity is rarely compared to explicit biodiversity data at multiple scales (Gamon et al., 2020; Torresani et al., 2024), but linking them in a spatially explicit way would benefit global conservation efforts. Biodiversity repositories (e.g. the Global Biodiversity Information Facility) and available aerial hyperspectral images (e.g. NASA's upcoming Surface Biology & Geology satellite) could be leveraged to fill gaps due to missing or incomplete data in either dataset with an improved understanding of the spectral diversity-biodiversity relationship. To evaluate the SVH and to elucidate patterns in plant community dynamics, I pair plot-level and community-level biodiversity data with aerial hyperspectral imagery collected at Blandy Experimental Farm and answer the following questions:

1. How do alpha, beta, and gamma biodiversity and spectral diversity compare in an early successional plant community?
2. How does integrating spectral variability inform our understanding of ecosystem dynamics in this system?

3. Do patterns in alpha spectral diversity and alpha biodiversity support the SVH at this scale in this ecosystem?

Methods

2.1 Study site

Aerial imagery and vegetation composition data were collected in 2021 at the ~280 ha biological field station Blandy Experimental Farm (BEF) biological field station in northwestern Virginia (39.06°N, 78.07°W). The early successional vegetation communities surveyed were last disturbed ~25 years prior. Communities were located on low-relief topography within ~500 m of each other. Invasive plant species, including *Elaeagnus umbellata* (autumn olive) and *Rhamnus davurica* (Dahurian buckthorn), were present within a heterogeneous matrix of native and non-native forbs, graminoids, shrubs, and trees. Commonly occurring forb and shrub species include *Rubus spp.* and *Solidago altissima* (tall goldenrod). Commonly occurring tree species include *Maclura pomifera* (Osage orange) and *Gleditsia triacanthos* (honey locust). Plots 5 m x 5 m in size were randomly selected in the landscape but stratified with either high (>25% relative plot cover) or low (<25% relative plot cover) levels of *R. davurica* invasion.

2.2 Data collection & post processing

2.2.1 Aerial hyperspectral imagery

Aerial hyperspectral images were collected by fixed-wing aircraft by the National Ecological Observatory Network (NEON) Aerial Observation Platform (AOP), which collects data on a near-annual basis during times with > 90% maximum greenness (> DOY 150 at BEF). Reflectance images were corrected by NEON for atmospheric and illumination effects using the

Atmospheric and Topographic Correction (ATCOR) and stitched together on an orthorectified UTM projection with 1 m spatial resolution.

Spectral data cubes were downloaded from NEON's Application Programming Interface using the `neonUtilities` R package (Lunch et al., 2024) for locations that overlapped with surveyed vegetation plots. Quadrats slightly larger than the surveyed plot size (6 m x 6 m rather than 5 m x 5 m) were extracted from the reflectance data cubes to provide a slight buffer for plots not oriented perfectly parallel to compass directions. The final dataset included reflectance data restricted to VNIR bands (400 to 1100 nm) for 36 pixels centered on the coordinates of each individual plot location. Non-vegetation and shadow pixels were removed from the images, which resulted in a loss of pixels in several plots due to cloud cover. Last, all pixels were examined for irregularities that would suggest their removal.

Because of variable cloud cover in images, the number of well-lit vegetation pixels from the aerial imagery in each plot differed. To ensure that spectral diversity would not be driven by the number of pixels (e.g. if more pixels would automatically demonstrate greater diversity), I assessed the relationship between sample size and variability. I found that when randomly selecting pixels from plots, variability saturated at 15 pixels (out of 36 maximum). Thus, any plots with fewer than 15 pixels were eliminated, which removed ten and left ten plots, five of which were highly invaded and five of which were not.

2.2.2 Vegetation surveys

Vegetation surveys were completed in each plot using a point-frame method to determine plant species composition. The point-frame method establishes a theoretical grid over the 25 m² plot with vertices at every 0.5 m, for a total of 121 vertices. Every plant species touching each vertex was recorded, and relative frequencies of each species were calculated (Bergman, 2022).

2.3 Calculating diversity metrics

2.3.1 Spectral diversity

The spectral diversities within and among plant communities were assessed using a common metric for spectral diversity, the coefficient of variation (CV), which is the standard deviation of reflectance in each band normalized by the mean reflectance (Gholizadeh et al., 2018; Hall et al., 2010; Oindo et al., 2002; R. Wang et al., 2018). Variance is used synonymously with spectral diversity and is not only argued to be the most direct route to quantifying spectral diversity, as it doesn't require *a priori* decisions about the appropriate number of categories to use to classify pixels into "spectral species," but it also allows for comparison across regions and ecotypes (Laliberté et al., 2020; Figure 1).

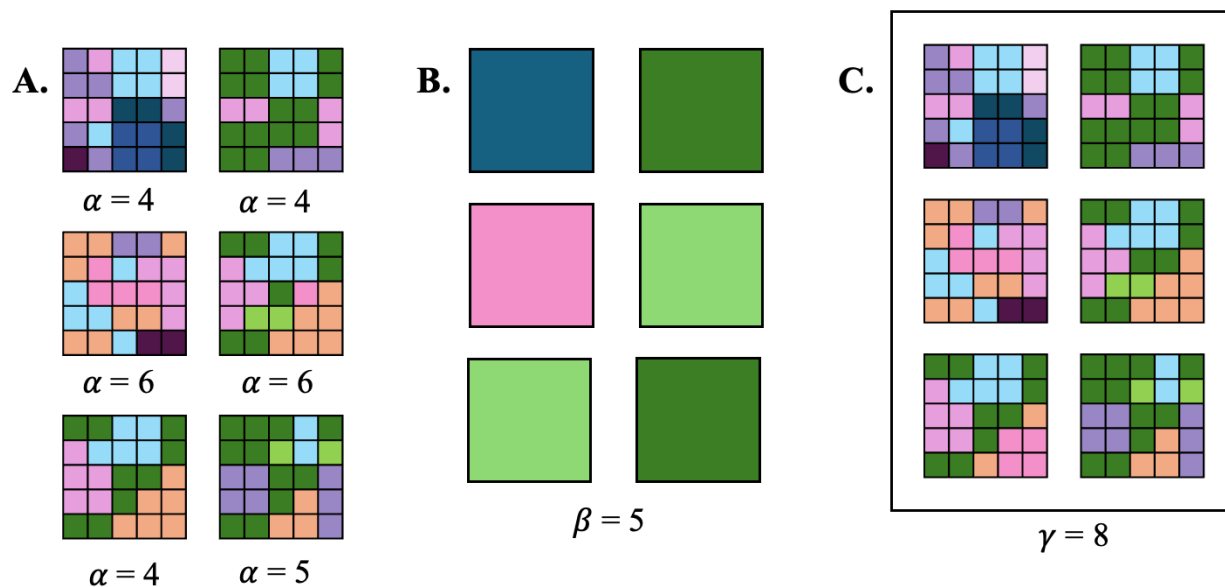


Figure 1. A theoretical diagram of alpha (A), beta (B), and gamma (C) spectral diversity. Although this demonstrates spectral "categories" (seen as different colors), calculating the coefficient of variation (the normalized standard deviation) provides a similar summary but without requiring *a priori* decisions about the appropriate number of categories to use to classify.

The CV was calculated for every band within plots (alpha spectral diversity) and across all plots (gamma spectral diversity). Beta spectral diversity was derived by dividing gamma by the mean alpha spectral diversity. The wavelength-specific spectral diversity metrics at each scale (alpha, beta, and gamma) were compared. To simplify the analysis of spectral diversity, several summary statistics of CV were calculated (e.g. the mean, maximum, range, and percent of bands with variability in the 67th percentile or greater) for several spectral regions (e.g. across all bands, grouped by spectral regions 100 nm in width, and grouped by biologically meaningful band ranges). The band ranges selected as biologically meaningful had been found to be associated with vegetation traits in aerial imagery in temperate forests (Table 1).

Table 1. Spectral regions as ranges of bands found to predict specific traits in empirical studies that used aerial hyperspectral remote sensing to model traits in temperate, broadleaf forests. Because these spectral regions were used in Table 2 their codes are included here for reference.

Spectral region	Linked trait	Code	Reference
460-540 nm	Chlorophyll, N	$CV_{\text{chlor, N}}$	(Hoeppner et al., 2020; R. Wang et al., 2018)
550-600 nm	Chlorophyll, carotenoids, N	$CV_{\text{chlor, car, N (GY)}}$	(Hoeppner et al., 2020; J. Wang et al., 2016; Z. Wang et al., 2020; Yang et al., 2016)
600-690 nm	Chlorophyll	CV_{chlor}	(Hoeppner et al., 2020)
690-760 nm	Chlorophyll, carotenoids, N	$CV_{\text{chlor, car, N (RE)}}$	(Hoeppner et al., 2020; Muraoka et al., 2013; J. Wang et al., 2016; Z. Wang et al., 2020; Yang et al., 2016)
800-850 nm	Canopy structure	$CV_{\text{canopy structure}}$	(J. Wang et al., 2016)
940 nm	Leaf mass per area (LMA)	CV_{LMA}	(Z. Wang et al., 2020)

2.3.2 Biodiversity

Two biodiversity metrics were calculated from the species composition data: species richness (Equation 1; Whittaker 1960) and Shannon diversity (Equation 2; Shannon, 1948). Species richness does not consider the abundance of each species, whereas Shannon's diversity index incorporates both richness and evenness into one metric. The total number of species in each plot and across all plots, representing alpha species richness and gamma species richness, respectively, were directly calculated from the species composition data. The beta species richness was calculated by dividing the gamma by the mean alpha. Shannon diversity was also calculated directly for the alpha level as the negative sum of the relative frequency of each species multiplied by the natural log of its relative frequency within each plot.

Richness: s (Equation 1)

Shannon diversity: $-\sum_{i=1}^s p_i \ln(p_i)$ (Equation 2)

Where s is total number of species in a plot (alpha) or in the entire landscape (gamma)

p_i is the relative frequency of the i^{th} species in the plot (alpha) or in the entire landscape (gamma)

2.4 Comparing biodiversity and spectral diversity

The relationship between each spectral diversity metric and biodiversity metric within each plot (alpha) was examined for correlation using a linear regression to assess whether the SVH is supported at this scale in this ecosystem. The biodiversity metrics (richness and Shannon diversity) were also visually compared to all single-value spectral diversity metrics described in 2.3.1 for each plot to determine their agreement with the theoretical positive correlation of the SVH (Figure 2).

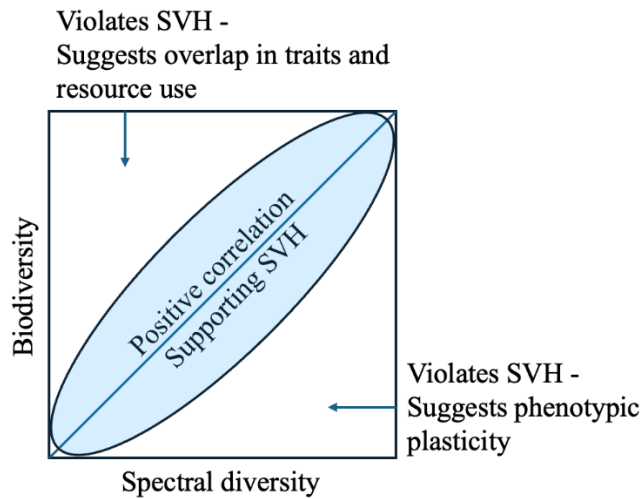


Figure 2. The theoretical positive correlation between spectral diversity and biodiversity that would support the SVH. Regions above the line violate the SVH assumption with low spectral diversity and high biodiversity, which suggest overlap in functional traits and likely resource use. Regions below the line violate the SVH assumption with high spectral diversity but low biodiversity, which suggests phenotypic plasticity at the plot level.

3. Results

3.1 Overall patterns in alpha, beta, and gamma biodiversity and spectral diversity

Across all plots, alpha (plot-level) richness ranged from 7 to 16 species, with a mean alpha richness of 11.9 ± 0.74 species. Gamma richness (total species across all plots) was 43, and beta diversity was 3.61. Across all plots, alpha (plot-level) Shannon diversity ranged from 0.85 to 1.83, with a mean of 1.39 ± 0.1 (Table 2). The overall mean of alpha (plot-level) CV across all bands (CV_{mean} in Table 2) ranged from 0.04 to 0.14, with a mean alpha CV across all plots of 0.09 ± 0.01 . Gamma CV averaged across all bands was 0.14, and beta CV was 1.6. The alpha and beta spectral variability in specific spectral regions followed similar patterns to the overall mean across all bands, with means of alpha spectral variability ~ 0.08 to 0.11, means of gamma spectral variability ~ 0.12 to 0.16, and means of beta spectral variability ~ 1.5 to 1.7 (Table 2).

The lowest mean alpha spectral variabilities (0.08 mean across all plots) were observed in spectral regions associated with chlorophyll, carotenoids, N (Hoeppepner et al., 2020; Muraoka et al., 2013; J. Wang et al., 2016; Z. Wang et al., 2020; Yang et al., 2016) and structural traits (canopy structure and LMA; J. Wang et al., 2016 and Z. Wang et al., 2020), or the green-yellow, red edge, and NIR spectral regions. The lowest beta spectral variabilities (<1.5) were also observed in spectral regions associated with chlorophyll, carotenoids, and N (Hoeppepner et al., 2020; J. Wang et al., 2016; Z. Wang et al., 2020; Yang et al., 2016) or the green-yellow spectral region. The greatest mean alpha spectral variabilities (0.11 mean across all plots) were observed in spectral regions associated with chlorophyll (Hoeppepner et al., 2020), or the orange-red spectral region. The greatest beta spectral variabilities were observed in spectral regions associated with LMA (Z. Wang et al., 2020; Table 2).

Table 2. Alpha, beta, and gamma biodiversity and spectral diversity. Biodiversity metrics, richness and Shannon diversity, were calculated from species composition data, and spectral diversity metrics were calculated from extracted quadrats in NEON aerial imagery as average CV across different ranges of bands: over all bands (CV_{mean}) and over ranges of bands found to predict specific traits in empirical studies (see Table 1).

Diversity metric		$\text{Alpha}_{\text{mean}}$	$\text{Alpha}_{\text{range}}$	Beta	Gamma	
Biodiversity	Richness	11.90 ± 0.74	[7, 16]	3.61	43	
	Shannon diversity	$1.39 \pm .10$	[0.85, 1.83]	---	---	
	Overall	CV_{mean}	0.09 ± 0.01	[0.04, 0.14]	1.6	0.14
Spectral diversity	Biologically meaningful regions	$CV_{\text{chlor, N}}$	0.09 ± 0.01	[0.04, 0.15]	1.54	0.14
		$CV_{\text{chlor, car, N}}$ (GY)	0.08 ± 0.01	[0.03, 0.14]	1.46	0.12
		CV_{chlor}	0.11 ± 0.1	[0.06, 0.17]	1.53	0.16
		$CV_{\text{chlor, car, N}}$ (RE)	0.08 ± 0.01	[0.04, 0.17]	1.60	0.13
		$CV_{\text{canopy structure}}$	0.08 ± 0.2	[0.04, 0.19]	1.59	0.13
		CV_{LMA}	0.08 ± 0.2	[0.04, 0.18]	1.66	0.14

3.1.2 Alpha, beta, and gamma spectral diversity over spectral regions

Alpha and gamma spectral variability were greater in the blue and orange-red spectral regions than other spectral regions, and gamma spectral variability was slightly greater than alpha spectral variability in the red edge. Beta spectral variability was greatest in the blue, red edge, low- and mid-NIR spectral regions (Table 2, Figure 3).

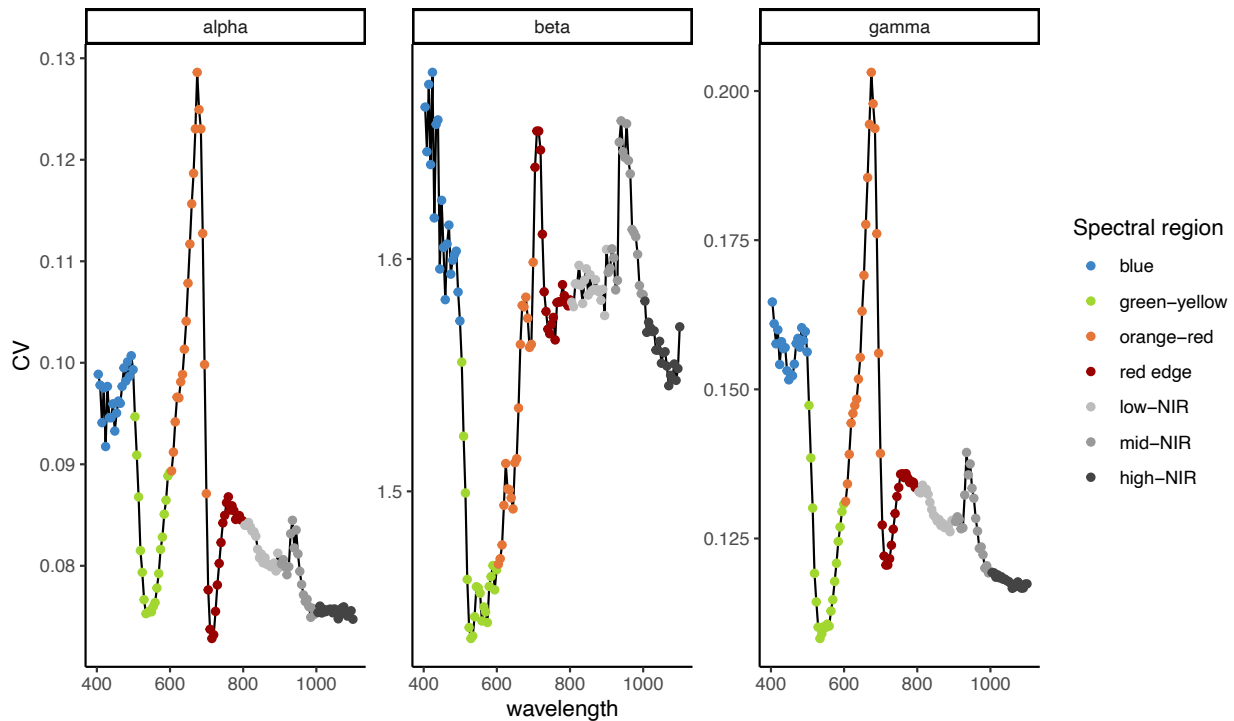


Figure 3. Alpha, beta, and gamma spectral diversity, calculated as the coefficient of variation (CV) at each level for each band.

3.2 Plot-level comparisons of spectral diversity and biodiversity a semi-invaded early successional plant community

There were no significant relationships between plot-level (alpha) biodiversity metrics and their corresponding spectral diversity metric ($p > 0.05$). In plot-level comparisons of spectral diversity and both biodiversity metrics, four of the ten plots adhered to the theoretical positive

relationship between spectral diversity and biodiversity suggested by the SVH (Figure 2). Three of those four plots were less invaded (plots 6, 7, and 8), and the other (plot 4) was invaded by the invasive shrubs *E. umbellata* and *R. davurica*.

Plots that fell outside of the theoretical positive spectral diversity- biodiversity relationship exhibited either low spectral diversity paired with high biodiversity or high spectral diversity paired with low biodiversity (Figure 4). Three plots supported the SVH in only one of the two biodiversity metrics; plot 1, which was heavily invaded by *R. davurica* (78% relative cover), showed agreement with Shannon diversity but not richness, and plots 9 and 10, which were also heavily invaded by *R. davurica* (32% and 29% relative cover), showed agreement with richness but not Shannon diversity. Two plots fell beyond the positive correlation range in both biodiversity metrics, one of which was highly invaded (plot 2), which fell above the range, and two of which were not, which respectively fell above and below the range (plots 3 and 5; Table S2).

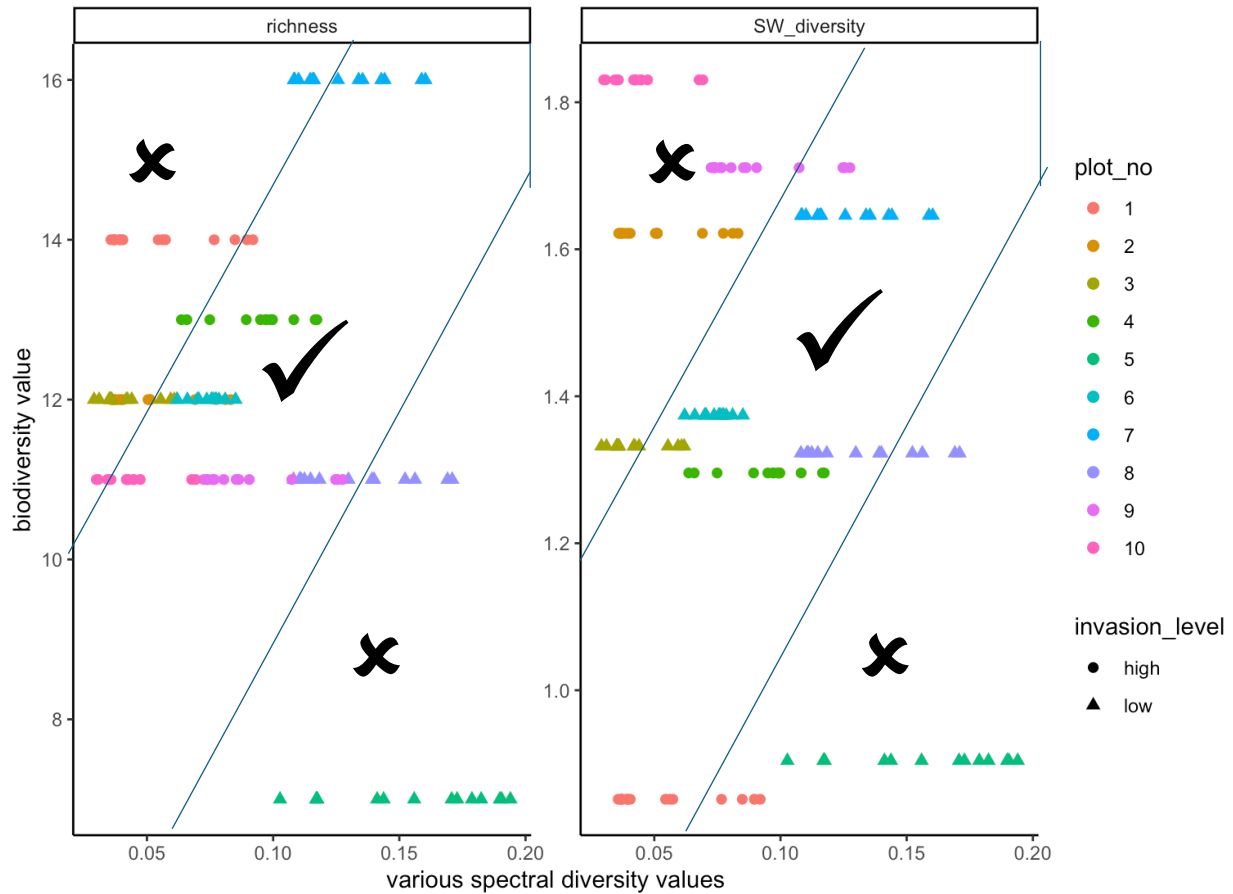


Figure 4. Assessment of various spectral diversity values for each plot (1 through 10) compared to biodiversity values calculated from field-based species composition data. A diagonal segment through the middle of each relationship provided an estimate of plots that fell near the theoretical positive relationship of the SVH and those that did not. If a majority of spectral diversity values fell within the positive relationship boundary for either biodiversity metric, it was considered in agreement with the SVH (the region with a checkmark). Plots with a majority of metrics above or below the line were not in agreement with the SVH (regions with an X). Additional details about each plot can be found in Table S2.

4. Discussion

4.1 Understanding ecosystem dynamics through the lens of alpha, beta, and gamma diversity

Spectral diversity can elucidate dynamics of this landscape. Niche partitioning suggests ecosystem stability. Ecosystems can exhibit niche partitioning and therefore stability in some traits and not in others (Adler et al., 2013). Therefore, examining the spectral diversity of each spectral region relative to others can suggest which traits are more stable and how traits vary across the landscape. The greater alpha and gamma spectral variabilities observed in the orange-red and blue regions compared to other regions suggest that the traits associated with those regions (e.g. chlorophyll absorption bands) vary most among pixels, regardless of observation at the plot-level or at the landscape scale. This suggests plot- and landscape-level niche partitioning in chlorophyll traits.

Both alpha and gamma spectral variabilities were lower in the green, red edge, and NIR than in other spectral regions. In the red edge, alpha spectral variability was least and less than that of gamma spectral variability. These results suggest lower variability in traits associated with those regions (e.g. structure, chlorophyll, carotenoids, and N). This suggests less niche partitioning in accessory photosynthetic traits and structure and therefore less stability (or more interspecific competition) in functions associated with those traits, either within plots (at the alpha or fine-scale level) or among individuals in the community (at the gamma or landscape-scale level). Additionally, the lower alpha spectral variability compared to gamma spectral variability in the red edge suggests that chlorophyll, carotenoids, and N are most similar at the plot level, with the least niche partitioning. This suggests that local plant community compositions may continue to change to maximize niche partitioning both in terms of structure and accessory pigments. The similar spectral patterns of within-plot (alpha) and landscape-level (gamma) spectral variability provide context for the spatial spectral heterogeneity (beta). The greatest beta spectral variability occurred

in the blue, red edge, and mid-NIR. This suggests that the traits that vary most across the landscape are also chlorophyll-related but also include accessory pigments (e.g. carotenoids), N (blue and red edge), and structure (NIR). This suggests that spatial environmental heterogeneity drives variability in community structural traits and accessory pigments.

The patterns in spectral variability suggest that plants within communities differ more in photosynthetic properties than they do in structure. Conversely, communities differ more in structure than they do in photosynthetic properties. If some communities are compositionally similar, but structurally and functionally different along the lines of pigments, N, and structure, that further supports the role of phenotypic plasticity in creating spectral heterogeneity at different scales and in different traits.

4.2 Evaluating plot-level agreement between diversity metrics and the SVH

More plots exhibited either high biodiversity and low spectral diversity or low biodiversity and high spectral diversity than plots that exhibited a positive relationship between spectral diversity and biodiversity, and I therefore conclude that the SVH is not supported for these communities. Of the ten plots surveyed, four agreed with the SVH in both biodiversity metrics, three agreed in one biodiversity metric, and three did not agree in either metric. The four plots in agreement in both biodiversity metrics had moderate spectral diversity and biodiversity, and three of them were not highly invaded (plots 6, 7, and 8). The fourth (plot 4) was not only heavily invaded (>25% cover) by *R. davurica* but was also heavily invaded (>25% cover) by another invasive shrub, *E. umbellata*. These plant communities demonstrated relatively high spectral and biodiversity, which indicates functional diversity, species diversity, and long-term coexistence, due to niche partitioning (Rocchini et al., 2021).

Three plots (plots 1, 9, and 10) adhered to the SVH in only one of the two biodiversity metrics. Plot 1, which was heavily invaded by *R. davurica* (78% relative cover), showed agreement between spectral diversity and Shannon diversity but not richness. The lack of evenness in this plot likely made richness a less appropriate and potentially misleading biodiversity metric. Abundance- or evenness-based measures often better align with spectral heterogeneity, because, unlike richness as a metric, they acknowledge the stronger influence of dominant species on the landscape relative to rarer species (Madonsela et al., 2017; Oldeland et al., 2010; Torresani et al., 2018; R. Wang et al., 2018; Xu et al., 2022). In the case of plot 1, 13 of the 14 species comprised ~22% of the relative cover and therefore the overall spectral reflectance of the plot. The low Shannon diversity biodiversity metric did, however, agree with the low spectral diversity for plot 1. The combined low alpha spectral diversity and evenness-influenced biodiversity metric suggest that a few plant species with similar traits dominate this plant community (Rocchini et al. 2021), which also aligns with the expected competitive traits of invasive plants (Cavender-Bares et al., 2020; Matongera et al., 2016), and which is supported by the species composition of this plot and dominant *R. davurica* cover.

Plots 9 and 10, which were also heavily invaded by *R. davurica* (32% and 29% relative cover, respectively), had low spectral diversity and showed agreement with richness (also low) but not Shannon diversity (greater than richness due to relative evenness). This potentially suggests that very even, but less diverse (and potentially invaded), plots may not have good agreement with the SVH, especially when traits and resource use drive spectral similarities. The species compositions of these plots were more even than plot 1, with *R. davurica* cover at ~30%, the second most abundant species ~20%, and the third ~18%.

Three plots exhibited patterns outside of the positive correlation range in both biodiversity metrics. One of the plots was highly invaded (plot 2) and two were not (plots 3 and 5). Whether each plot fell above or below the positive correlation area did not vary by level of invasion. Plots 2 and 3, both of which had a single functional type or species with a near-majority or majority of relative cover (52% relative cover of *R. davurica* and 44% relative graminoid cover, respectively), both fell above the line due to low spectral diversity but high biodiversity. The relationships between biodiversity and spectral diversity across communities were likely driven by different mechanisms.

Plot 2, with a high invasion of *R. davurica* had low spectral diversity because it was invaded by a shrub with homogenizing impacts (Bergman et al., in preparation). Plot 3, with a near majority of grass cover potentially had low spectral diversity because of the size and structure of grasses, which may not be well-suited for meter-sized pixels. Although forest environments have illustrated the SVH relatively frequently, grasslands may require finer spatial resolutions for spectral diversity to align with biodiversity (R. Wang et al., 2018). Plot 5, which had 74% *M. pomifera* cover, fell below the line due to high spectral diversity but low species diversity. This is the only plot in this study where phenotypic plasticity appears to drive a violation of the SVH, and that plasticity appears to occur within a single tree canopy.

4.3 Other considerations

In addition to the mechanisms causing a lack of agreement with the SVH outlined above, there are other factors that could make this community contradict the SVH. Because the plant community is characterized by a mixture of grasses, forbs, shrubs, and trees, it is vertically complex, which may look less complex in remote sensing data due to taller vegetation obscuring

or shading lower-lying plants (Conti et al., 2021). Additionally, the sampling plots used in this study were small and relatively near each other. Larger sampling plots, which provide a broader range in species and heterogeneity, improve the SVH relationship (Gholizadeh et al., 2022; Hauser et al., 2021; Oldeland et al., 2010; Robertson et al., 2023).

4.4 Future work

Remote sensing and aerial imagery provide a relatively uniform, robust, and affordable approach to repeat Earth observation (Cavender-Bares et al., 2020; Foody & Cutler, 2003; Nagendra, 2001; Pettorelli et al., 2014; Rocchini et al., 2010; Skidmore et al., 2021). With increases in computing power, cloud storage, and the availability of abundant biodiversity data, evaluating the relationship between spectral diversity in remotely sensed images and plant diversity in different ecosystems, at different scales, and across time and space is not only increasingly possible but also increasingly important to biodiversity conservation efforts. Linking spectral and biodiversity data in a spatially explicit way will support complementary uses of biodiversity and spectral data (e.g. gap filling across datasets) and interoperability to answer ecological questions about community dynamics and broader ecosystem functioning.

5. Conclusion

The primary goals of this study were to assess alpha, beta, and gamma biodiversity and spectral diversity in this early successional plant community and how integrating spectral variability informs our understanding of ecosystem dynamics in this system. I found that alpha, beta, and gamma biodiversity metrics indicated that 7 to 16 species were found in each plot, with a mean of ~12 species, and 43 species were observed at the landscape level, and a beta biodiversity metric of 4 for variability among plots across the landscape. These traits may or may not align with

species diversity and compositional differences within and among plots, but they can still provide information about niche partitioning at different scales. The patterns in spectral variability suggest that biochemical traits vary more than structural traits do within plots, whereas structural traits vary more than biochemical traits among them.

The third goal was to assess how well patterns of alpha spectral diversity and biological diversity support the SVH at this scale in this ecosystem. Overall, this invaded early successional plant community did not exhibit patterns consistent with the SVH. Invaded plots agreed with the SVH less often than non-invaded plots did. The lack of agreement in invaded plots was linked to a combination of misaligned biodiversity metrics (e.g. higher evenness with few species or low evenness with many species) and the low spectral diversity that tends to be seen in invaded plots. The two non-invaded plots that did not agree with the SVH appeared to exhibit phenotypic plasticity (within canopy spectral variability) and scale exceptions. Despite the overall lack of agreement with the SVH at this scale in this early successional plant community, plot-specific patterns provide context for the lack of agreement. These methods also provide a framework through which the SVH can be evaluated and assessed across times and scales to improve applications.

Chapter 6: Conclusion

This dissertation applies the concept of spectral variability to two practical applications: first, to detect invasive plant species in remotely sensed imagery, and then, to elucidate ecological patterns of plant traits and communities. The variability among species at different points in the growing season, across years, and across scales can elucidate the best times and approaches to detect invasive plant species for management efforts. Spectral variability within species can be used to better understand when and which functional traits may vary. Variability in images can also be used to understand plant community dynamics across time and space.

The results in chapters 2 and 3 demonstrate that using hyperspectral imagery in concert with both UAV and fixed-wing aircraft can be useful in detecting and monitoring ecosystems invaded by *A. altissima*, *R. davurica*, and *E. umbellata*. In Chapter 2, detection algorithms were generated and applied to fine-scale UAV (drone) images from seven different dates across the growing season. In Chapter 3, detection algorithms were generated using both fine-scale UAV images from 2020 and coarser-scale fixed-wing aircraft NEON images from four different years (2016, 2017, 2019, and 2021), then were applied to each year of NEON images. Detection was most accurate when applying drone-based algorithms to drone-based images and least accurate when applying drone-based algorithms to NEON-based images. Both accuracy and key differentiating spectral features varied across the growing season and across years.

In drone images, all three species could be accurately detected in June using blue-green, green-yellow, and red edge spectral regions (450 to 510, 560 to 580, and 710 to 720 nm), along with additional species-specific spectral regions. For times when accuracy of detection is high, resulting in few false positives and negatives, such as June, single classification results can be used independently with good results, however, the flexible sampling and multi-month nature of drone-

based data collection has the potential to improve accuracy by combining classifications across times. In addition to accurate detection in June, all three species were also detectable at other points in the growing season: *R. davurica* in September, *A. altissima* in October, and *E. umbellata* on nearly every collection date. The lack of consistency in drone-based algorithms across the growing season for *A. altissima* and *R. davurica* suggests that *in situ* or date-specific detection algorithms may be more useful than a standard algorithm across the entire growing season, though a standard drone-based detection algorithm may be more applicable for *E. umbellata* detection. These results illustrate the usefulness of the very fine spatial resolution of drone-based imagery as well as the flexible sampling time that drone-based observation allows, which incorporates phenological features into detection algorithms.

In NEON images, all three species could be detected with >50% user and producer accuracies in at least two years using both drone-based detection algorithms and NEON-based detection algorithms. Transforming and resampling drone images both increased the number of important spectral regions in detection algorithms, though neither guaranteed an increase in detection accuracy. Classification algorithms developed from the NEON images themselves had greater detection accuracy than those developed from drone images, as they eliminated temporal and scale differences, but spectral features that were important to detection often varied across years.

Spectral features important to the accurate detection of *A. altissima* were consistent within each platform but not across platforms, which suggests that its spectral features are not universal across time and/or space. Spectral features key to the accurate detection of *E. umbellata* were inconsistent, which suggests that they are resolution dependent. In addition to inconsistent spectral features, detection of *E. umbellata* was the least accurate of the three species in NEON images,

which is in stark comparison to the 100% detection accuracy in drone-based images during mid-growing season, further highlighting the resolution dependence of *E. umbellata* detection. *R. davurica* had the greatest consistency in features that allowed for its detection using either platform, although the features changed, which suggests at least some variability associated with time and space.

These UAV- and fixed-wing aircraft-based detection methods can be extended to other regions, ecosystems, and species for monitoring and management efforts. The inconsistencies within and across approaches highlight the importance of temporal and spatial variability in detecting invasive plant species, even within a single site. This highlights the need for further exploration of the range of reflectances that are possible across all bands in reflectance profiles, across time (e.g. growing seasons, years) and space (e.g. ecosystems, latitudes) (Ji et al., 2024; Yang et al., 2016). Understanding how hyperspectral reflectances vary across a growing season and among seasons will also be crucial in utilizing data from satellite missions with repeat visits, e.g. SBG and EnMap. It also highlights the importance of context and the need for more generally applicable detection algorithms. The analysis of the inconsistencies across detection algorithms also elucidates the importance of considering time and space, not only in the detection of invasive plant species, but also in answering ecological questions.

Chapters 4 and 5 demonstrate temporal, spatial, and ecological exceptions to the SVH using fine-scale hyperspectral imagery. Chapter 4 examines spectral variability of organizational scales nested within vegetation communities, comparing among-species variability to within-species and within-canopy variability. Chapter 5 examines spectral variability of vegetation communities, comparing the spectral variability among and within differentially invaded plots. Each demonstrated temporal, spatial, and ecological exceptions to the SVH.

I found that variability among species was greatest early in the growing season, supporting the SVH. As the growing season progressed, however, both within-individual and among-individual spectral variability increasingly exceeded among-species variability in more spectral regions and to a greater degree, which suggests that more traits become increasingly variable at finer organizational scales as leaves mature. The contribution of among-community spectral variation suggests that some observed species-specific among-individual spectral variability was likely caused by spatial heterogeneity. Later in the growing season, the total within- and among-individual spectral variability contributed to over half of the total observed spectral variability in spectral regions associated with biochemical traits, and among-individual variability was also >30% in spectral regions associated with canopy structure.

The results suggest that differences within individual canopies and among individuals of a species are greater than differences among species, particularly in biochemical traits, from mid-growing season and into the start of fall senescence. Therefore, species-based assumptions about traits in mid- to late growing season may neglect considerable variability among individuals within species and within individuals. As functional traits can be used to make generalizable predictions across organizational and spatial scales, understanding trait variation at different scales and times can facilitate answering major questions in community ecology to further the understanding of plant communities and ecosystems. Spectroscopy can be used to this end and will benefit from increasingly available hyperspectral airborne data and new satellite missions.

In the fifth chapter, I found that spectral variability within plots was greater in biochemical traits than in structural traits, but among plots was greater in structural traits than biochemical traits, which suggest stability in different traits at different scales. This ecosystem did not fully agree with the SVH. Plot-specific patterns provide context for the mechanisms resulting in the lack

of agreement with the SVH: a combination of misaligned biodiversity metrics (e.g. higher evenness with few species or low evenness with many species), the low spectral diversity that tends to be seen in invaded plots, phenotypic plasticity (within canopy spectral variability) and scale exceptions. The methods also provide a framework through which the SVH can be evaluated and assessed across times and scales to improve applications.

Together, these two chapters highlight 1) the importance of variability within species over space and time, 2) the importance of evenness and trait variability in using remote sensing to examine ecological communities, and 3) the importance of scale. The spectral phenotype is the combination of genetic information and response to the environment of a plant over the course of its lifetime, which drives within-species spectral variability. Chapters 4 and 5 demonstrate that the spectral phenotype varies among and within individuals, within a growing season (over time) and within different vegetation communities (over space). These two chapters further highlight the need to explore the ways in which the spectral phenotype results in a range of reflectance signatures for both individual species as well as vegetation communities, to better apply remotely sensed imagery to ecological questions.

There is also a connection between detecting invasive plant species and these violations of the SVH. Although spectral signatures can vary within a species to different degrees in different contexts, invasive plants could still often be detected with reasonable accuracy. An additional analysis (see Appendix E) determined that this could be attributed to two patterns: 1) the traits that differ, and therefore the associated spectral regions with the greatest variability, do not necessarily overlap with the spectral regions that are key to detection, and 2) the spectral features that differentiate a species of interest from all other species are not based on the entirety of among-species variability.

Remote sensing provides us with an abundance of data, which can translate to ecological understanding when applied correctly. By identifying the importance of within-canopy and among-canopy variability across a growing season, within-species variability in spectra across years, and varying relationships between biodiversity and spectral diversity, I highlight the importance of considering how time and space impact the range of traits and spectra within species in the context of a semi-invaded mid-Atlantic successional field. This analysis can and should be extended to additional contexts, including additional years, species, and ecosystems to improve our understanding of these relationships both in management applications and in answering ecological questions; I provide a methodological framework to do so.

References

- Adler, P. B., Fajardo, A., Kleinhesselink, A. R., & Kraft, N. J. B. (2013). Trait-based tests of coexistence mechanisms. *Ecology Letters*, *16*(10), 1294–1306.
<https://doi.org/10.1111/ele.12157>
- Albert, C. H., Thuiller, W., Yoccoz, N. G., Soudant, A., Boucher, F., Saccone, P., & Lavorel, S. (2010). Intraspecific functional variability: extent, structure and sources of variation. *Journal of Ecology*, *98*(3), 604–613. <https://doi.org/10.1111/j.1365-2745.2010.01651.x>
- Alvarez-Vanhard, E., Corpetti, T., & Houet, T. (2021). UAV & satellite synergies for optical remote sensing applications: A literature review. *Science of Remote Sensing*, *3*, 100019.
<https://doi.org/10.1016/j.srs.2021.100019>
- Aneece, I., & Epstein, H. (2017). Identifying invasive plant species using field spectroscopy in the VNIR region in successional systems of north-central Virginia. *International Journal of Remote Sensing*, *38*, 100–122. <https://doi.org/10.1080/01431161.2016.1259682>
- Asner, G., & Vitousek, P. (2005). Remote analysis of biological invasion and biogeochemical change. *Proceedings of the National Academy of Sciences of the United States of America*, *102*, 4383–6. <https://doi.org/10.1073/pnas.0500823102>
- Asner, G. P., Martin, R. E., Knapp, D. E., Tupayachi, R., Anderson, C. B., Sinca, F., et al. (2017). Airborne laser-guided imaging spectroscopy to map forest trait diversity and guide conservation. *Science*, *355*(6323), 385–389. <https://doi.org/10.1126/science.aaj1987>
- Asner, Gregory P. (1998). Biophysical and Biochemical Sources of Variability in Canopy Reflectance. *Remote Sensing of Environment*, *64*(3), 234–253.
[https://doi.org/10.1016/S0034-4257\(98\)00014-5](https://doi.org/10.1016/S0034-4257(98)00014-5)

- Asner, Gregory P., & Martin, R. E. (2008a). Airborne spectranomics: mapping canopy chemical and taxonomic diversity in tropical forests. *Frontiers in Ecology and the Environment*, 7(5), 269–276. <https://doi.org/10.1890/070152>
- Asner, Gregory P., & Martin, R. E. (2008b). Spectral and chemical analysis of tropical forests: Scaling from leaf to canopy levels. *Remote Sensing of Environment*, 112(10), 3958–3970. <https://doi.org/10.1016/j.rse.2008.07.003>
- Asner, Gregory P., Knapp, D. E., Kennedy-Bowdoin, T., Jones, M. O., Martin, R. E., Boardman, J., & Hughes, R. F. (2008). Invasive species detection in Hawaiian rainforests using airborne imaging spectroscopy and LiDAR. *Remote Sensing of Environment*, 112(5), 1942–1955. <https://doi.org/10.1016/j.rse.2007.11.016>
- Asner, Gregory P., Anderson, C. B., Martin, R. E., Tupayachi, R., Knapp, D. E., & Sinca, F. (2015). Landscape biogeochemistry reflected in shifting distributions of chemical traits in the Amazon forest canopy. *Nature Geoscience*, 8(7), 567–573. <https://doi.org/10.1038/ngeo2443>
- Auger, S., & Shipley, B. (2013). Inter-specific and intra-specific trait variation along short environmental gradients in an old-growth temperate forest. *Journal of Vegetation Science*, 24(3), 419–428. <https://doi.org/10.1111/j.1654-1103.2012.01473.x>
- Azadnia, R., Rajabipour, A., Jamshidi, B., & Omid, M. (2023). New approach for rapid estimation of leaf nitrogen, phosphorus, and potassium contents in apple-trees using Vis/NIR spectroscopy based on wavelength selection coupled with machine learning. *Computers and Electronics in Agriculture*, 207, 107746. <https://doi.org/10.1016/j.compag.2023.107746>

- Barnosky, A., Matzke, N., Tomiya, S., Wogan, G., Swartz, B., Quental, T., et al. (2011). Has the Earth's Sixth Mass Extinction Already Arrived? *Nature*. *Nature*, *471*, 51–7.
<https://doi.org/10.1038/nature09678>
- Bellard, C., Thuiller, W., Leroy, B., Genovesi, P., Bakkenes, M., & Courchamp, F. (2013). Will climate change promote future invasions? *Global Change Biology*, *19*(12), 3740–3748.
<https://doi.org/10.1111/gcb.12344>
- Bergman, Z. (2022, March 6). *Novel Weaponry in the Arsenal of an Invasive Shrub (Dahurian Buckthorn)*. University of Virginia, Environmental Sciences - Graduate School of Arts and Sciences, MS (Master of Science), 2022, Charlottesville, VA. Retrieved from
<https://doi.org/10.18130/1esd-rz94>
- Besson, M., Alison, J., Bjerge, K., Gorochowski, T. E., Høye, T. T., Jucker, T., et al. (2022). Towards the fully automated monitoring of ecological communities. *Ecology Letters*, *25*(12), 2753–2775. <https://doi.org/10.1111/ele.14123>
- Blackburn, G. A. (2007). Hyperspectral remote sensing of plant pigments. *Journal of Experimental Botany*, *58*(4), 855–867. <https://doi.org/10.1093/jxb/erl123>
- Bolnick, D. I., Svanbäck, R., Fordyce, J. A., Yang, L. H., Davis, J. M., Hulsey, C. D., & Forister, M. L. (2003). The ecology of individuals: incidence and implications of individual specialization. *The American Naturalist*, *161*(1), 1–28. <https://doi.org/10.1086/343878>
- Boochs, F., Kupfer, G., Dockter, K., & Kuhbauch, W. (1990). Shape of the red edge as vitality indicator for plants. *International Journal of Remote Sensing*, *11*(10), 1741–1753.
<https://doi.org/10.1080/01431169008955127>

- Bradshaw, A. D. (1965). Evolutionary Significance of Phenotypic Plasticity in Plants. In E. W. Caspari & J. M. Thoday (Eds.), *Advances in Genetics* (Vol. 13, pp. 115–155). Academic Press. [https://doi.org/10.1016/S0065-2660\(08\)60048-6](https://doi.org/10.1016/S0065-2660(08)60048-6)
- Burkholder, A. (2010). Seasonal trends in separability of leaf reflectance spectra for *Ailanthus altissima* and four other tree species. *Graduate Theses, Dissertations, and Problem Reports*. <https://doi.org/10.33915/etd.701>
- Burkholder, A., Warner, T., Culp, M., & Landenberger, R. (2011). Seasonal Trends in Separability of Leaf Reflectance Spectra for *Ailanthus altissima* and Four Other Tree Species. *Photogrammetric Engineering and Remote Sensing*, 77, 793–804. <https://doi.org/10.14358/PERS.77.8.793>
- Buschmann, C., & Nagel, E. (1993). In vivo spectroscopy and internal optics of leaves as basis for remote sensing of vegetation. *International Journal of Remote Sensing*, 14(4), 711–722. <https://doi.org/10.1080/01431169308904370>
- Bush, A., Sollmann, R., Wilting, A., Bohmann, K., Cole, B., Balzter, H., et al. (2017). Connecting Earth observation to high-throughput biodiversity data. *Nature Ecology & Evolution*, 1(7), 1–9. <https://doi.org/10.1038/s41559-017-0176>
- Cadotte, M. W., Cavender-Bares, J., Tilman, D., & Oakley, T. H. (2009). Using Phylogenetic, Functional and Trait Diversity to Understand Patterns of Plant Community Productivity. *PLOS ONE*, 4(5), e5695. <https://doi.org/10.1371/journal.pone.0005695>
- Cardina, J., Johnson, G., & Sparrow, D. (1997). The nature and consequence of weed spatial distribution. *Weed Science*, 45, 364–373. <https://doi.org/10.1017/S0043174500092997>
- Cardinale, B. J. (2011). Biodiversity improves water quality through niche partitioning. *Nature*, 472(7341), 86–89. <https://doi.org/10.1038/nature09904>

- Carradori, S., Cairone, F., Garzoli, S., Fabrizi, G., Iazzetti, A., Giusti, A. M., et al. (2020). Phytocomplex Characterization and Biological Evaluation of Powdered Fruits and Leaves from *Elaeagnus angustifolia*. *Molecules*, 25(9), 2021.
<https://doi.org/10.3390/molecules25092021>
- Carson, H. W., Lass, L. W., & Callihan, R. H. (1995). Detection of Yellow Hawkweed (*Hieracium pratense*) with High Resolution Multispectral Digital Imagery. *Weed Technology*, 9(3), 477–483.
- Castro, K., Sanchez-Azofeifa, G. A., & Caelli, T. (2004). Discrimination of lianas and trees with leaf-level hyperspectral data. *Remote Sensing of Environment*, 90, 353–372.
<https://doi.org/10.1016/j.rse.2004.01.013>
- Castro-Esau, K. L., Sánchez-Azofeifa, G. A., Rivard, B., Wright, S. J., & Quesada, M. (2006). Variability in leaf optical properties of Mesoamerican trees and the potential for species classification. *American Journal of Botany*, 93(4), 517–530.
<https://doi.org/10.3732/ajb.93.4.517>
- Cavender-Bares, J., Meireles, J. E., Couture, J. J., Kaproth, M. A., Kingdon, C. C., Singh, A., et al. (2016). Associations of leaf spectra with genetic and phylogenetic variation in oaks: Prospects for remote detection of biodiversity. *Remote Sensing*, 8(3), 221.
<https://doi.org/10.3390/rs8030221>
- Cavender-Bares, J., Schweiger, A. K., Pinto-Ledezma, J. N., & Meireles, J. E. (2020). Applying Remote Sensing to Biodiversity Science. In J. Cavender-Bares, J. A. Gamon, & P. A. Townsend (Eds.), *Remote Sensing of Plant Biodiversity* (pp. 13–42). Cham: Springer International Publishing. https://doi.org/10.1007/978-3-030-33157-3_2

- Chance, C. M., Coops, N. C., Plowright, A. A., Tooke, T. R., Christen, A., & Aven, N. (2016). Invasive Shrub Mapping in an Urban Environment from Hyperspectral and LiDAR-Derived Attributes. *Frontiers in Plant Science*, 7. <https://doi.org/10.3389/fpls.2016.01528>
- Chesson, P. (2000). Mechanisms of Maintenance of Species Diversity. *Annual Review of Ecology and Systematics*, 31(1), 343–366. <https://doi.org/10.1146/annurev.ecolsys.31.1.343>
- Clark, C. M., Flynn, D. F. B., Butterfield, B. J., & Reich, P. B. (2012). Testing the Link between Functional Diversity and Ecosystem Functioning in a Minnesota Grassland Experiment. *PLOS ONE*, 7(12), e52821. <https://doi.org/10.1371/journal.pone.0052821>
- Clark, M., Roberts, D., & Clark, D. (2005). Hyperspectral discrimination of tropical rain forest tree species at leaf to crown scales. *Remote Sensing of Environment*, 96, 375–398. <https://doi.org/10.1016/j.rse.2005.03.009>
- Clark, M. L., Roberts, D. A., & Clark, D. B. (2005). Hyperspectral discrimination of tropical rain forest tree species at leaf to crown scales. *Remote Sensing of Environment*, 96(3), 375–398. <https://doi.org/10.1016/j.rse.2005.03.009>
- Cochrane, M. A. (2000). Using vegetation reflectance variability for species level classification of hyperspectral data. *International Journal of Remote Sensing*, 21(10), 2075–2087. <https://doi.org/10.1080/01431160050021303>
- Conti, L., Malavasi, M., Galland, T., Komárek, J., Lagner, O., Carmona, C. P., et al. (2021). The relationship between species and spectral diversity in grassland communities is mediated by their vertical complexity. *Applied Vegetation Science*, 24(3). <https://doi.org/10.1111/avsc.12600>

- Cornwell, W. K., Schwilk, L. D. W., & Ackerly, D. D. (2006). A trait-based test for habitat filtering: convex hull volume. *Ecology*, *87*(6), 1465–1471. [https://doi.org/10.1890/0012-9658\(2006\)87\[1465:attfhf\]2.0.co;2](https://doi.org/10.1890/0012-9658(2006)87[1465:attfhf]2.0.co;2)
- Daughtry, C. S. T., Walthall, C. L., Kim, M. S., de Colstoun, E. B., & McMurtrey, J. E. (2000). Estimating Corn Leaf Chlorophyll Concentration from Leaf and Canopy Reflectance. *Remote Sensing of Environment*, *74*(2), 229–239. [https://doi.org/10.1016/S0034-4257\(00\)00113-9](https://doi.org/10.1016/S0034-4257(00)00113-9)
- Dawson, T. P., & Curran, P. J. (1998). Technical note A new technique for interpolating the reflectance red edge position. *International Journal of Remote Sensing*, *19*(11), 2133–2139. <https://doi.org/10.1080/014311698214910>
- Dawson, W., Moser, D., van Kleunen, M., Kreft, H., Pergl, J., Pyšek, P., et al. (2017). Global hotspots and correlates of alien species richness across taxonomic groups. *Nature Ecology & Evolution*, *1*(7), 1–7. <https://doi.org/10.1038/s41559-017-0186>
- Díaz, S., Kattge, J., Cornelissen, J. H. C., Wright, I. J., Lavorel, S., Dray, S., et al. (2016). The global spectrum of plant form and function. *Nature*, *529*(7585), 167–171. <https://doi.org/10.1038/nature16489>
- Dietze, M. C., Fox, A., Beck-Johnson, L. M., Betancourt, J. L., Hooten, M. B., Jarnevich, C. S., et al. (2018). Iterative near-term ecological forecasting: Needs, opportunities, and challenges. *Proceedings of the National Academy of Sciences*, *115*(7), 1424–1432. <https://doi.org/10.1073/pnas.1710231115>
- Diruit, W., Le Bris, A., Bajjouk, T., Richier, S., Helias, M., Burel, T., et al. (2022). Seaweed Habitats on the Shore: Characterization through Hyperspectral UAV Imagery and Field Sampling. *Remote Sensing*, *14*(13), 3124. <https://doi.org/10.3390/rs14133124>

- Dmitriev, P. A., Kozlovsky, B. L., Kupriushkin, D. P., Dmitrieva, A. A., Rajput, V. D., Chokheli, V. A., et al. (2022). Assessment of Invasive and Weed Species by Hyperspectral Imagery in Agrocenoses Ecosystem. *Remote Sensing*, 14(10), 2442.
<https://doi.org/10.3390/rs14102442>
- Dronova, I., Taddeo, S., Hemes, K. S., Knox, S. H., Valach, A., Oikawa, P. Y., et al. (2021). Remotely sensed phenological heterogeneity of restored wetlands: linking vegetation structure and function. *Agricultural and Forest Meteorology*, 296, 108215.
<https://doi.org/10.1016/j.agrformet.2020.108215>
- Ecke, S., Dempewolf, J., Frey, J., Schwaller, A., Endres, E., Klemmt, H.-J., et al. (2022). UAV-Based Forest Health Monitoring: A Systematic Review. *Remote Sensing*, 14(13), 3205.
<https://doi.org/10.3390/rs14133205>
- Ehrenfeld, J. G. (2004). Implications of Invasive Species for Belowground Community and Nutrient Processes. *Weed Technology*, 18, 1232–1235.
- Ehrenfeld, J. G., Kourtev, P., & Huang, W. (2001). Changes in Soil Functions Following Invasions of Exotic Understory Plants in Deciduous Forests. *Ecological Applications*, 11(5), 1287–1300. [https://doi.org/10.1890/1051-0761\(2001\)011\[1287:CISFFI\]2.0.CO;2](https://doi.org/10.1890/1051-0761(2001)011[1287:CISFFI]2.0.CO;2)
- Ely, K. S., Burnett, A. C., Lieberman-Cribbin, W., Serbin, S. P., & Rogers, A. (2019). Spectroscopy can predict key leaf traits associated with source–sink balance and carbon–nitrogen status. *Journal of Experimental Botany*, 70(6), 1789–1799.
<https://doi.org/10.1093/jxb/erz061>
- Ewald, M., Aerts, R., Lenoir, J., Fassnacht, F. E., Nicolas, M., Skowronek, S., et al. (2018). LiDAR derived forest structure data improves predictions of canopy N and P

- concentrations from imaging spectroscopy. *Remote Sensing of Environment*, 211, 13–25.
<https://doi.org/10.1016/j.rse.2018.03.038>
- Fassnacht, F. E., Müllerová, J., Conti, L., Malavasi, M., & Schmidtlein, S. (2022). About the link between biodiversity and spectral variation. *Applied Vegetation Science*, 25(1), e12643.
<https://doi.org/10.1111/avsc.12643>
- Féret, J.-B., & Asner, G. P. (2014). Mapping tropical forest canopy diversity using high-fidelity imaging spectroscopy. *Ecological Applications: A Publication of the Ecological Society of America*, 24(6), 1289–1296. <https://doi.org/10.1890/13-1824.1>
- Fischer, B., Smith, M., & Pau, G. (2023). rhdf5: R Interface to HDF5 (Version 2.46.1). Retrieved from <http://bioconductor.org/packages/rhdf5/>
- Foody, G. M., & Cutler, M. (2003). Tree biodiversity in protected and logged Bornean tropical rain forest and its measurement by satellite remote sensing. *Journal of Biogeography*, 30, 1053–1066.
- Gaertner, M., Den Breeyen, A., Hui, C., & Richardson, D. (2009). Impacts of alien plant invasions on species richness in Mediterranean-type ecosystems: a meta-analysis. *Progress in Physical Geography*, 33, 319–338.
<https://doi.org/10.1177/0309133309341607>
- Gamon, J. A., Wang, R., Gholizadeh, H., Zutta, B., Townsend, P. A., & Cavender-Bares, J. (2020). Consideration of Scale in Remote Sensing of Biodiversity. In J. Cavender-Bares, J. A. Gamon, & P. A. Townsend (Eds.), *Remote Sensing of Plant Biodiversity* (pp. 425–447). Cham: Springer International Publishing. https://doi.org/10.1007/978-3-030-33157-3_16

- Gao, B., Yu, L., Ren, L., Zhan, Z., & Luo, Y. (2023). Early Detection of *Dendroctonus valens* Infestation at Tree Level with a Hyperspectral UAV Image. *Remote Sensing*, *15*(2), 407. <https://doi.org/10.3390/rs15020407>
- Geller, G., Cavender-Bares, J., Gamon, J., McDonald, K., Podest, E., Townsend, P., & Ustin, S. (2020). Epilogue: Toward a Global Biodiversity Monitoring System (pp. 519–526). https://doi.org/10.1007/978-3-030-33157-3_20
- Gholizadeh, H., Gamon, J. A., Zygielbaum, A. I., Wang, R., Schweiger, A. K., & Cavender-Bares, J. (2018). Remote sensing of biodiversity: Soil correction and data dimension reduction methods improve assessment of α -diversity (species richness) in prairie ecosystems. *Remote Sensing of Environment*, *206*, 240–253. <https://doi.org/10.1016/j.rse.2017.12.014>
- Gholizadeh, H., Dixon, A. P., Pan, K. H., McMillan, N. A., Hamilton, R. G., Fuhlendorf, S. D., et al. (2022). Using airborne and DESIS imaging spectroscopy to map plant diversity across the largest contiguous tract of tallgrass prairie on earth. *Remote Sensing of Environment*, *281*, 113254. <https://doi.org/10.1016/j.rse.2022.113254>
- Giordan, D., Hayakawa, Y., Nex, F., Remondino, F., & Tarolli, P. (2018). Review article: the use of remotely piloted aircraft systems (RPASs) for natural hazards monitoring and management. *Natural Hazards and Earth System Sciences*, *18*(4), 1079–1096. <https://doi.org/10.5194/nhess-18-1079-2018>
- Gómez-Aparicio, L., & Canham, C. (2008). Neighborhood models of the effects of invasive tree species on ecosystem processes. *Ecological Monographs*, *78*, 69–86. <https://doi.org/10.1890/06-2036.1>

- Grant, L. (1987). Diffuse and specular characteristics of leaf reflectance. *Remote Sensing of Environment*, 22(2), 309–322. [https://doi.org/10.1016/0034-4257\(87\)90064-2](https://doi.org/10.1016/0034-4257(87)90064-2)
- Gurevitch, J., & Padilla, D. K. (2004). Are invasive species a major cause of extinctions? *Trends in Ecology & Evolution*, 19(9), 470–474. <https://doi.org/10.1016/j.tree.2004.07.005>
- Hall, K., Johansson, L. j., Sykes, M. t., Reitalu, T., Larsson, K., & Prentice, H. c. (2010). Inventorying management status and plant species richness in semi-natural grasslands using high spatial resolution imagery. *Applied Vegetation Science*, 13(2), 221–233. <https://doi.org/10.1111/j.1654-109X.2009.01063.x>
- Hamilton, R., Megown, K., Lachowski, H., & Campbell, R. (2006). *Mapping Russian olive: using remote sensing to map an invasive tree.*
- Hauser, L. T., Féret, J.-B., An Binh, N., van der Windt, N., Sil, Â. F., Timmermans, J., et al. (2021). Towards scalable estimation of plant functional diversity from Sentinel-2: In-situ validation in a heterogeneous (semi-)natural landscape. *Remote Sensing of Environment*, 262, 112505. <https://doi.org/10.1016/j.rse.2021.112505>
- He, L., Chen, W., Leblanc, S. G., Lovitt, J., Arsenault, A., Schmelzer, I., et al. (2021). Integration of multi-scale remote sensing data for reindeer lichen fractional cover mapping in Eastern Canada. *Remote Sensing of Environment*, 267, 112731. <https://doi.org/10.1016/j.rse.2021.112731>
- Hill, J., Buddenbaum, H., & Townsend, P. (2019). Imaging Spectroscopy of Forest Ecosystems: Perspectives for the Use of Space-borne Hyperspectral Earth Observation Systems. *Surveys in Geophysics*, 40. <https://doi.org/10.1007/s10712-019-09514-2>
- Hochberg, E., Roberts, D., Dennison, P., & Hulley, G. (2015). Special issue on the Hyperspectral Infrared Imager (HyspIRI): Emerging science in terrestrial and aquatic ecology, radiation

- balance and hazards. *Remote Sensing of Environment*, 167.
<https://doi.org/10.1016/j.rse.2015.06.011>
- Hoeppner, J. M., Skidmore, A. K., Darvishzadeh, R., Heurich, M., Chang, H.-C., & Gara, T. W. (2020). Mapping Canopy Chlorophyll Content in a Temperate Forest Using Airborne Hyperspectral Data. *Remote Sensing*, 12(21), 3573. <https://doi.org/10.3390/rs12213573>
- Homolova, L., Malenovský, Z., Clevers, J. G. P. W., Garcia-Santos, G., & Schaepman, M. (2013). Review of optical-based remote sensing for plant trait mapping. *Ecological Complexity*, 15. <https://doi.org/10.1016/j.ecocom.2013.06.003>
- Horn, H. S. (1971). *Adaptive Geometry of Trees (MPB-3), Volume 3*. Princeton University Press.
<https://doi.org/10.2307/j.ctvx5w9x8>
- Horn, H. S. (1975). Forest Succession. *Scientific American*, 232(5), 90–101.
- Huang, C.-Y., & Asner, G. P. (2009). Applications of remote sensing to alien invasive plant studies. *Sensors (Basel, Switzerland)*, 9(6), 4869–4889.
<https://doi.org/10.3390/s90604869>
- Huelsman, K., Epstein, H., Yang, X., Mullori, L., Červená, L., & Walker, R. (2023). Spectral variability in fine-scale drone-based imaging spectroscopy does not impede detection of target invasive plant species. *Frontiers in Remote Sensing*, 3. Retrieved from
<https://www.frontiersin.org/articles/10.3389/frsen.2022.1085808>
- Jacquemoud, S., Verhoef, W., Baret, F., Bacour, C., Zarco-Tejada, P. J., Asner, G. P., et al. (2009). PROSPECT+SAIL models: A review of use for vegetation characterization. *Remote Sensing of Environment*, 113, S56–S66. <https://doi.org/10.1016/j.rse.2008.01.026>

- Jetz, W., Cavender-Bares, J., Pavlick, R., Schimel, D., Davis, F. W., Asner, G. P., et al. (2016). Monitoring plant functional diversity from space. *Nature Plants*, 2(3), 1–5.
<https://doi.org/10.1038/nplants.2016.24>
- Ji, F., Li, F., Hao, D., Shiklomanov, A. N., Yang, X., Townsend, P. A., et al. (2024). Unveiling the transferability of PLSR models for leaf trait estimation: lessons from a comprehensive analysis with a novel global dataset. *New Phytologist*, 243(1), 111–131.
<https://doi.org/10.1111/nph.19807>
- Jónsdóttir, I. S., Halbritter, A. H., Christiansen, C. T., Althuizen, I. H. J., Haugum, S. V., Henn, J. J., et al. (2022). Intraspecific trait variability is a key feature underlying high Arctic plant community resistance to climate warming. *Ecological Monographs*, n/a(n/a), e1555.
<https://doi.org/10.1002/ecm.1555>
- Jost, L. (2007). Partitioning Diversity Into Independent Alpha and Beta Components. *Ecology*, 88, 2427–39. <https://doi.org/10.1890/06-1736.1>
- Jung, V., Violle, C., Mondy, C., Hoffmann, L., & Muller, S. (2010). Intraspecific variability and trait-based community assembly. *Journal of Ecology*, 98(5), 1134–1140.
<https://doi.org/10.1111/j.1365-2745.2010.01687.x>
- Kattenborn, T., Fassnacht, F. E., & Schmidlein, S. (2019). Differentiating plant functional types using reflectance: which traits make the difference? *Remote Sensing in Ecology and Conservation*, 5(1), 5–19. <https://doi.org/10.1002/rse2.86>
- Kaufmann, H., Segl, K., Guanter, L., Hofer, S., Förster, K.-P., Stuffer, T., et al. (2008). Environmental Mapping and Analysis Program (EnMAP) - Recent Advances and Status (Vol. 4, pp. 109–112). Presented at the International Geoscience and Remote Sensing Symposium (IGARSS). <https://doi.org/10.1109/IGARSS.2008.4779668>

- Kays, R., Crofoot, M. C., Jetz, W., & Wikelski, M. (2015). Terrestrial animal tracking as an eye on life and planet. *Science*, *348*(6240), aaa2478. <https://doi.org/10.1126/science.aaa2478>
- Kazakou, E., Violle, C., Roumet, C., Navas, M.-L., Vile, D., Kattge, J., & Garnier, E. (2014). Are trait-based species rankings consistent across data sets and spatial scales? *Journal of Vegetation Science*, *25*(1), 235–247. <https://doi.org/10.1111/jvs.12066>
- Kganyago, M., Odindi, J., Adjorlolo, C., & Mhangara, P. (2017). Selecting a subset of spectral bands for mapping invasive alien plants: a case of discriminating *Parthenium hysterophorus* using field spectroscopy data. *International Journal of Remote Sensing*, *38*(20), 5608–5625. <https://doi.org/10.1080/01431161.2017.1343510>
- Kimothi, M. M., & Dasari, A. (2010). Methodology to map the spread of an invasive plant (*Lantana camara* L.) in forest ecosystems using Indian remote sensing satellite data. *International Journal of Remote Sensing*, *31*(12), 3273–3289. <https://doi.org/10.1080/01431160903121126>
- Kirk, N., Kannemeyer, R., Greenaway, A., MacDonald, E., & Stronge, D. (2019). Understanding attitudes on new technologies to manage invasive species. *Pacific Conservation Biology*, *26*. <https://doi.org/10.1071/PC18080>
- Kokaly, R., Asner, G., Ollinger, S., Martin, M., & Wessman, C. A. (2009). Characterizing canopy biochemistry from imaging spectroscopy and its application to ecosystem studies. *Remote Sensing of Environment*, *113*. <https://doi.org/10.1016/j.rse.2008.10.018>
- Kothari, S., Beauchamp-Rioux, R., Blanchard, F., Crofts, A. L., Girard, A., Guilbeault-Mayers, X., et al. (2023). Predicting leaf traits across functional groups using reflectance spectroscopy. *New Phytologist*, *238*(2), 549–566. <https://doi.org/10.1111/nph.18713>

- Laliberté, E., Schweiger, A. K., & Legendre, P. (2020). Partitioning plant spectral diversity into alpha and beta components. *Ecology Letters*, 23(2), 370–380.
<https://doi.org/10.1111/ele.13429>
- Liao, C., Peng, R., Luo, Y., Zhou, X., Wu, X., Fang, C., et al. (2008). Altered ecosystem carbon and nitrogen cycles by plant invasion: a meta-analysis. *The New Phytologist*, 177(3), 706–714. <https://doi.org/10.1111/j.1469-8137.2007.02290.x>
- Liland, K. H., Mevik, B.-H., Wehrens, R., & Hiemstra, P. (2022, July 16). pls: Partial Least Squares and Principal Component Regression (Version 2.8-1). Retrieved from <https://CRAN.R-project.org/package=pls>
- Lovett, G., Weiss, M., Liebhold, A., Holmes, T., Leung, B., Lambert, K., et al. (2016). Nonnative forest insects and pathogens in the United States: Impacts and policy options. *Ecological Applications*, 26. <https://doi.org/10.1890/15-1176>
- Lunch, C., Laney, C., Mietkiewicz, N., Sokol, E., Cawley, K., & Network), N. (National E. O. (2024, January 9). neonUtilities: Utilities for Working with NEON Data (Version 2.4.1). Retrieved from <https://cran.r-project.org/web/packages/neonUtilities/index.html>
- Madonsela, S., Cho, M., Ramoelo, A., & Mutanga, O. (2017). Remote sensing of species diversity using Landsat 8 spectral variables. *ISPRS Journal of Photogrammetry and Remote Sensing*, 133. <https://doi.org/10.1016/j.isprsjprs.2017.10.008>
- Mahlein, A.-K., Steiner, U., Dehne, H.-W., & Oerke, E.-C. (2010). Spectral signatures of sugar beet leaves for the detection and differentiation of diseases. *Precision Agriculture*, 11(4), 413–431. <https://doi.org/10.1007/s11119-010-9180-7>

- Malinich, E., Lynn-Bell, N., & Kourtev, P. S. (2017). The effect of the invasive *Elaeagnus umbellata* on soil microbial communities depends on proximity of soils to plants. *Ecosphere*, 8(5), e01827. <https://doi.org/10.1002/ecs2.1827>
- Marais, D. L. D., Hernandez, K. M., & Juenger, T. E. (2013). Genotype-by-Environment Interaction and Plasticity: Exploring Genomic Responses of Plants to the Abiotic Environment. *Annual Review of Ecology, Evolution, and Systematics*, 44(Volume 44, 2013), 5–29. <https://doi.org/10.1146/annurev-ecolsys-110512-135806>
- Marconi, S., Weinstein, B. G., Zou, S., Bohlman, S. A., Zare, A., Singh, A., et al. (2022). Continental-scale hyperspectral tree species classification in the United States National Ecological Observatory Network. *Remote Sensing of Environment*, 282, 113264. <https://doi.org/10.1016/j.rse.2022.113264>
- Marks, C. O. (2007). The Causes of Variation in Tree Seedling Traits: The Roles of Environmental Selection Versus Chance. *Evolution*, 61(2), 455–469. <https://doi.org/10.1111/j.1742-4658.2007.00021.x>
- Martin, M. E., & Aber, J. D. (1997). High Spectral Resolution Remote Sensing of Forest Canopy Lignin, Nitrogen, and Ecosystem Processes. *Ecological Applications*, 7(2), 431–443. [https://doi.org/10.1890/1051-0761\(1997\)007\[0431:HSRRSO\]2.0.CO;2](https://doi.org/10.1890/1051-0761(1997)007[0431:HSRRSO]2.0.CO;2)
- Martinez, B., Reaser, J. K., Dehgan, A., Zamft, B., Baisch, D., McCormick, C., et al. (2020). Technology innovation: advancing capacities for the early detection of and rapid response to invasive species. *Biological Invasions*, 22(1), 75–100. <https://doi.org/10.1007/s10530-019-02146-y>

- Mascaro, J., & Schnitzer, S. A. (2007). *Rhamnus cathartica* L. (Common Buckthorn) as an Ecosystem Dominant in Southern Wisconsin Forests. *Northeastern Naturalist*, *14*(3), 387–402.
- Matongera, T., Mutanga, O., & Lottering, R. (2016). Detection and mapping of bracken fern weeds using multispectral remotely sensed data: A review of progress and challenges. *Geocarto International*, *33*, 1–31. <https://doi.org/10.1080/10106049.2016.1240719>
- McGill, B. J., Enquist, B. J., Weiher, E., & Westoby, M. (2006). Rebuilding community ecology from functional traits. *Trends in Ecology & Evolution*, *21*(4), 178–185. <https://doi.org/10.1016/j.tree.2006.02.002>
- McManus, K. M., Asner, G. P., Martin, R. E., Dexter, K. G., Kress, W. J., & Field, C. B. (2016). Phylogenetic Structure of Foliar Spectral Traits in Tropical Forest Canopies. *Remote Sensing*, *8*(3), 196. <https://doi.org/10.3390/rs8030196>
- Messier, J., McGill, B. J., & Lechowicz, M. J. (2010). How do traits vary across ecological scales? A case for trait-based ecology. *Ecology Letters*, *13*(7), 838–848. <https://doi.org/10.1111/j.1461-0248.2010.01476.x>
- Milla, R., Escudero, A., & Iriondo, J. M. (2009). Inherited variability in multiple traits determines fitness in populations of an annual legume from contrasting latitudinal origins. *Annals of Botany*, *103*(8), 1279–1289. <https://doi.org/10.1093/aob/mcp068>
- Miller, J. H., Manning, S. T., & Enloe, S. F. (2013). A management guide for invasive plants in southern forests. *Gen. Tech. Rep. SRS-131*. Asheville, NC: U.S. Department of Agriculture Forest Service, Southern Research Station. 120 p., 131, 1–120.

- Mishra, P., mohd asaari, mohd shahrimie, Herrero-Langreo, A., Lohumi, S., Diezma, B., & Scheunders, P. (2017). Close range hyperspectral imaging of plants: A review. *Biosystems Engineering*, *164*, 49–67. <https://doi.org/10.1016/j.biosystemseng.2017.09.009>
- Muraoka, H., Noda, H. M., Nagai, S., Motohka, T., Saitoh, T. M., Nasahara, K. N., & Saigusa, N. (2013). Spectral vegetation indices as the indicator of canopy photosynthetic productivity in a deciduous broadleaf forest. *Journal of Plant Ecology*, *6*(5), 393–407. <https://doi.org/10.1093/jpe/rts037>
- Mutanga, O., Skidmore, A. K., & Prins, H. H. T. (2004). Predicting in situ pasture quality in the Kruger national Park, South Africa, using continuum removed absorption features. *Remote Sensing of Environment*, *89*(2), 393–408. <https://doi.org/10.1016/j.rse.2003.11.001>
- Nagendra, H. (2001). Review article. Using remote sensing to assess biodiversity. *International Journal of Remote Sensing*, *22*, 2377–2400. <https://doi.org/10.1080/01431160117096>
- Naumann, J. C., Bissett, S. N., Young, D. R., Edwards, J., & Anderson, J. E. (2010). Diurnal patterns of photosynthesis, chlorophyll fluorescence, and PRI to evaluate water stress in the invasive species, *Elaeagnus umbellata* Thunb. *Trees*, *24*(2), 237–245. <https://doi.org/10.1007/s00468-009-0394-0>
- Neuwirthová, E., Kuusk, A., Lhotáková, Z., Kuusk, J., Albrechtová, J., & Hallik, L. (2021). Leaf Age Matters in Remote Sensing: Taking Ground Truth for Spectroscopic Studies in Hemiboreal Deciduous Trees with Continuous Leaf Formation. *Remote Sensing*, *13*(7), 1353. <https://doi.org/10.3390/rs13071353>

- Nguyen, D. V., & Rocke, D. M. (2002). Multi-class cancer classification via partial least squares with gene expression profiles. *Bioinformatics (Oxford, England)*, *18*(9), 1216–1226.
<https://doi.org/10.1093/bioinformatics/18.9.1216>
- Oindo, B., Skidmore, A., & de By, R. (2002). Interannual variability of NDVI and species richness in Kenya. *International Journal of Remote Sensing*, *23*.
<https://doi.org/10.1080/01431160010014819>
- Oldeland, J., Wesuls, D., Rocchini, D., Schmidt, M., & Jürgens, N. (2010). Does using species abundance data improve estimates of species diversity from remotely sensed spectral heterogeneity? *Ecological Indicators*, *10*(2), 390–396.
<https://doi.org/10.1016/j.ecolind.2009.07.012>
- Oliphant, A. J., Wynne, R. H., Zipper, C. E., Ford, W. M., Donovan, P. F., & Li, J. (2017). Autumn olive (*Elaeagnus umbellata*) presence and proliferation on former surface coal mines in Eastern USA. *Biological Invasions*, *19*(1), 179–195.
<https://doi.org/10.1007/s10530-016-1271-6>
- Ollinger, S. V. (2011). Sources of variability in canopy reflectance and the convergent properties of plants. *New Phytologist*, *189*(2), 375–394. <https://doi.org/10.1111/j.1469-8137.2010.03536.x>
- Oppelt, N., & Mauser, W. (2004). Hyperspectral monitoring of physiological parameters of wheat during a vegetation period using AVIS data. *International Journal of Remote Sensing - INT J REMOTE SENS*, *25*, 145–159.
<https://doi.org/10.1080/0143116031000115300>

- Palmer, M. W., Earls, P. G., Hoagland, B. W., White, P. S., & Wohlgemuth, T. (2002). Quantitative tools for perfecting species lists. *Environmetrics*, *13*(2), 121–137. <https://doi.org/10.1002/env.516>
- Papp, L., van Leeuwen, B., Szilassi, P., Tobak, Z., Szatmári, J., Árvai, M., et al. (2021). Monitoring Invasive Plant Species Using Hyperspectral Remote Sensing Data. *Land*, *10*(1), 29. <https://doi.org/10.3390/land10010029>
- Peerbhay, K., Mutanga, O., Lottering, R., Bangamwabo, V., & Ismail, R. (2016). Detecting bugweed (*Solanum mauritianum*) abundance in plantation forestry using multisource remote sensing. *ISPRS Journal of Photogrammetry and Remote Sensing*, *C*(121), 167–176. <https://doi.org/10.1016/j.isprsjprs.2016.09.014>
- Peña, M. A., Cruz, P., & Roig, M. (2013). The effect of spectral and spatial degradation of hyperspectral imagery for the Sclerophyll tree species classification. *International Journal of Remote Sensing*, *34*(20), 7113–7130. <https://doi.org/10.1080/01431161.2013.817712>
- Pereira, H. M., Ferrier, S., Walters, M., Geller, G. N., Jongman, R. H. G., Scholes, R. J., et al. (2013). Essential Biodiversity Variables. *Science*, *339*(6117), 277–278. <https://doi.org/10.1126/science.1229931>
- Pérez-Enciso, M., & Tenenhaus, M. (2003). Prediction of clinical outcome with microarray data: a partial least squares discriminant analysis (PLS-DA) approach. *Human Genetics*, *112*(5–6), 581–592. <https://doi.org/10.1007/s00439-003-0921-9>
- Petchey, O. L., Pontarp, M., Massie, T. M., Kéfi, S., Ozgul, A., Weilenmann, M., et al. (2015). The ecological forecast horizon, and examples of its uses and determinants. *Ecology Letters*, *18*(7), 597–611. <https://doi.org/10.1111/ele.12443>

- Pettorelli, N., Safi, K., & Turner, W. (2014). Satellite remote sensing, biodiversity research and conservation of the future. *Philosophical Transactions of the Royal Society B: Biological Sciences*, 369(1643), 20130190. <https://doi.org/10.1098/rstb.2013.0190>
- Pettorelli, N., Bühne, H. S. to, Tulloch, A., Dubois, G., Macinnis-Ng, C., Queirós, A. M., et al. (2018). Satellite remote sensing of ecosystem functions: opportunities, challenges and way forward. *Remote Sensing in Ecology and Conservation*, 4(2), 71–93. <https://doi.org/10.1002/rse2.59>
- Pimm, S. L., Alibhai, S., Bergl, R., Dehgan, A., Giri, C., Jewell, Z., et al. (2015). Emerging Technologies to Conserve Biodiversity. *Trends in Ecology & Evolution*, 30(11), 685–696. <https://doi.org/10.1016/j.tree.2015.08.008>
- Pyšek, P., Pergl, J., Essl, F., Lenzner, B., Dawson, W., Kreft, H., et al. (2017). Naturalized alien flora of the world: Species diversity, taxonomic and phylogenetic patterns, geographic distribution and global hotspots of plant invasion. *Preslia*, 89, 203–274. <https://doi.org/10.23855/preslia.2017.203>
- Rapaport, T., Hochberg, U., Rachmilevitch, S., & Karnieli, A. (2014). The Effect of Differential Growth Rates across Plants on Spectral Predictions of Physiological Parameters. *PLOS ONE*, 9(2), e88930. <https://doi.org/10.1371/journal.pone.0088930>
- Reaser, J. K., Burgiel, S. W., Kirkey, J., Brantley, K. A., Veatch, S. D., & Burgos-Rodríguez, J. (2020). The early detection of and rapid response (EDRR) to invasive species: a conceptual framework and federal capacities assessment. *Biological Invasions*, 22(1), 1–19. <https://doi.org/10.1007/s10530-019-02156-w>
- Reich, P. B. (2014). The world-wide ‘fast–slow’ plant economics spectrum: a traits manifesto. *Journal of Ecology*, 102(2), 275–301. <https://doi.org/10.1111/1365-2745.12211>

- Roberts, D., Ustin, S., Ogunjemiyo, S., Greenberg, J., Dobrowski, S., Chen, J., & Hinckley, T. (2004). Spectral and Structural Measures of Northwest Forest Vegetation at Leaf to Landscape Scales. *Ecosystems*, 7, 545–562. <https://doi.org/10.1007/s10021-004-0144-5>
- Roberts, D. A., Ustin, S. L., Ogunjemiyo, S., Greenberg, J., Dobrowski, S. Z., Chen, J., & Hinckley, T. M. (2004). Spectral and Structural Measures of Northwest Forest Vegetation at Leaf to Landscape Scales. *Ecosystems*, 7(5), 545–562.
- Robertson, K. M., Simonson, E., Ramirez-Bullon, N., Poulter, B., & Carter, R. (2023). Effects of Spatial Resolution, Mapping Window Size, and Spectral Species Clustering on Remote Sensing of Plant Beta Diversity Using biodivMapR and Hyperspectral Imagery. *Journal of Geophysical Research: Biogeosciences*, 128(7), e2022JG007350. <https://doi.org/10.1029/2022JG007350>
- Rocchini, D., Chiarucci, A., & Loiselle, S. (2004). Testing the spectral variation hypothesis by using satellite multispectral images. *Acta Oecologica*, 26, 117–120. <https://doi.org/10.1016/j.actao.2004.03.008>
- Rocchini, D., Balkenhol, N., Carter, G., Foody, G., Gillespie, T., He, K., et al. (2010). Remotely sensed spectral heterogeneity as a proxy of species diversity: Recent advances and open challenges. *Ecological Informatics*, 5, 318–329. <https://doi.org/10.1016/j.ecoinf.2010.06.001>
- Rocchini, D., Salvatori, N., Beierkuhnlein, C., Chiarucci, A., de Boissieu, F., Förster, M., et al. (2021). From local spectral species to global spectral communities: A benchmark for ecosystem diversity estimate by remote sensing. *Ecological Informatics*, 61, 101195. <https://doi.org/10.1016/j.ecoinf.2020.101195>

- Rodriguez, R., Perroy, R. L., Leary, J., Jenkins, D., Panoff, M., Mandel, T., & Perez, P. (2021). Comparing Interpretation of High-Resolution Aerial Imagery by Humans and Artificial Intelligence to Detect an Invasive Tree Species. *Remote Sensing*, *13*(17), 3503. <https://doi.org/10.3390/rs13173503>
- Rohart, F., Gonzalez, I., & Dejean, S. (2016). mixOmics: Omics Data Integration Project. R package version 6.1.1. Retrieved January 29, 2024, from <https://cran.r-project.org/web/packages/mixOmics/index.html>
- Royimani, L., Mutanga, O., Odindi, J., & Matongera, T. (2018). Advancements in satellite remote sensing for mapping and monitoring of Alien Invasive Plant species (AIPs). *Physics and Chemistry of the Earth, Parts A/B/C*, *112*. <https://doi.org/10.1016/j.pce.2018.12.004>
- Rozendaal, D. M. A., Hurtado, V. H., & Poorter, L. (2006). Plasticity in leaf traits of 38 tropical tree species in response to light; relationships with light demand and adult stature. *Functional Ecology*, *20*(2), 207–216. <https://doi.org/10.1111/j.1365-2435.2006.01105.x>
- Sabat-Tomala, A., Raczko, E., & Zagajewski, B. (2020). Comparison of Support Vector Machine and Random Forest Algorithms for Invasive and Expansive Species Classification Using Airborne Hyperspectral Data. *Remote Sensing*, *12*(3), 516. <https://doi.org/10.3390/rs12030516>
- Sabat-Tomala, A., Raczko, E., & Zagajewski, B. (2022). Mapping Invasive Plant Species with Hyperspectral Data Based on Iterative Accuracy Assessment Techniques. *Remote Sensing*, *14*(1), 64. <https://doi.org/10.3390/rs14010064>

- Sanchez-Azofeifa, G. A., Calvo-Alvarado, J., Espírito-Santo, M., Fernandes, G., Powers, J., & Quesada, M. (2013). Tropical Dry Forests in the Americas: The Tropi-Dry Endeavor (pp. 1–16).
- Scheiner, S. (1993). Genetics and Evolution of Phenotypic Plasticity. *Annual Review of Ecology, Evolution and Systematic*, 24, 35–68.
<https://doi.org/10.1146/annurev.es.24.110193.000343>
- Schmidt, K. S., & Skidmore, A. (2003). Spectral discrimination of vegetation types in a coastal wetland. *Remote Sensing of Environment*, 85, 92–108. [https://doi.org/10.1016/S0034-4257\(02\)00196-7](https://doi.org/10.1016/S0034-4257(02)00196-7)
- Schmidtlein, S., & Fassnacht, F. E. (2017). The spectral variability hypothesis does not hold across landscapes. *Remote Sensing of Environment*, 192, 114–125.
<https://doi.org/10.1016/j.rse.2017.01.036>
- Scholes, R. J., Walters, M., Turak, E., Saarenmaa, H., Heip, C. H., Tuama, É. Ó., et al. (2012). Building a global observing system for biodiversity. *Current Opinion in Environmental Sustainability*, 4(1), 139–146. <https://doi.org/10.1016/j.cosust.2011.12.005>
- Schweiger, A. K., Cavender-Bares, J., Townsend, P. A., Hobbie, S. E., Madritch, M. D., Wang, R., et al. (2018). Plant spectral diversity integrates functional and phylogenetic components of biodiversity and predicts ecosystem function. *Nature Ecology & Evolution*, 2(6), 976–982. <https://doi.org/10.1038/s41559-018-0551-1>
- Seebens, H., Blackburn, T. M., Dyer, E. E., Genovesi, P., Hulme, P. E., Jeschke, J. M., et al. (2017). No saturation in the accumulation of alien species worldwide. *Nature Communications*, 8(1), 14435. <https://doi.org/10.1038/ncomms14435>

- Serbin, S. P., Singh, A., McNeil, B. E., Kingdon, C. C., & Townsend, P. A. (2014). Spectroscopic determination of leaf morphological and biochemical traits for northern temperate and boreal tree species. *Ecological Applications*, *24*(7), 1651–1669. <https://doi.org/10.1890/13-2110.1>
- Shannon, C. E. (1948). A Mathematical Theory of Communication. *Bell System Technical Journal*, *27*(3), 379–423. <https://doi.org/10.1002/j.1538-7305.1948.tb01338.x>
- Siefert, A., Violle, C., Chalmandrier, L., Albert, C. H., Taudiere, A., Fajardo, A., et al. (2015). A global meta-analysis of the relative extent of intraspecific trait variation in plant communities. *Ecology Letters*, *18*(12), 1406–1419. <https://doi.org/10.1111/ele.12508>
- Sims, D. A., & Gamon, J. A. (2002). Relationships between leaf pigment content and spectral reflectance across a wide range of species, leaf structures and developmental stages. *Remote Sensing of Environment*, *81*(2), 337–354. [https://doi.org/10.1016/S0034-4257\(02\)00010-X](https://doi.org/10.1016/S0034-4257(02)00010-X)
- Singh, K. K., Surasinghe, T. D., & Frazier, A. E. (2024). Systematic review and best practices for drone remote sensing of invasive plants. *Methods in Ecology and Evolution*, *15*(6), 998–1015. <https://doi.org/10.1111/2041-210X.14330>
- Skidmore, A. K., Coops, N. C., Neinavaz, E., Ali, A., Schaepman, M. E., Paganini, M., et al. (2021). Priority list of biodiversity metrics to observe from space. *Nature Ecology and Evolution*, *5*(7), 896–906. <https://doi.org/10.1038/s41559-021-01451-x>
- Skowronek, S., Ewald, M., Isermann, M., Van De Kerchove, R., Lenoir, J., Aerts, R., et al. (2017). Mapping an invasive bryophyte species using hyperspectral remote sensing data. *Biological Invasions*, *19*, 239–254.

- Slaton, M. R., Raymond Hunt, E., & Smith, W. K. (2001). Estimating near-infrared leaf reflectance from leaf structural characteristics. *American Journal of Botany*, 88(2), 278–284.
- Stevens, A., & Ramirez-Lopez, L. (2022). An introduction to the prospectr package. (Version 0.2.6.).
- Sun, A. Y., & Scanlon, B. R. (2019). How can Big Data and machine learning benefit environment and water management: a survey of methods, applications, and future directions. *Environmental Research Letters*, 14(7), 073001. <https://doi.org/10.1088/1748-9326/ab1b7d>
- Thenkabail, P. S., Gumma, M. K., Teluguntla, P., & Mohammed, I. A. (2014). Hyperspectral Remote Sensing of Vegetation and Agricultural Crops. *Photogrammetric Engineering & Remote Sensing (PE&RS)*, 80(8), 697–723.
- Torresani, M., Duccio, R., Marc, Z., Ruth, S., & Tonon, G. (2018). Testing the spectral variation hypothesis by using the RAO-Q index to estimate forest biodiversity: Effect of spatial resolution (pp. 1183–1186). <https://doi.org/10.1109/IGARSS.2018.8666630>
- Torresani, M., Rossi, C., Perrone, M., Hauser, L. T., Féret, J.-B., Moudrý, V., et al. (2024). Reviewing the spectral variation hypothesis: Twenty years in the tumultuous sea of biodiversity estimation by remote sensing. *Ecological Informatics*, 102702. <https://doi.org/10.1016/j.ecoinf.2024.102702>
- Townsend, P. A., Serbin, S. P., Kruger, E. L., & Gamon, J. A. (2013). Disentangling the contribution of biological and physical properties of leaves and canopies in imaging spectroscopy data. *Proceedings of the National Academy of Sciences of the United States of America*, 110(12), E1074. <https://doi.org/10.1073/pnas.1300952110>

- Treurnicht, M., Pagel, J., Tonnabel, J., Esler, K. J., Slingsby, J. A., & Schurr, F. M. (2020). Functional traits explain the Hutchinsonian niches of plant species. *Global Ecology and Biogeography*, 29(3), 534–545. <https://doi.org/10.1111/geb.13048>
- Turner, W. (2014). Sensing biodiversity. *Science*, 346(6207), 301–302. <https://doi.org/10.1126/science.1256014>
- Ustin, S. L., & Gamon, J. A. (2010). Remote sensing of plant functional types. *The New Phytologist*, 186(4), 795–816. <https://doi.org/10.1111/j.1469-8137.2010.03284.x>
- Ustin, S. L., Roberts, D. A., Gamon, J. A., Asner, G. P., & Green, R. O. (2004). Using Imaging Spectroscopy to Study Ecosystem Processes and Properties. *BioScience*, 54(6), 523–534. [https://doi.org/10.1641/0006-3568\(2004\)054\[0523:U1STSE\]2.0.CO;2](https://doi.org/10.1641/0006-3568(2004)054[0523:U1STSE]2.0.CO;2)
- Vellend, M., & Geber, M. A. (2005). Connections between species diversity and genetic diversity. *Ecology Letters*, 8(7), 767–781. <https://doi.org/10.1111/j.1461-0248.2005.00775.x>
- Virginia Invasive Species Advisory Committee. (2018). *Virginia Invasive Species Management Plan*. (Natural Heritage Technical Document No. 18– 09). Virginia Department of Conservation and Recreation.
- Wang, J., Cheng, Y., Zhang, J., Müller, C., & Cai, Z. (2016). Soil gross nitrogen transformations along a secondary succession transect in the north subtropical forest ecosystem of southwest China. *Geoderma*, 280, 88–95. <https://doi.org/10.1016/j.geoderma.2016.06.016>
- Wang, J., Song, G., Liddell, M., Morellato, P., Lee, C., Yang, D., et al. (2023). An ecologically-constrained deep learning model for tropical leaf phenology monitoring using

- PlanetScope satellites. *Remote Sensing of Environment*, 286, 113429.
<https://doi.org/10.1016/j.rse.2022.113429>
- Wang, R., & Gamon, J. A. (2019). Remote sensing of terrestrial plant biodiversity. *Remote Sensing of Environment*, 231, 111218. <https://doi.org/10.1016/j.rse.2019.111218>
- Wang, R., Gamon, J. A., Cavender-Bares, J., Townsend, P. A., & Zyguelbaum, A. I. (2018). The spatial sensitivity of the spectral diversity–biodiversity relationship: an experimental test in a prairie grassland. *Ecological Applications*, 28(2), 541–556.
- Wang, Z., Chlus, A., Geygan, R., Ye, Z., Zheng, T., Singh, A., et al. (2020). Foliar functional traits from imaging spectroscopy across biomes in eastern North America. *New Phytologist*, 228(2), 494–511. <https://doi.org/10.1111/nph.16711>
- Whittaker, R. H. (1972). Evolution and Measurement of Species Diversity. *Taxon*, 21(2/3), 213–251. <https://doi.org/10.2307/1218190>
- Woolley, J. (1971). Reflectance and transmittance of light by leaves. *Plant Physiology*.
<https://doi.org/10.1104/PP.47.5.656>
- Wright, I. J., Reich, P. B., Westoby, M., Ackerly, D. D., Baruch, Z., Bongers, F., et al. (2004). The worldwide leaf economics spectrum. *Nature*, 428(6985), 821–827.
<https://doi.org/10.1038/nature02403>
- Xiao, Y., Zhao, W., Zhou, D., & Gong, H. (2014). Sensitivity Analysis of Vegetation Reflectance to Biochemical and Biophysical Variables at Leaf, Canopy, and Regional Scales. *Geoscience and Remote Sensing, IEEE Transactions On*, 52, 4014–4024.
<https://doi.org/10.1109/TGRS.2013.2278838>

- Xu, C., Zeng, Y., Zheng, Z., Zhao, D., Liu, W., Ma, Z., & Wu, B. (2022). Assessing the Impact of Soil on Species Diversity Estimation Based on UAV Imaging Spectroscopy in a Natural Alpine Steppe. *Remote Sensing*, *14*(3), 671. <https://doi.org/10.3390/rs14030671>
- Yang, X., Tang, J., Mustard, J. F., Wu, J., Zhao, K., Serbin, S., & Lee, J.-E. (2016). Seasonal variability of multiple leaf traits captured by leaf spectroscopy at two temperate deciduous forests. *Remote Sensing of Environment*, *179*, 1–12. <https://doi.org/10.1016/j.rse.2016.03.026>
- Zarco-Tejada, P., Miller, J., Harron, J., Hu, B., Noland, T., Goel, N., et al. (2004). Needle Chlorophyll content estimation through model inversion using hyperspectral data from Boreal Conifer Forest Canopies. *Remote Sensing of Environment*, *89*, 189–199. <https://doi.org/10.1016/j.rse.2002.06.002>
- Zeileis, A., & Grothendieck, G. (2005). **zoo** : S3 Infrastructure for Regular and Irregular Time Series. *Journal of Statistical Software*, *14*(6). <https://doi.org/10.18637/jss.v014.i06>

Appendix A: Supplemental Figures Chapter 2

Table S1: Errors (Omission and Commission) and Accuracies (User and Producer) for each detection algorithm for each species of interest.

Species of interest	DOY	Omission	Commission	User Accuracy	Producer Accuracy	Accuracy Classification
Ai_al	160	100%	29%	71%	0%	poor detection
Ai_al	178	0%	34%	66%	100%	good detection but sensitive
Ai_al	249	100%	37%	63%	0%	poor detection
Ai al	276	0%	9%	91%	100%	good overall accuracy
El_um	106	25%	16%	84%	75%	good overall accuracy
El_um	134	38%	0%	100%	63%	poor detection
El_um	160	0%	0%	100%	100%	good overall accuracy
El_um	178	0%	0%	100%	100%	good overall accuracy
El_um	249	0%	0%	100%	100%	good overall accuracy
El_um	276	13%	10%	90%	88%	good overall accuracy
El um	309	25%	23%	77%	75%	good overall accuracy
Rh_da	106	60%	44%	56%	40%	poor detection
Rh_da	134	63%	40%	60%	38%	poor detection
Rh_da	160	13%	22%	78%	88%	good overall accuracy
Rh_da	178	25%	24%	76%	75%	good overall accuracy
Rh_da	249	13%	57%	43%	88%	good detection but sensitive
Rh_da	276	63%	50%	50%	38%	poor detection
Rh_da	309	50%	22%	78%	50%	poor detection

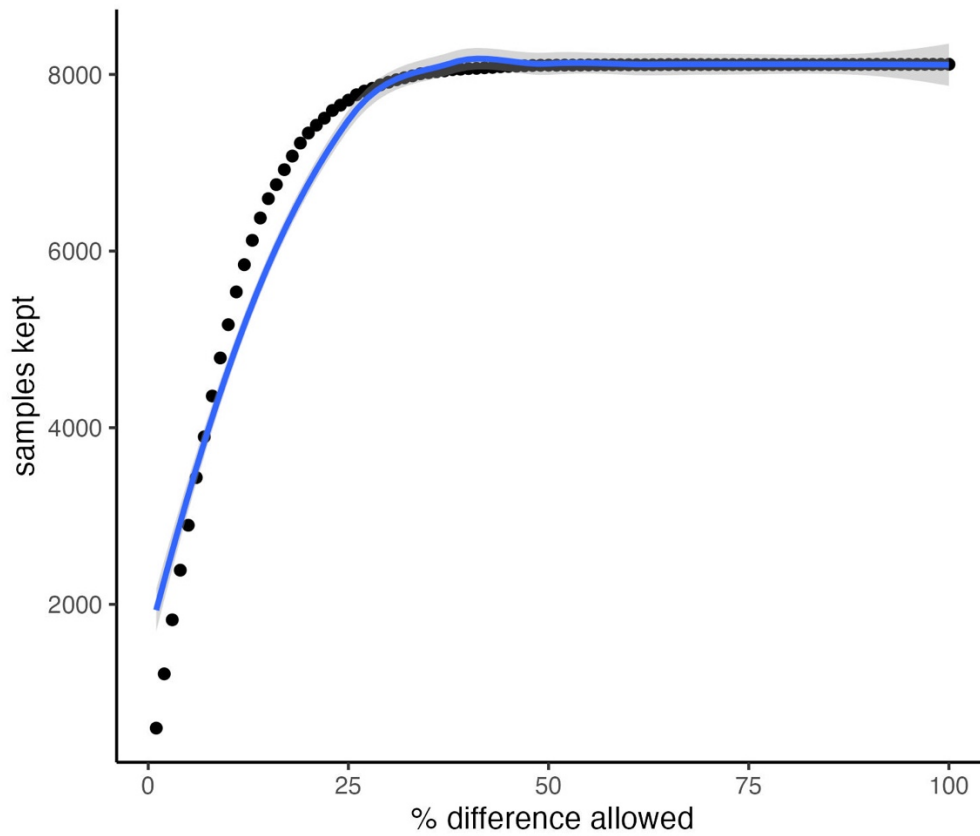


Figure S1: The number of samples (pixels) kept during outlier removal. On the x-axis is the percent difference allowed between each pixel's overall mean reflectance (across all wavelengths) and the entire canopy. The shoulder occurs around 25-30%.

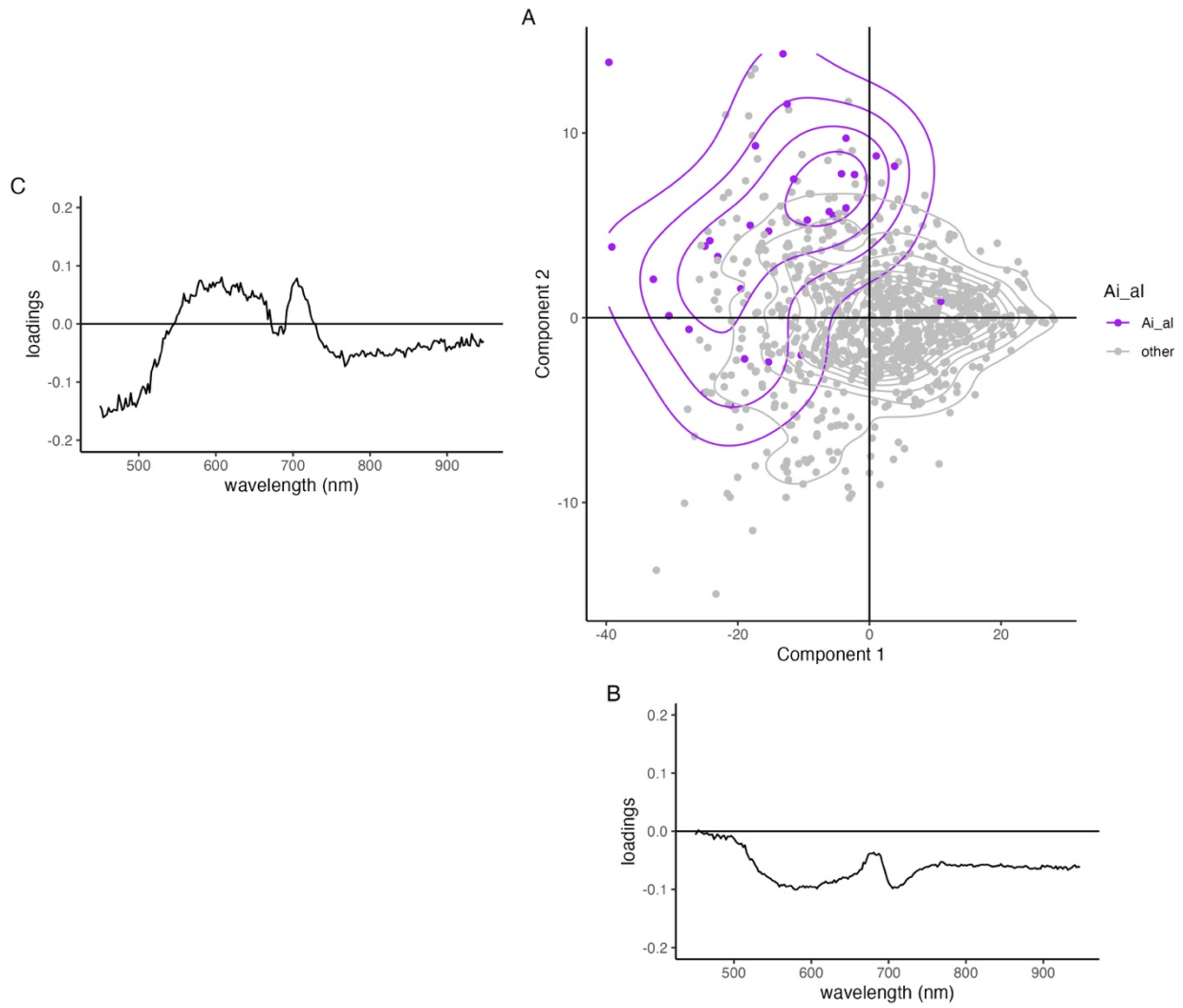


Figure S2. A) Location of all *A. altissima* training pixels (purple) and all other species (grey) in component space in PLS-DA for DOY 276. B) Shown below the x-axis is Component 1, and C) beside the y-axis are the loadings for each wavelength in Component 2.

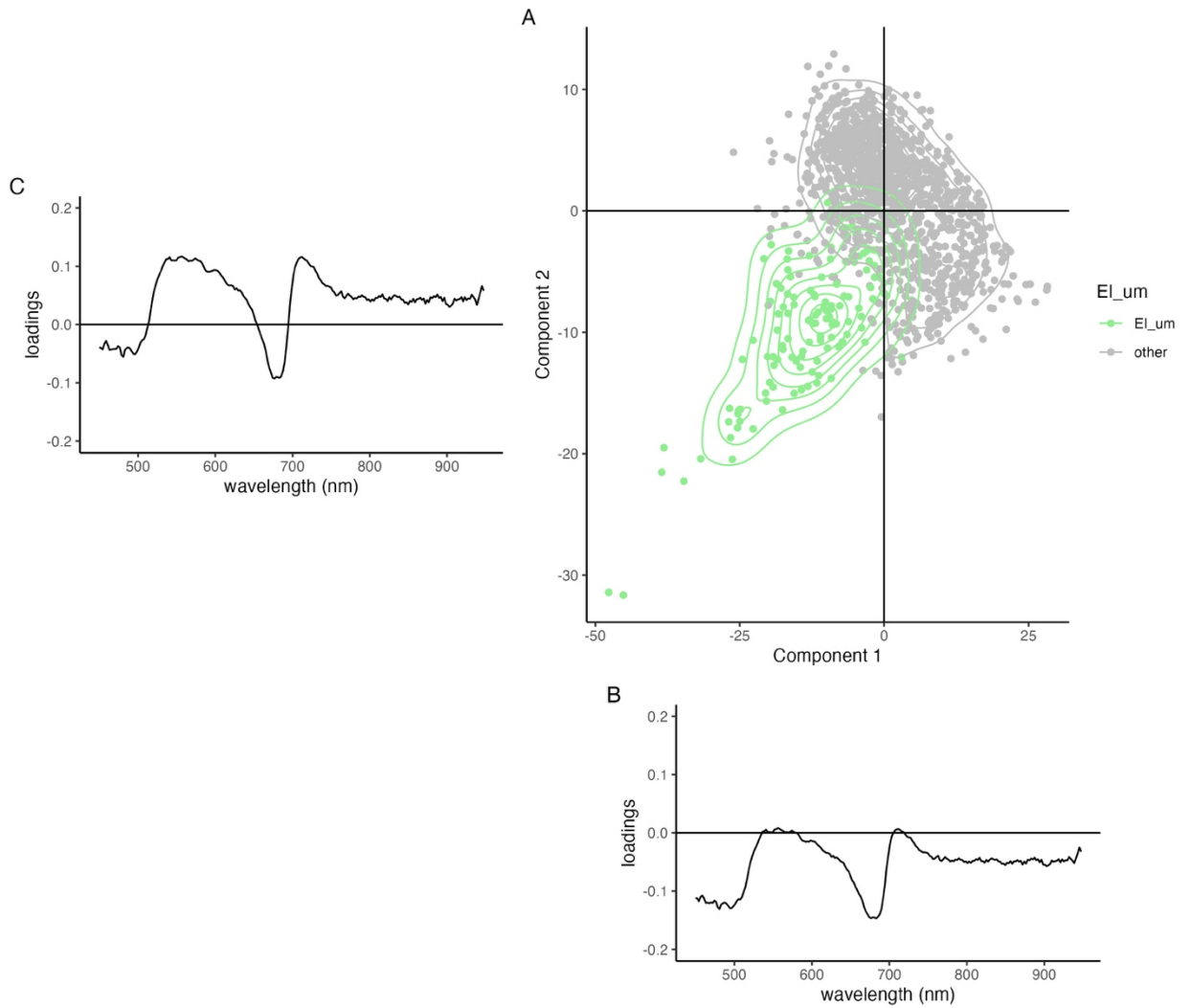


Figure S3. A) Location of all *E. umbellata* training pixels (light green) and all other species (grey) in component space in PLS-DA for June 26 (DOY 178). B) Shown below the x-axis is Component 1, and C) beside the y-axis are the loadings for each wavelength in Component 2.

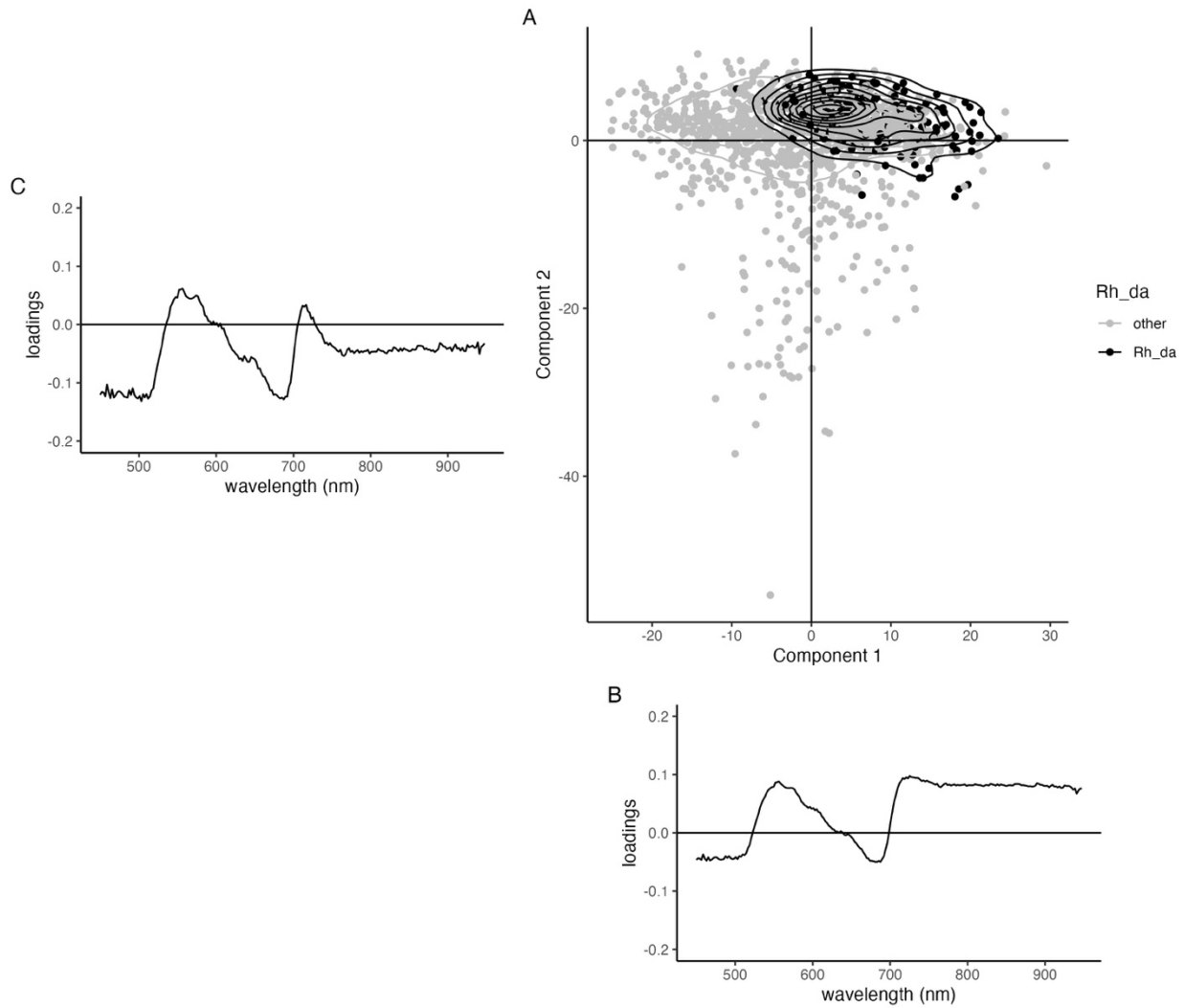


Figure S4. A) Location of all *R. davurica* training pixels (black) and all other species (grey) in component space in PLS-DA for June 26 (DOY 178). B) Shown below the x-axis is Component 1, and C) beside the y-axis are the loadings for each wavelength in Component 2.

Appendix B: Supplemental Figures Chapter 3

Table S1: Classification accuracy results as user accuracy (UA) and producer accuracy (PA) for detection of each species of interest (*A. altissima*, *E. umbellata*, and *R. davurica*) in NEON images from 2016, 2017, 2019, and 2021 (listed in the “Testing (NEON)” column) using either fine- or coarser-resolution hyperspectral drone imagery (listed in the “Training (drone)” column as C for coarse or F for fine-resolution). Reflectance data were either transformed (“T” in the “Transformed” column) or untransformed (“NT” in the “Trans” column). The most accurate strictness level is also reported (“L+” is most lenient, “L” is moderately lenient, “S” is strict, and “S +” is most strict).

Species of interest	Testing (NEON)	Training (drone)	Trans	Most accurate strictness level	UA	PA
<i>A. altissima</i>	2016	C	NT	L +	52%	57%
<i>A. altissima</i>	2017	C	NT	L +	56%	60%
<i>A. altissima</i>	2017	C	T	S	53%	60%
<i>A. altissima</i>	2021	F	T	L +	58%	100%
<i>E. umbellata</i>	2017	F	T	S +	51%	86%
<i>E. umbellata</i>	2021	F	NT	S +	59%	71%
<i>R. davurica</i>	2017	C	NT	L	62%	60%
<i>R. davurica</i>	2019	F	NT	L	65%	67%
<i>R. davurica</i>	2019	F	NT	S	54%	67%
<i>R. davurica</i>	2019	F	T	S	73%	67%
<i>R. davurica</i>	2019	F	T	S +	88%	67%
<i>R. davurica</i>	2019	C	NT	S +	54%	67%

Table S2: Classification accuracy results as user accuracy (UA) and producer accuracy (PA) for detection of each species of interest (*A. altissima*, *E. umbellata*, and *R. davurica*) in NEON images from 2016, 2017, 2019, and 2021 using that year’s images (listed in the “Testing & Training (NEON)” column). Reflectance data were either transformed (“T” in the “Transformed” column) or untransformed (“NT” in the “Transformed” column). The most accurate strictness level is also reported (“L+” is most lenient, “L” is moderately lenient, “S” is strict, and “S +” is most strict).

Species of interest	Testing & Training (NEON)	Transformed	Most accurate strictness level	UA	PA
<i>A. altissima</i>	2017	NT	L	69%	75%
<i>A. altissima</i>	2017	NT	L +	51%	75%
<i>A. altissima</i>	2017	T	L	69%	100%
<i>A. altissima</i>	2017	T	L +	63%	100%
<i>A. altissima</i>	2019	NT	S	56%	60%
<i>A. altissima</i>	2019	NT	S +	69%	60%
<i>A. altissima</i>	2019	T	L	67%	80%
<i>A. altissima</i>	2019	T	S	93%	60%
<i>A. altissima</i>	2019	T	L +	53%	100%
<i>A. altissima</i>	2021	T	L	78%	100%
<i>A. altissima</i>	2021	T	S	97%	100%
<i>A. altissima</i>	2021	T	L +	78%	100%
<i>A. altissima</i>	2021	T	S +	97%	100%

Species of interest	Testing & Training (NEON)	Transformed	Most accurate strictness level	UA	PA
<i>E. umbellata</i>	2016	NT	S	73%	67%
<i>E. umbellata</i>	2016	NT	S +	81%	67%
<i>E. umbellata</i>	2016	T	L	53%	80%
<i>E. umbellata</i>	2016	T	S	74%	80%
<i>E. umbellata</i>	2016	T	S +	82%	60%
<i>E. umbellata</i>	2017	NT	L	58%	80%
<i>E. umbellata</i>	2017	NT	S	68%	60%
<i>E. umbellata</i>	2017	NT	S +	79%	60%
<i>E. umbellata</i>	2017	T	L	56%	67%
<i>E. umbellata</i>	2017	T	S	67%	67%
<i>E. umbellata</i>	2017	T	S +	83%	67%
<i>R. davurica</i>	2017	NT	S	63%	75%
<i>R. davurica</i>	2017	NT	S +	80%	75%
<i>R. davurica</i>	2017	T	L	64%	75%
<i>R. davurica</i>	2017	T	S	68%	75%
<i>R. davurica</i>	2017	T	S +	85%	75%
<i>R. davurica</i>	2019	NT	L	58%	100%
<i>R. davurica</i>	2019	NT	S	79%	100%
<i>R. davurica</i>	2019	NT	S +	89%	100%
<i>R. davurica</i>	2019	T	L	67%	100%
<i>R. davurica</i>	2019	T	S	65%	100%
<i>R. davurica</i>	2019	T	L +	57%	100%
<i>R. davurica</i>	2019	T	S +	80%	100%

Appendix C: Supplemental Figures Chapter 4

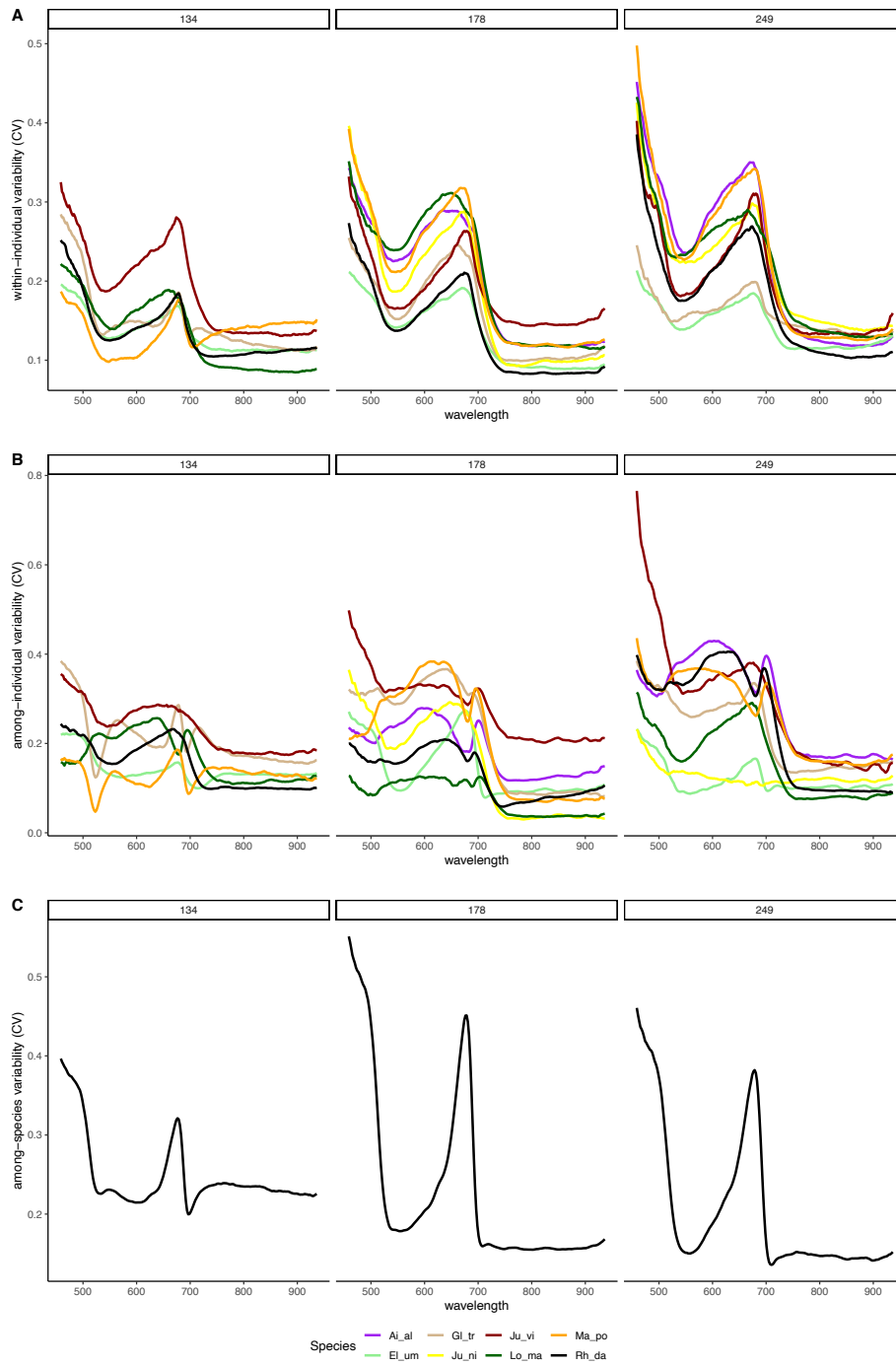


Figure S1. CV at each organizational scale for each species. These values were presented in the body of the manuscript as a ratio of the finer-scale variability compared to among-species variability in each band.

Table S1. Summary of variability at each finer organizational scale (“scale”, within and among individuals of a species), compared to among-species variability for each day (“DOY”): which species had ratios > 1 (“Species with ratio > 1”). Then statistics about the greatest CV ratio: which species, band, and the magnitude (“Maximum CV ratio: Species (band), value”)

scale	DOY	Species with ratio > 1	Maximum CV ratio: Species (band), value
within individuals	134	Ju_vi	Ju_vi (695 nm), 1.1
within individuals	178	Ai_al, Ju_ni, Lo_ma, Ma_po, Gl_tr, Ju_vi	Lo_ma (703 nm), 1.4
within individuals	249	all	Lo_ma (707 nm), 1.7
among individuals	134	Gl_tr, Ju_vi, Lo_ma	Ju_vi (697 nm), 1.3
among individuals	178	Ai_al, Gl_tr, Ju_ni, Ju_vi, Ma_po	Ju_vi (705 nm), 2.0
among individuals	249	Ju_vi, Ai_al, Gl_tr, Lo_ma, Ma_po, Rh_da	Ai_al (707 nm), 2.8

Appendix D: Supplemental Figures Chapter 5

Table 1S. Alpha, beta, and gamma biodiversity and spectral diversity. Biodiversity metrics, richness and Shannon diversity, were calculated from species composition data, and spectral diversity metrics were calculated from extracted quadrats in NEON aerial imagery as average CV across all bands in 100 nm-wide spectral regions.

Diversity metric		Alpha _{mean}	Alpha _{range}	Beta	Gamma
Biodiversity	Richness	11.90 ± 0.74	[7, 16]	3.61	43
	Shannon diversity	1.39 ± .10	[0.85, 1.83]	0.30	0.4
Spectral diversity	CV _{blue}	0.10 ± 0.01	[0.04, 0.16]	1.62	0.16
	CV _{green-yellow}	0.08 ± 0.01	[0.03, 0.14]	1.47	0.12
	CV _{orange-red}	0.11 ± 0.01	[0.06, 0.17]	1.53	0.16
	CV _{red edge}	0.08 ± 0.02	[0.04, 0.19]	1.59	0.13
	CV _{low NIR}	0.08 ± 0.02	[0.04, 0.19]	1.59	0.13
	CV _{mid NIR}	0.08 ± 0.02	[0.03, 0.18]	1.62	0.13
	CV _{high NIR}	0.08 ± 0.01	[0.03, 0.17]	1.56	0.12

Table S2: Plot-level species composition details for each plot, (“Plot”, “Invasion level,” which is how invaded the plot is by *R. davurica* and *E. umbellata*, and “Top species (relative cover),” the most abundantly sampled species and its relative number of hits, which translates approximately to relative cover for use with the Shannon diversity index. The “Spectral diversity” reports the single metric of mean CV across all VNIR bands (“Overall CV_{mean}”). The Richness and Shannon diversity indices are provided, along with an “X” if the plot’s spectral diversity values did not fall near the positive relationship line and instead fell above or below it, or a checkmark if the plot did fall on the positive relationship line.

Plot details			Spectral diversity	Biodiversity metrics and SVH agreement	
Plot	Invasion level	Top species (relative cover)	Overall CV _{mean}	Richness	Shannon diversity
1	high	<i>R. davurica</i> (78%)	0.05	14 ✘	0.85 ✓
2	high	<i>R. davurica</i> (52%)	0.05	12 ✘	1.62 ✘
3	low	graminoid <i>spp</i> (44%)	0.04	12 ✘	1.33 ✘
4	high	<i>E. umbellata</i> (34%)	0.09	13 ✓	1.30 ✓
5	low	<i>M. pomifera</i> (74%)	0.16	7 ✘	0.90 ✘
6	low	<i>Rubus spp.</i> (43%)	0.07	12 ✓	1.37 ✓
7	low	<i>Rubus spp.</i> (50%)	0.13	16 ✓	1.65 ✓
8	low	<i>Rubus spp.</i> (56%)	0.13	11 ✓	1.32 ✓
9	high	<i>R. davurica</i> (32%)	0.09	11 ✓	1.71 ✘
10	high	<i>R.davurica</i> (29%)	0.04	11 ✓	1.83 ✘

Appendix E: Spectral variability in fine-scale drone-based imaging spectroscopy does not impede detection of target invasive plant species

This is a published manuscript in a special issue of Frontiers in Remote Sensing: Women in Remote Sensing and was a preliminary study for Chapter 2.

Abstract:

Land managers are making concerted efforts to control the spread of invasive plants, a task that demands extensive ecosystem monitoring, for which unoccupied aerial vehicles (UAVs or drones) are becoming increasingly popular. UAV imagery has high spatial resolution, which may positively or negatively affect plant species differentiation. We assessed this impact on detection of invasive plant species *Ailanthus altissima* (tree of heaven) and *Elaeagnus umbellata* (autumn olive) using fine-resolution images collected in northwestern Virginia in June 2020 by a UAV with a Headwall Hyperspec visible and near-infrared hyperspectral imager. Though *E. umbellata* had greater intraspecific relative to interspecific variability than *A. altissima*, the classification accuracy was greater for *E. umbellata* (95%) than for *A. altissima* (66%). This suggests that differences between species of interest and others are not necessarily obscured by intraspecific variability. Therefore, the benefits of UAV-based spectroscopy for species identification outweigh potential variability in fine resolution imagery.

1. Introduction

Globally, invasive plants pose significant threats to natural ecosystems (Gurevitch & Padilla, 2004) and biodiversity (Gaertner et al., 2009; Kimothi & Dasari, 2010; Peerbhay et al., 2016). Across the state of Virginia, invasive, non-native plants are radically altering natural environments by inhibiting the growth of native species upon which native wildlife and insects depend (Miller et al., 2013). These widespread changes in species composition also have broader impacts on soil chemistry and forest canopies, with effects on dynamics of carbon, nutrients, water, and energy (Liao et al., 2008; Lovett et al., 2016).

Ailanthus altissima (tree of heaven) is a notably widespread and harmful invasive tree not only in Virginia but across the U.S. (Burkholder, 2010). It tends to impact the soil chemistry and species composition of ecosystems in which it is present by: increasing nutrient cycling rates; increasing soil C, N, K, and Mg; and encouraging the encroachment of other plant species that thrive in high nutrient environments (Gómez-Aparicio & Canham, 2008). *Elaeagnus umbellata* (autumn olive) is a common invasive shrub; as of 2017, it was found on 39,000 ha in the U.S. (Oliphant et al., 2017). It has a relationship with N-fixing endosymbionts and affects nitrifying (ammonium-oxidizing) microorganisms (Malinich et al., 2017; Naumann et al., 2010), and therefore is especially competitive in disturbed areas with N-poor soils (Malinich et al., 2017). In addition to its tolerance of nutrient-poor conditions, *E. umbellata* is also drought resistant and able to survive in a wide range of soil moisture conditions (Malinich et al., 2017; Naumann et al., 2010). Last, it can outcompete native plants after establishment due to its dense shading (Oliphant et al., 2017).

Land managers are making concerted efforts to control the spread of invasive plant species, a task that demands extensive ecosystem monitoring (Miller et al., 2013). Traditional approaches

to ecosystem observation and monitoring are satellite-based and ground-based. Each approach, however, has caveats. Satellite imagery covers large areas but cannot provide fine-scale details, whereas ground surveying, despite its ability to provide fine-scale details, is labor intensive, and is challenging for surveying broad areas. Unoccupied aerial vehicles (UAVs) provide data on an intermediate scale, with much higher spatial resolution than satellite data and with more spatial coverage than ground surveys (Alvarez-Vanhard et al., 2021). As UAVs merge the benefits of more traditional satellite-based and ground-based monitoring, they are becoming an increasingly popular means to observe ecosystems, including invasive plant species monitoring (Sun & Scanlon, 2019).

Whereas UAVs are becoming increasingly popular as a vehicle for invasive plant species monitoring, spectroscopy has been and continues to be used for the remote sensing of plant and ecosystem observation. Spectroscopy, which includes a large number of narrow, contiguous bands, provides detailed spectral information (Chance et al., 2016; Kaufmann et al., 2008), which is influenced by differences in biophysical and biochemical characteristics of plants (Matongera et al., 2016; Z. Wang et al., 2020; Yang et al., 2016), including: pigments (Mahlein et al., 2010; Xiao et al., 2014), such as chlorophyll (Gregory P. Asner & Martin, 2008b; Chance et al., 2016; Thenkabail et al., 2014), anthocyanins, and carotenoids (Blackburn, 2007); plant water and vegetation stress (Thenkabail et al., 2014); and leaf N, P, and K (Gregory P. Asner & Martin, 2008b; Chance et al., 2016; Mutanga et al., 2004; Thenkabail et al., 2014). Thus, spectroscopic data, which serve as an indication of plant chemical and structural properties, vary within and across ecosystems (Martin & Aber, 1997; Ustin et al., 2004).

Spectra are strongly related to certain biochemical and structural plant traits (Jacquemoud et al. 2009; Kattenborn et al. 2019; Ollinger 2010). Generally, greater spectral variation is

associated with species or trait variation (Palmer et al., 2002). Certain wavelengths, such as those associated with upper-canopy pigments, water, and nitrogen, can be analyzed to differentiate among species. Intraspecific (within species) trait variability, however, is sometimes similar to or even greater than interspecific (among species) variation (Jung et al. 2010; Messier et al. 2010; Leps et al. 2011; Auger & Shipley 2013).

Though imaging spectroscopy has been previously used to identify individual plant species (Mishra et al., 2017), particularly invasive species (Aneece & Epstein, 2017; Chance et al., 2016; Kganyago et al., 2017; Skowronek et al., 2017), using spectroscopic sensors in concert with UAVs is a relatively new application for these technologies. Whereas a few UAV-based studies have been successful in identifying individual plant species, this has been accomplished in large monocultures where the target plant is easily distinguished from the surrounding vegetation (Huang & Asner, 2009).

Additionally, UAV imagery has much finer spatial resolution than satellites. It is not known, however, whether the very fine spatial resolution of data provided by UAVs is beneficial or detrimental to the process of differentiation. Smaller pixel size overcomes the challenge of averaged spectral properties of large pixel sizes over heterogeneous landscapes (Underwood et al., 2007). Peña et al. (2013), for example, found that increased resolution from 2.4 m to 1.2 m increased the differentiability of tree species by 25%. Similarly, Roberts et al. (2004) found that plant species were least distinct at the stand scale and most distinct at the branch scale, a scale similar to that of Peña et al. (2013). Detection of invasive plant species is likely improved by the fine spatial resolution that a UAV can achieve, as it does not require large and homogeneous infestation stands. With very fine spatial resolution, however, spectral variation among pixels will be greater than with coarser spatial resolution, which yields a smoothing effect of extreme values

(Palmer 2000, 2002). It is expected, then, that spectral variation will be greater with decreasing spatial resolution. It is essential to understand the mechanisms that allow for the detection of target invasive plant species within these fine-resolution images.

To explore the fundamental questions of whether variability caused by fine-resolution spectroscopy enhances or impedes the ability to differentiate plant species, we collected images during the 2020 growing season from forest canopies in northwestern Virginia at the Blandy Experimental Farm (BEF), where invasive species are present and common. We address the following questions:

1. Over which wavelengths do intra-individual and intraspecific variability of target invasive plant species exceed interspecific variability?
2. Can the spectral signal from individual pixels within a tree crown be used to effectively detect target invasive plant species in an image?
3. How much does intra-individual and intraspecific variability of target invasive plant species impede the ability to differentiate among species?

2. Methods

2.1 Study Site

Blandy Experimental Farm (BEF), a biological field station owned by the University of Virginia, is located in the Shenandoah Valley in northwestern Virginia (39.06°N, 78.07°W). At 190 m elevation, BEF has a mean annual precipitation of 975 mm, a mean annual temperature of 12°C, and a mean July high temperature of 31.5°C. It contains 80 ha of old fields in various stages of succession (Bowers, 1997).

Aerial spectroscopic data collection took place over three 1-ha fields at BEF, based on their abundance of the invasive plant species of interest, *A. altissima* and *E. umbellata*, along with several other trees, shrubs, forbs, and grasses. The fields are in early- to mid-successional stages and are approximately 20, 25, and 30 years in age. Each field is located on low-relief topography.

2.2 Data collection and image post-processing

Spectroscopic images were collected using a DJI Matrice 600 Pro drone equipped with a high-precision GPS system and an imaging spectrometer (Nano-Hyperspec, Headwall Photonics, Bolton, MA). The imaging spectrometer has a spectral range of 400 to 1000 nm (in the visible and NIR portions of the electromagnetic spectrum), with a spectral resolution of 2 to 3 nm over 270 spectral bands. Flight plans over each field were created using Universal Ground Control Software (UgCS), in which the UAV would fly in straight lines at a consistent height of 48 m above the ground to obtain images with 3 cm pixels. The imaging spectrometer was programmed to capture images along the flight plan using HyperSpec III software (Headwall Photonics, Bolton, MA).

Images were collected in the middle of the growing season in late June (DOY 178), midday between 10h and 15h to reduce bidirectional reflectance distribution function (BRDF) effects and under consistent sky conditions. This date of collection was chosen for its proximity to when the National Ecological Observatory Network (NEON) collects spectroscopic images using a fixed-wing aircraft with coarser resolution (approximately 1 m resolution, compared to 0.03 m resolution). Collected spectroscopic images were adjusted for incoming and scattered solar radiation using a sampled dark reference at the time of flight and a grey scale reference tarp with known reflectance located in the flight scene, respectively. Using HyperSpec III software, terrain

and perspective effects were removed with a 1-m digital elevation model provided by the US Geological Survey, and a mosaic of multiple images was created.

2.3 Image sampling

Individuals of 16 tree and shrub species and plant types (*A. altissima*, *Celastrus orbiculatus*, *E. umbellata*, *Gleditsia triacanthos*, *Galium verum*, *Machura pomifera*, *Juglans nigra*, *Juniperus virginiana*, *Lonicera japonica*, *Lonicera maackii*, *Pinus virginiana*, *Rhamnus davurica*, *Rubus sp.*, *Solidago altissima*, *Symphoricarpos orbiculatus*, and graminoids) were identified in each of the three fields (E, EM, and M) using a high-precision GPS and used to catalogue individuals within imagery. If a given species was present in images of a field, up to eight individuals were selected for analysis. In cases where fewer than eight individuals were present, as many as were present were sampled.

Within the images, 15 well-lit and representative pixels were selected for spectral sampling from each individual. To remove outliers, a mean was taken across all wavelengths for each reflectance spectrum of a pixel, and a mean was calculated in a similar fashion for all 15 pixels from each individual. Any pixel within an individual that differed more than 25% from the mean of the individual was removed from the dataset. This removed approximately 1% of pixels from observation.

2.4 Assessing variability due to fine-scale images

Both relative and absolute intraspecific (among individuals within a species) spectral variability were calculated. Relative variability was determined using the coefficient of variation (CV), which compares the variability among the means of each individual to the grand mean of

the species. Absolute variability was determined using standard deviation (SD). CV and SD were calculated across all wavelengths for each species. Interspecific (among species) spectral variability was also quantified using CV and SD for comparison to intraspecific variability.

To differentiate *A. altissima* and *E. umbellata*, individuals from Fields E and M were used to train an algorithm with Partial Least Squares Discriminant Analysis (PLS-DA) using the pls R package (Liland et al., 2022). To create an algorithm to detect *A. altissima*, pixels known to be species other than *A. altissima* were recoded into “other” and were separated from *A. altissima*. The same process was followed for *E. umbellata*. Once an algorithm was established using reflectance at each wavelength to separate *A. altissima* and *E. umbellata* pixels in the component space from other species, it was applied to a testing dataset using Field EM, to test the effectiveness of each algorithm. The algorithms to detect *A. altissima* and *E. umbellata* with PLS-DA on the training data were applied to each pixel in the testing dataset. Because the pls R package applies the PLS-DA algorithm to each pixel in both components, only pixels categorized as the species of interest in both components were classified as the species of interest, while pixels categorized as the species of interest in only one component were not.

Then the percentage of pixels within each individual tree or shrub was calculated for each class, and if over half the pixels were classified as the species of interest, the individual was classified as the species of interest. If fewer than half the pixels were classified as the species of interest, the individual was classified as other species. This was done for all individuals using each algorithm to detect both *A. altissima* and *E. umbellata*. Following classification, omission error (false negatives), commission error (false positives), overall accuracy, and Matthew’s Correlation Coefficient (MCC; Equation 1) were calculated. MCC uses the balance of true positives (TP), true negatives (TN), false positives (FP), and false negatives (FN) and can range from -1 to 1, where

-1 is entirely incorrect classification and 1 is entirely correct classification. An MCC value of 0 represents classification due to chance.

$$\frac{(TP*TN)-(FP*FN)}{\sqrt{(TP+FP)*(TP+FN)*(TN+FP)*(TN+FN)}} \quad (\text{Equation 1})$$

3. Results

3.1 Intra-individual and intraspecific variability relative to interspecific variability

The CV of intra-individual variability exceeded the CV of interspecific variability at 454 nm, 514 to 663 nm and 694 to 714 nm in *A. altissima*, with the greatest ratio of intra-individual to interspecific variability of 1.42 occurring at 701 nm. The SD of intra-individual variability of *E. umbellata* did not exceed the SD of interspecific variability (Figure 1A). The SD of intra-individual variability exceeded the SD of interspecific variability in *A. altissima* at 530 nm, 570 nm, 574 nm, 583 to 645 nm, 696 to 714 nm, and 940 nm and in *E. umbellata* from 450 to 530 nm and 585 to 705 nm. The greatest ratio of intra-individual to interspecific variability of 1.18 in *A. altissima* occurred at 703 nm and at 459 nm with a ratio of 1.35 in *E. umbellata* (Figure 1B).

The CV of intraspecific variability exceeded interspecific variability in *A. altissima* from 527 to 641 nm and 699 to 719 nm and in *E. umbellata* from 516 to 521 nm, 603 to 667 nm, and 690 to 703 nm. The greatest ratio of intraspecific to interspecific variability of 1.29 in *A. altissima* occurred at 703 nm and 1.29 in *E. umbellata* at 696 nm (Figure 2A). The SD of intraspecific variability in *A. altissima* exceeded the SD of interspecific variability at 603 nm, 607 nm, and from 701 to 719 nm and in *E. umbellata* from 450 to 530 nm and 585 to 705 nm. The greatest ratio of intraspecific to interspecific variability of 1.16 in *A. altissima* occurred at 707 nm and 2.04 in *E. umbellata* at 690 nm (Figure 2B).

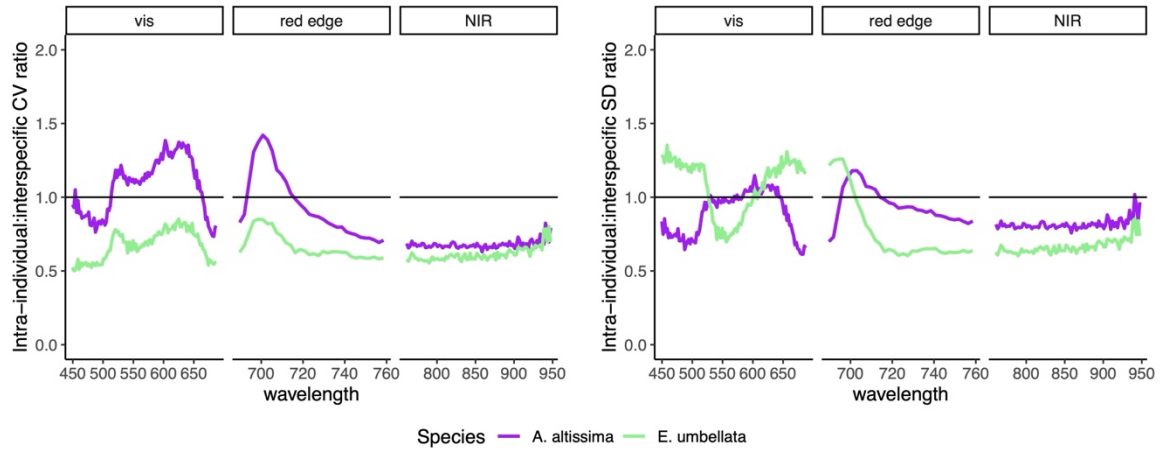


Figure 1. Ratio of intra-individual (within individuals, averaged for a single species) to interspecific (among species) coefficient of variation (CV; the variation normalized by mean, B) and standard deviation (SD, B) across all wavelengths. Spectra are split into visible, red edge, and near-infrared regions. Ratio values over 1 indicate variability that is greater on average within individuals of a species than among species.

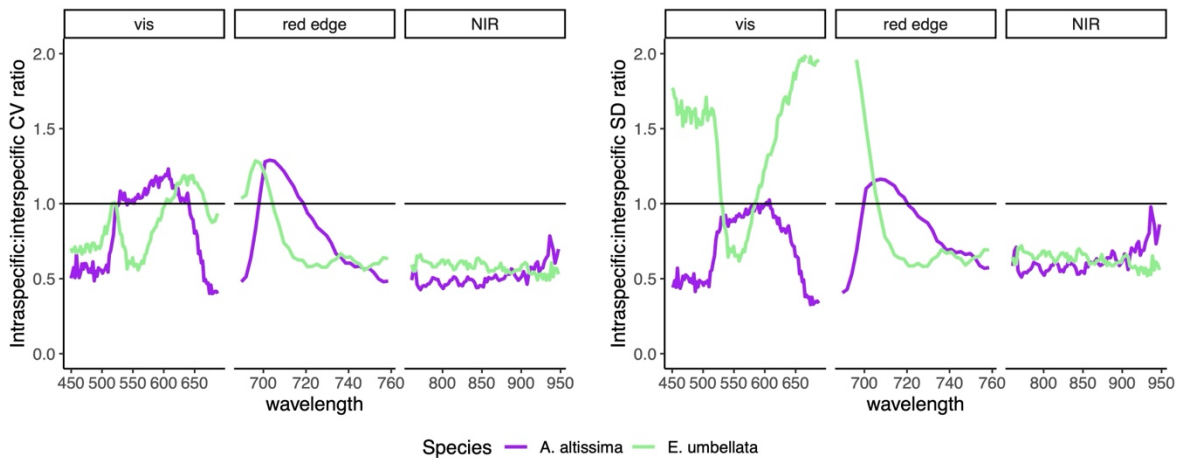


Figure 2. Ratio of intraspecific (within individuals, averaged for a single species) to interspecific (among species) coefficient of variation (CV; the variation normalized by mean, B) and standard deviation (SD, B) across all wavelengths. Spectra are split into visible, red edge, and near-infrared regions. Ratio values over 1 indicate variability that is greater on average among individuals within a species than among species.

3.2 Detection using pixel spectra

The two components of the PLS-DA used to differentiate *A. altissima* pixels from all other species explained a total of 81% of variability in the training data (36% in component 1, and 45% in component 2). *A. altissima* separated most from other species in component 1 and overlapped considerably in the component space (Figure 3A). Wavelengths in the NIR region (763-935 nm) loaded heavily in component 1 (Figure 3B), and wavelengths in the green to yellow spectral region (525-590 nm) loaded heavily in component 2, with the greatest loading values occurring around 540-550 nm (Figure 3C). The two components of the PLS-DA to differentiate *E. umbellata* pixels from all other species explained a total of 72% of variability in the training data (46% in component 1, and 26% in component 2). Unlike *A. altissima*, which separated most in component 1, *E. umbellata* separated from other species in both components and overlapped much less in the component space (Figure 4A). Wavelengths in the blue to green spectral regions (450-510 nm) loaded heavily in component 1 in the negative direction, with a maximum magnitude occurring around 480 nm (Figure 4B). Wavelengths in the red edge region (705-725 nm) loaded most heavily in component 2 (Figure 4C).

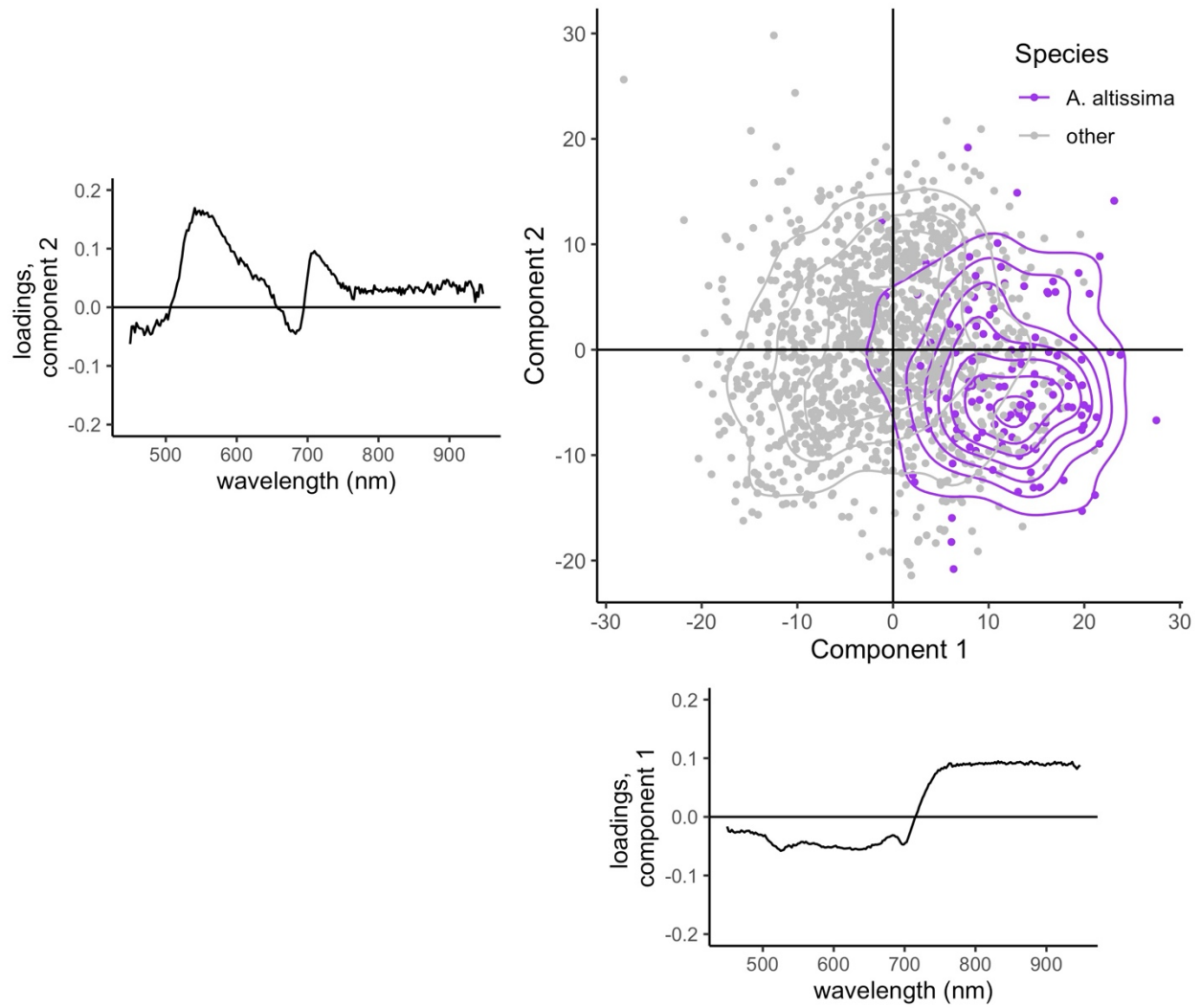


Figure 3. A) Location of all *A. altissima* training pixels (purple) and all other species (grey) in component space. B) Shown below the x-axis is Component 1, and C) beside the y-axis are the loadings for each wavelength in Component 2.

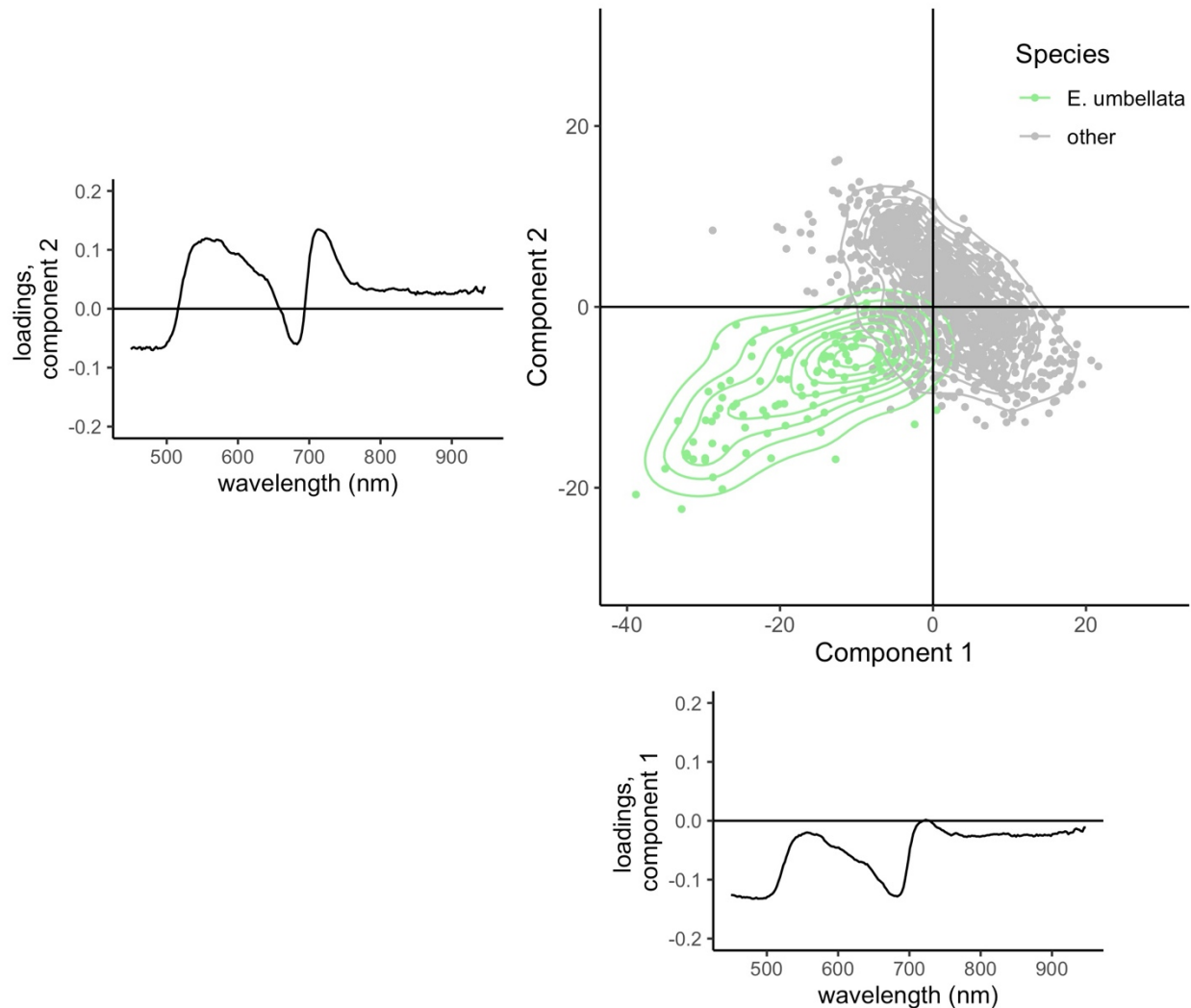


Figure 4. A) Location of all *E. umbellata* training pixels (light green) and all other species (grey) in component space. B) Shown below the x-axis is Component 1, and C) beside the y-axis are the loadings for each wavelength in Component 2.

Applying the algorithm to the test field to detect *A. altissima* provided an overall accuracy of 66%, with all 3 *A. altissima* individuals (5% of all individuals) falsely classified as not *A. altissima* and 17 individuals (29% of individuals) falsely classified as *A. altissima*. Of the 17 individuals incorrectly classified as *A. altissima*, 5 were *Lonicera maackii*, an invasive shrub, and 3 were *Maclura pomifera* and *Rhamnus davurica*. Overall accuracy to detect *E. umbellata* was

95%, with 7 out of 8 individuals correctly classified as *E. umbellata* and 2 individuals falsely classified as *E. umbellata* (Table 1).

Table 1. Accuracy of the algorithm to detect *A. altissima* and *E. umbellata* in a test field. Individuals were classified based on the classification in each component. True positives and negatives and false positives and negatives are given as number of individuals out of 59 total individuals.

	True positive	True negative	Omission error (false negative)	Commission error (false positive)	Overall Accuracy (%)	Matthew's Correlation Coefficient
<i>A. altissima</i>	0	39	3	17	66%	-0.15
<i>E. umbellata</i>	7	49	1	2	95%	0.96

3.3 Variability and differentiation

Wavelengths in the visible spectral region with a ratio of relative intra-individual to interspecific variability (CV) greater than 1 also loaded heavily in component 2 in the PLS-DA to separate *A. altissima* from other species in discriminant analysis (Figure 5A). Wavelengths in the visible and red edge spectral regions with a ratio of absolute intra-individual to interspecific variability (SD) greater than 1 also loaded heavily in component 1 to separate *E. umbellata* from other species in discriminant analysis (Figure 5B).

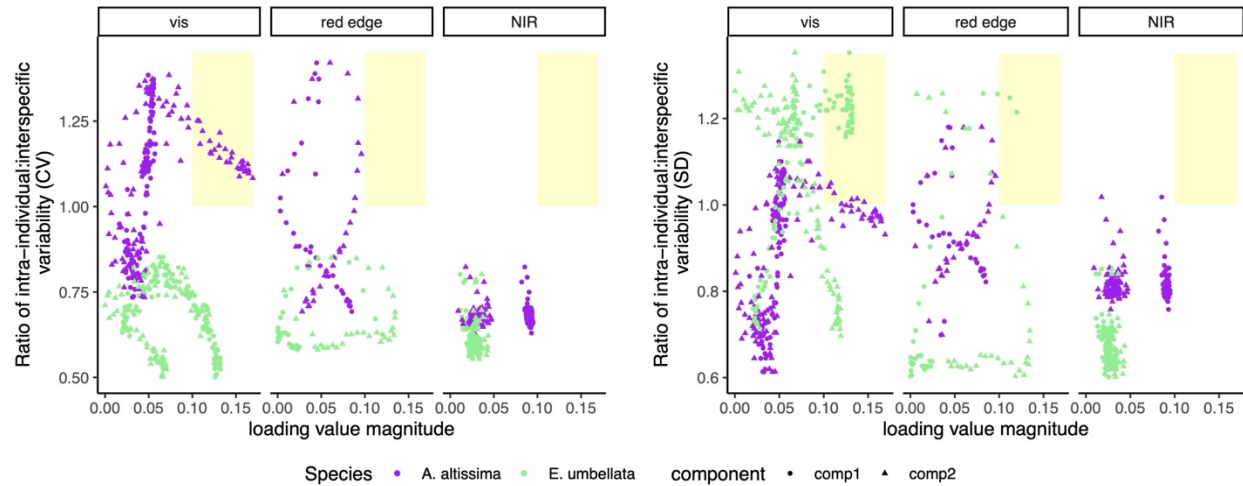


Figure 5. Magnitude of loading values for a given wavelength plotted against the ratio of relative and absolute intra-individual to interspecific variability, given as CV (A) and SD (B), respectively, for that wavelength. Component 1 and component 2 are shown as circles and triangles, respectively, and *A. altissima* and *E. umbellata* are purple and green, respectively. Wavelengths that both load heavily and have high intra-individual variability relative to interspecific variability are shaded in yellow.

Wavelengths in the visible spectral region with a ratio of relative intraspecific to interspecific variability (CV) greater than 1 also loaded heavily in component 2 to separate *A. altissima* from other species in discriminant analysis (Figure 6A). Wavelengths in the visible and red edge spectral regions with ratios of relative and absolute intraspecific to interspecific variability (CV and SD, respectively) greater than 1 also loaded heavily in component 1 to separate *E. umbellata* from other species in discriminant analysis (Figure 6B).

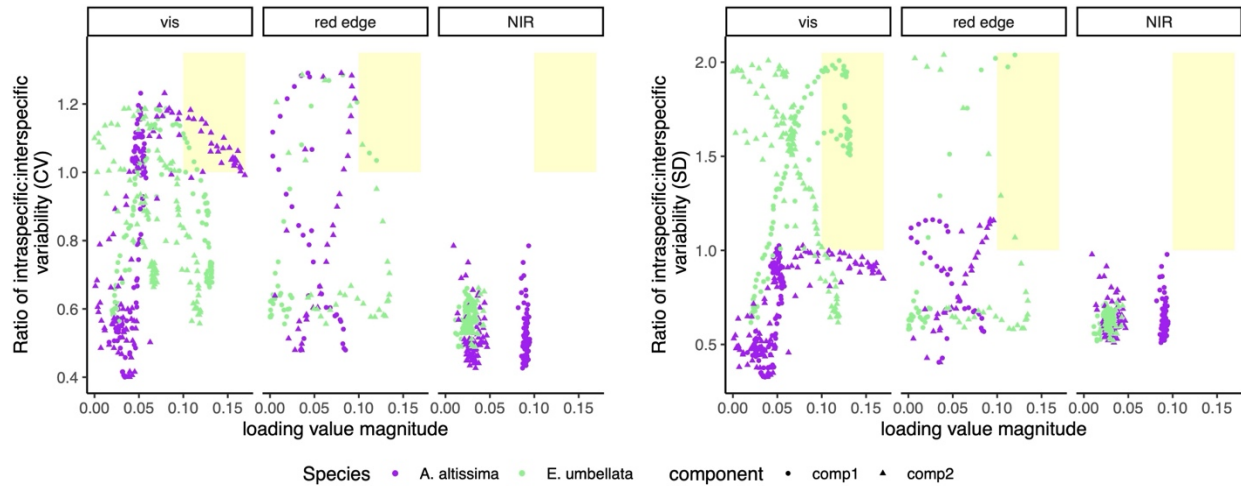


Figure 6. Magnitude of loading values for a given wavelength plotted against the ratio of relative and absolute intra-individual to interspecific variability, given as CV (A) and SD (B), respectively, for that wavelength. Component 1 and component 2 are shown as circles and triangles, respectively, and *A. altissima* and *E. umbellata* are purple and green, respectively. Wavelengths that both load heavily and have high intra-individual variability relative to interspecific variability are shaded in yellow.

4. Discussion

Regions in which both relative and absolute intra-individual variability exceed interspecific variability are of interest, as they may hinder differentiation of species. In the case of intra-individual variability in *A. altissima*, those wavelengths would be: 530 nm, 570 nm, 574 nm, 583 to 645 nm, 696 to 714 nm. As relative intra-individual variability of *E. umbellata* did not exceed interspecific variability, its greater absolute variability relative to interspecific variability can be attributed to its high reflectance in blue and red spectral regions relative to other species. Wavelengths with both relative and absolute intraspecific variability that exceeded interspecific variability were 603 nm, 607 nm, and 701 to 719 nm in *A. altissima* and 516 to 521 nm, 603 to

667 nm, and 690 to 703 nm in *E. umbellata*. These results imply that the combination of intra-individual and intraspecific variability may impede classification of *A. altissima*, particularly around 603 nm, 607 nm, and 701 nm, in which both relative and absolute intra-individual and intraspecific variability exceed interspecific variability. Because relative intra-individual variability in *E. umbellata* did not exceed interspecific variability, overall variability may not impede classification to the same extent as with *A. altissima*.

Spectral signals from individual pixels detected *E. umbellata* better than *A. altissima*. Although *E. umbellata* demonstrated relative intraspecific variability about twice that of interspecific variability, the absolute variability among *E. umbellata* individuals exceeded interspecific variability over fewer wavelengths than *A. altissima*, and absolute variability within *E. umbellata* individuals did not exceed interspecific variability over any wavelengths. These patterns of variability do not definitively suggest that intra-individual or intraspecific variability impacted classification. The amount of overlap in locations of pixels in the component space, however, does suggest other factors impact classification. In the PLS-DA component space, *A. altissima* overlapped with other species more than *E. umbellata* did. This suggests that despite high intraspecific variability in *E. umbellata*, it was still differentiable from other species, while *A. altissima* had more in common with other species, particularly *L. maackii*, *M. pomifera*, and *R. davurica*.

The overlap between wavelengths with high variability and wavelengths with high loading values suggests *some* intra-individual and intraspecific variability may impede detection of these two invasive plant species, especially *E. umbellata*, which had greater variability relative to interspecific variability than *A. altissima*. The classification results, however, suggest that differences between the species of interest and all other species are more important than the

variability among all species, which is what the interspecific variability represents. These results suggest that intra-individual and intraspecific variability are not the only factors impacting detection, as classification of *E. umbellata* was more accurate.

Traditional hyperspectral data collection efforts are inadequate on the basis of either time or space. For example, satellite data, though temporally robust and therefore providing phenological data, are often too coarse in resolution to detect individual tree and shrub canopies. Collection by fixed-wing aircraft has a finer spatial resolution but is typically collected at much lower frequency, often on an annual basis. Fixed-wing aircraft data collection also requires an open field, which can be a challenge in some forest studies. UAV-based data collection combines the spatial and temporal benefits of each data collection method to provide data with high temporal and spatial resolution. These results suggest the very fine, leaf-scale resolution of hyperspectral data collected by UAV does not impede differentiation, but rather, the differences among the species of interest and all other species are most important. As these data were collected mid-growing season when phenological differences are least noticeable, utilizing additional dates for differentiation will likely improve detection of invasive plant species.

To my knowledge, this is the first effort to identify and map invasive plant species within heterogeneous vegetation communities of the northern Blue Ridge region in Virginia. From this project I will produce effective methodology in utilizing spectroscopy to identify and locate targeted invasive plants, particularly the invasive tree *A. altissima* and shrub *E. umbellata* from aerial images. The conclusion that differences among the species of interest and all other species is more important than intra-individual and intraspecific variability indicates that the temporal flexibility of sampling via UAV will aid this effort.